University of Southampton

Faculty of Physical Sciences and Engineering

School of engineering

Layer by layer (LbL) coating on urological devices to prevent biofilm formation

by

Maryam Mosayebi

Thesis for the degree of MPhil in Engineering and the Environment (7838)

October 2022

University of Southampton

Abstract

Urological devices, such as indwelling catheters and stents, are widely used to maintain urinary drainage when this is impaired by obstructions. However, the important function of these devices is frequently compromised by the formation of encrustation, which can lead to complications such as blockages, urinary tract infections (UTIs), and retained devices that are difficult to remove. Encrustation occurs by precipitation of solid crystals from urine onto the surface of a device and is frequently promoted and mediated by urease-producing bacteria (such as Proteus mirabilis). The net result is the formation of crystalline biofilms, i.e., bacterial biofilms embedding crystalline structures, showing enhanced resistance against antibiotic treatment. Complications due to encrustation negatively impact on a patient's quality of life and cause significant financial burden on healthcare providers. Various approaches have been investigated to address these challenges, including the development of new device geometries and the use of different types of materials and surface coatings. However, a comprehensive solution that prevents the formation of crystalline biofilms and avoids device failure remains elusive. The formation of crystalline biofilms is influenced by a range of conditions, including the urinary flow field and the chemical and micro-biological composition of urine, which may differ between patients and depend upon where the device is placed within the urinary tract. Devices that can be customized to resist crystalline biofilm formation for a set of specific environmental conditions, or that address multiple causative mechanisms governing the development of encrustation, are a potential solution to this ongoing challenge. Layer-by-layer (LbL) assembly is a technique for depositing multilayer coatings that is capable of nano-scale control over the layer's composition and thickness. Individual layers are typically deposited from a solution or suspension onto a charged substrate via electrostatic attraction, leading to charge reversal of the coated surface, and enabling subsequent deposition of an oppositely charged moiety. A wide range of polyelectrolytes, other molecules, and particles can be deposited via LbL assembly, leading to multilayer coatings with many different potential combinations of materials, properties, and functions. LbL-assembled coatings with different surface chemistry, mechanical stiffness, and drug delivery capability have been reported with proven or potential infection-resistant functionality based on bactericidal or anti-adhesion effects. The high degree of control and flexibility that LbL assembly can achieve provides the opportunity to produce customized and multifunctional coatings for combatting crystalline biofilms and associated failures of urological devices. In this project, LbL assembly is used to produce multilayer coatings of Polyethyleneimine (PEI) and Polyacrylicacid (PAA) with different thickness and composition of the last deposited layer. The coatings were deposited onto Polydimethylsiloxane (PDMS) substrates, which is representative of materials commonly used for urinary catheters and stents. The coatings were characterized by microscopy for thickness and morphology, by nanoindentation for mechanical stiffness, and using bacterial cultures to assess microbiological properties. Results show that the proposed coatings can significantly prevent biofilm formation against common UTI bacteria *P. aeruginosa*, and the antimicrobial behavior can improve by increasing the thickness of coating.

Key words: Urinary system, urinary tract infections (UTIs), crystalline biofilms, encrustation, Layer by Layer (LbL) assembly

Table of Contents

Table of Tables

Table of Figures

Table of Figures

Table of Figures

Research Thesis: Declaration of Authorship

Print name: Maryam Mosayebi

Title of thesis: Layer by layer (LbL) coating on urological devices to prevent biofilm formation

I declare that this thesis and the work presented in it are my own and has been generated by me as the result of my own original research.

I confirm that:

1. This work was done wholly or mainly while in candidature for a research degree at this University;
2. Where any part of this thesis has previously been submitted for a degree or any other qualification at this University or any other institution, this has been clearly stated;
3. Where I have consulted the published work of others, this is always clearly attributed;
4. Where I have quoted from the work of others, the source is always given. With the exception of such quotations, this thesis is entirely my own work;
5. I have acknowledged all main sources of help;
6. Where the thesis is based on work done by myself jointly with others, I have made clear exactly what was done by others and what I have contributed myself;
7. None of this work has been published before submission or Parts of this work have been published as:-

Signature: Date:

Acknowledgements

This project would not have been possible without the support of my supervisory team Dr Andrew Hamilton, Dr Dario Carugo and Dr Ali Mosayyebi. I benefited greatly from the wealth of their knowledge and support throughout my research.

Special thanks to my parents for their endless support, without whom I would have not had the opportunity. I would also like to thank my sister Mrs Sarvin Nouroozi and Dr Gareth LuTheryn for their time, knowledge, skills, and support during this journey.

Definitions and Abbreviations

Urinary tract infections (UTIs)

National Institute for Health and Care Excellence (NICE)

National Health Service (NHS)

Crystalline biofilm (CB)

Layer by layer (LbL)

Polyethyleneimine (PEI)

Polyacrylic acid (PAA)

Escherichia coli (E. coli),

Proteus mirabilis (P. mirabilis)

Pseudomonas aeruginosa (P. aeruginosa)

Klebsiella pneumoniae (K. pneumoniae)

Streptococcus faecalis (S. faecalis)

Food and drug administration (FDA)

Bilayers (BLs)

Scanning electron microscopy (SEM)

Extra cellular matrix (ECM)

Polydimethylsiloxane (PDMS)

Optical density (OD)

Lysogeny broth (LB)

Chapter 1 Introduction

The urinary system is deputed to the regulation of blood volume and pressure, electrolytes levels, and excretion of waste products from the body. Dysfunction of this system can be complex to address and may result in severe systemic complications. If not effectively treated, dysfunction associated with impairment of urinary drainage can lead to a permanent inability to urinate, significant pain, and in some cases death [1]. Urinary stents and catheters are two of the most common devices that clinicians use as cost-effective and temporary solutions to address the impairment of urinary drainage. Stents are inserted in the upper urinary tract, between the kidneys and bladder, and used to restore urinary drainage when this is compromised by conditions such as tumors, kidney stones, or strictures. Catheters are used to manage urine flow within the lower urinary tract (i.e. distal to the bladder) [2], [3]. Despite their clinical utility, these devices suffer from limitations such as biofilm formation and encrustation, which can lead to urinary tract infections (UTIs) [4]. UTIs are the most common hospital-acquired infections, and the associated complications can significantly affect a patient's quality of life, negatively impacting on independence, ability to live and work normally, and mental as well as physical health [5]. They represent 19% of healthcare-associated infections, with half of these originating from a urinary catheter according to the UK National Institute for Health and Care Excellence (NICE) guidelines [6]. Around 2% of all primary care consultations are in connection with UTI-related symptoms, leading to 13.7% of antibiotic prescriptions in the UK National Health Service (NHS). The financial burden imposed on the NHS by UTIs is in the order of billions of pounds per year [7]. The average economic burden on healthcare providers ranges from £1.75 billion in the UK to £30 billion in the US annually [4].

As foreign objects to the body, stents and catheters can disrupt host defense mechanisms that protect the body against infection. In the case of catheters, bacteria can reach the urinary tract by transferring fecal or skin microbiota into the body. After device insertion, the inevitable relative movement of a catheter due to normal body motion can enhance this bacterial migration, enabling them to reach the bladder within 1–3 days. Clinical studies have reported that catheter associated UTIs (CAUTIs) are mainly caused by microorganisms that gain access to the urinary system by migrating along the outer surface of the catheter [8]. Contamination of collecting tubes or drainage bags used with urinary catheters is another possible route to infection that can occur in a large number of cases [9]. Bacterial colonization and migration in stents can occur both inside and outside the stent lumen [10]. Stents are typically deployed for more extensive periods of time (>1 week) compared to catheters (<1 week), with indwelling time directly correlating with incidence rates of encrustation [11]. It has been reported that biofilm formation can occur within 24 hours after stent

insertion in up to 90% of indwelling stents; this poses a considerable challenge, given the relatively longer deployment time for stents [12].

According to the literature, similar conditions lead to crystalline biofilm (CB) formation on both stents and catheters (Figure 1-1), but this is still an open question. The requirements for both devices differ in terms of indwelling time and environmental conditions, including urine pH and composition, administered drugs, and other patient-specific conditions. These differences explain why a one-fits-all solution is lacking for stents and catheters and for heterogeneous patient groups [13]–[16].

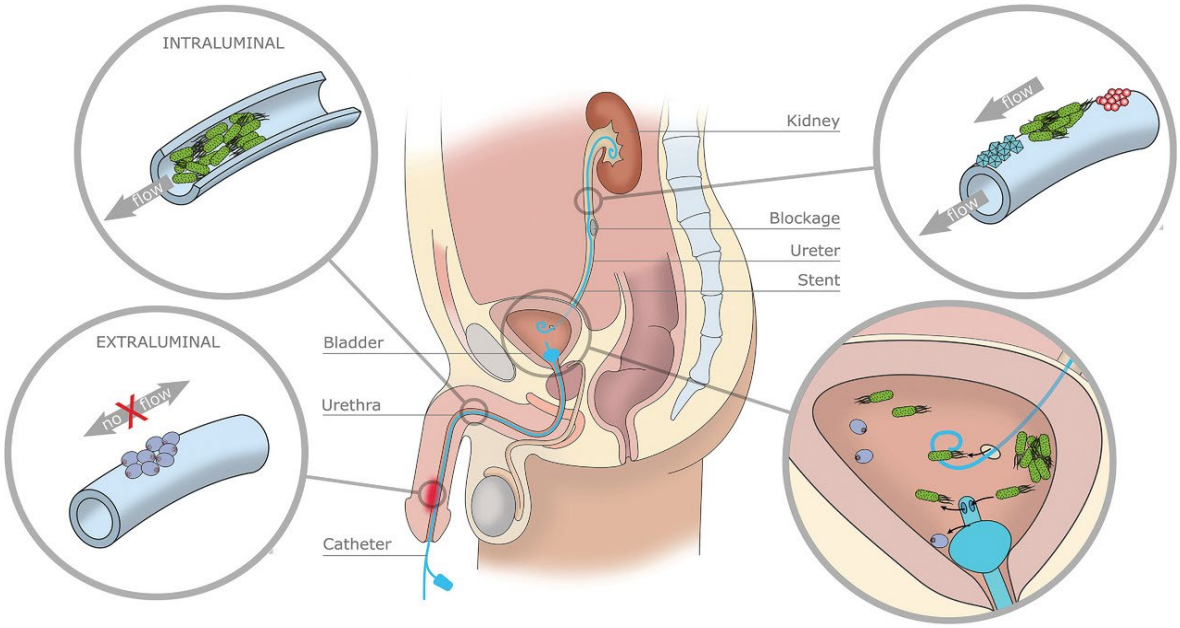

Figure 1-1 Cross section of urinary system in male body, showing urinary stent and catheters location [17].

Different strategies have been proposed to prevent the formation of CBs in stents and catheters, including new designs to enhance urinary drainage based on fluid mechanical modelling [18], [19] and changing the substrate material to vary its mechanical properties, morphology, or surface chemistry [20]. The application of coatings is another strategy which has been widely explored for improving the next generation of stents and catheters. Different types of antimicrobial surface coatings have been applied, including those comprising heavy metals, active pharmaceutical ingredients, polymers, colloids, biomolecules, or biological cells [21]–[23]. Although these various approaches have yielded promising outcomes, none of them has been shown to completely address the causative mechanisms governing the formation of CBs in urological devices, and they often lack clinical validation of efficacy against the associated complications. Layer by layer (LbL) assembly is a coating deposition technique that can combine many constituents to create multilayered coatings with the potential for addressing multiple causes and varying conditions leading to CB formation [24], [25]. Although LbL assembled coatings showed promising results in preventing biofilm

formation, their novelty and limited studies regarding their antimicrobial behavior make them an interesting subject for further investigations. The number of articles regarding materials and techniques to provide an antimicrobial LbL assembled coatings on urinary stents and catheters are very small in comparison to single layer antimicrobial coatings. However, their promising results in preventing biofilm formation and encrustation, shows there is a potential for more research in this area to help improving urological devices.

In this thesis, polyethyleneimine (PEI) and polyacrylic acid (PAA) were chosen as constituents for antimicrobial coatings due to their outstanding properties such as low cost, availability in large quantities, compatibility with LbL assembly, antimicrobial activity, and pH responsiveness [25]–[27]. Previous work has reported some promising results for the antimicrobial behavior of PEI/PAA coating [28]–[30] but this thesis will study the effect of thickness and mechanisms that can lead to antimicrobial activity against *P. aeruginosa* bacteria. After confirming the presence of the coating on PDMS and investigating thickness, stiffness, and antibiofilm activity (static cell work properties), PEI/PAA LbL assembled coatings were deposited on the surface of a commercially available catheter (Dover, 20 French (Fr), 100% silicone) and the antibiofilm activity was assessed under dynamic flow to replicate more realistic flow conditions in the urinary system. Chitosan was also incorporated as an additional constituent in the coatings produced and studied in this thesis. Chitosan has been used as an antimicrobial and degradable coating on the surface of urinary stents in previous studies [31]–[33], and so incorporation of chitosan to PEI/PAA coatings can potentially achieve degradability as an additional antimicrobial mechanism. Degradation of LbL assembled coatings including PEI,PAA and Chitosan were therefore studied by measuring thickness and monitoring thickness decreases over time upon exposure to enzymes expected in the urinary system.

Chapter 2 Literature review

2.1 Formation of CB

A description of the conditions that lead to CB formation helps to better understand the efficacy of coatings that are designed to disrupt the associated mechanisms and prevent UTIs. The progression of a device-associated UTI starts with bacterial adhesion, biofilm formation and growth, and leads to crystalline encrustation and device scaling. Upon deployment of a sterile urological device, a conditioning layer forms through adsorption of ions, minerals, proteins, lipids, and other biomolecules onto the device surface from the surrounding urine and tissues. This conditioning layer mediates bacterial adhesion, initially through reversible attachment *via* electrostatic interaction or the bacterial pili/flagella. This eventually leads to irreversible adhesion, mediated by bacterial adhesins and excretion of extracellular polymer substances. At the earlier stages of maturation, biofilms grow to thicknesses of ~10s of micrometers and bacteria within the biofilm are capable of sensing the external environment, communicating with adjacent cells, and transferring genetic information and plasmids (a process known as 'quorum sensing'). In the later stages, the bacterial population grows rapidly, and biofilm thickness can reach ~100s of micrometers. The breakdown of mature biofilms leads to release and dispersal of motile planktonic cells capable of adhering and forming biofilms in different locations [34]. Figure 2-1shows different steps of biofilm formation as described.

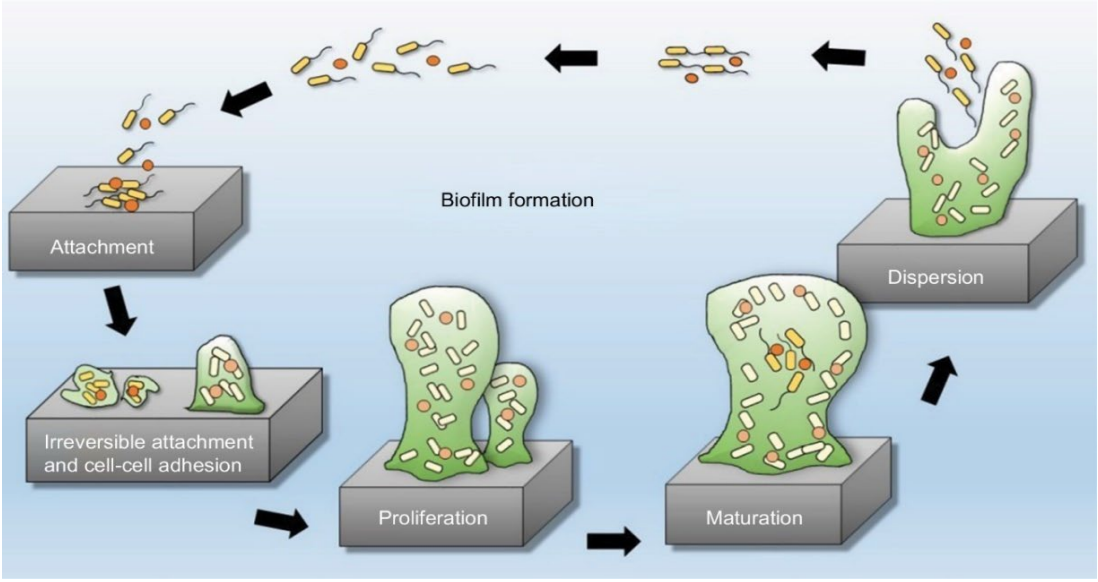

Figure 2-1 Different steps of biofilm formation including attachment, irreversible attachment, proliferation, maturation and dispersion [35].

A range of biofilm-forming microbes have been implicated in device-associated UTIs, including *Escherichia coli (E. coli)*, *Proteus mirabilis (P. mirabilis)*, *Pseudomonas aeruginosa* (*P. aeruginosa*), *Klebsiella pneumoniae (K. pneumoniae)* and *Streptococcus faecalis (S. faecalis).* These uropathogens are generally present in human urine and therefore can come into contact with both urinary stents and catheters [36], [37]. Biofilms play an important role in protecting microorganisms from the immune system, antibiotic drugs, and other physico-chemical disturbances. It has been reported that protection from biofilms can enable bacteria to withstand more than 1000-fold greater antibiotic concentrations than suspended (planktonic) bacteria [38].

In addition to microbiological constituents, urine also contains a large number of different minerals and chemicals including urea, uric acid, creatinine, sodium, potassium, ammonium, calcium, magnesium, chloride, oxalate, sulphate and phosphate. These solutes can form salt crystals such as magnesium ammonium phosphate, calcium carbonate, and calcium oxalate [39], which may deposit or precipitate on the surface of a urological device. Some of the uropathogens associated with UTIs (such as *P. mirabilis*) produce the enzyme urease, which in turn produces ammonia and carbon dioxide by hydrolyzing the urea present in urine. Increased concentration of ammonia causes elevation of urine pH, which in turn accelerates the rate of calcium and magnesium ammonium phosphate crystallization, leading to rapid encrustation of a device [9], [34]. The simultaneous formation of crystalline encrustation and excretion of extracellular polysaccharides by uropathogens, leads to the formation of CBs The combination and interaction of these two processes further enhances bacterial protection from the external environment, posing a significant challenge to the correct functioning of stents and catheters [37], [40]. shows steps of calcium oxalate crystal formation in human body.

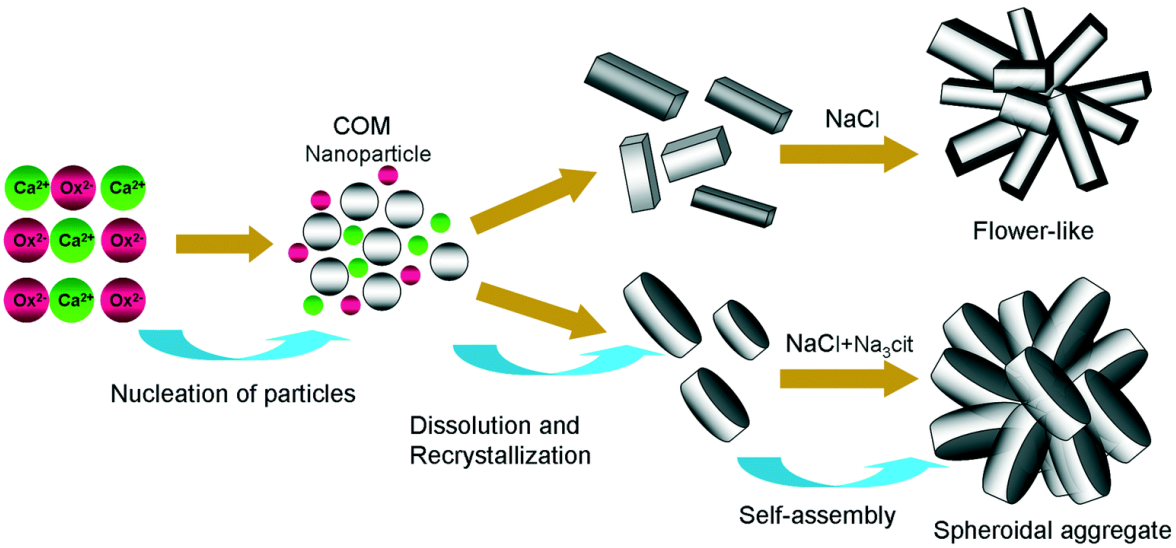

Figure 2-2 formation of calcium oxalate crystals in human body from Ca^{2+} and Ox^{2-} ions in solution [41].

2.2 Antimicrobial coatings on urological devices

The application of antimicrobial coatings to urinary stents and catheters is one of the potential strategies employed to prevent microbial colonization, CBs and, ultimately, related health complications (such as UTIs and device failures). A challenge to developing new antimicrobial coatings and implementing them clinically is the lack of studies demonstrating both in-vitro and in-vivo validation, as well as the limited standardization of test methods employed to assess their efficacy. Depending on the mechanism of action, these coating-based approaches can be divided into five major categories: (1) bactericidal coatings releasing bactericidal agents such as heavy metals, antibiotics, bactericidal enzymes, or bacteriophages that inhibit the biological activity of microorganisms near the surface of a device. (2) Contact killing coatings containing antimicrobial constituents that remain immobilized on a surface, such as antimicrobial peptides (AMPs), carbon nanotubes (CNTs) and graphene oxide (GO). (3) Antifouling coatings inhibiting bacterial attachment by disrupting conditioning layers and bacterial adhesion mechanisms. Hydrogels, polyzwitterions and cationic polymers are categorizing in this group. (4) Biofilm disruption coatings containing agents that interfere with the formation of a mature biofilm by dispersing the extracellular polymer substances (EPS) and interfering with quorum sensing. Finally, (5) coatings relying on bacterial interference, which incorporate benign bacteria inhibiting pathogenic bacteria from attaching to a surface. Summary of antimicrobial coating strategies that have been implemented on urinary catheters, and associated advantages and disadvantages is shown in Table 2-1 [11], [36], [49], [40], [42]–[48].

Table 2-1 Summary of antimicrobial coating strategies that have been implemented on urinary catheters, and associated advantages and disadvantages [11], [36], [49], [40], [42]–[48].

Strategy	**Type of Agent**	**Chemical Composition**	**Advantages**	**Disadvantages**
Bactericidal	Heavy metal	Silver [36], [47]	Reduction of CAUTI up to 3.7-fold in the short-term (1–3 days)	Accumulation of silver can cause damages toward the tissue, which is in contact with coated catheter, loses antimicrobial activity over long-term (2

				weeks) catheterization
	Antibiotics	Nitrofurazone, Gentamicin, Norfloxacin, Sparfloxacin, Vancomycin, Rifampin [36], [40], [48]	Bacterial inhibition for more than 100 days	May contribute to antimicrobial resistance; Nitrofurazone may lead to breast and ovarian tumours
	Bactericidal enzyme	Haloperoxidases, Chloroperoxidases, Lactoperoxidase [36], [49]	No antimicrobial resistance, and non-toxic for mammalian cells	High cost of complicated production and purification; likely deactivated by sterilization, storage, and transport
	Bacteriophage	Lytic phage, Lysogenic phage [36], [48]	No antimicrobial resistance, and non-toxic for mammalian cells	Unstable during sterilization and storage of catheter
Contact killing	AMP	An engineered arginine-tryptophan-rich peptide (CWR11), cysteine-modified Lasioglossin peptide [36], [40], [48]	Nontoxic for mammalian cells; reduces CAUTI up to 21 days	High pH sensitivity; antimicrobial resistance
	CNT & GO	Single-walled carbon nanotube (SWNT), hydrated GO (hGO) [25], [36]	Antimicrobial activity in the short-term (1 week)	Lack of clinical studies for long term use (2 weeks); needs more preclinical trials
Antifouling	Hydrogel	Polyethylene glycol (PEG) [44], [48]	Near complete eradication (>99%) of *S. aureus* after contact for up to 14 days	Can provoke anti-PEG immune response in significant portion of population (~25%),

	Polyzwitterion	Sulfobetaine methacrylate (SBMA); Poly(oxonorbornene) based zwitterion (PZI) [36], [49]	Biofilm formation was reduced against *P. aeruginosa* and *S. aureus* by 80%–90% up to 7 days	Breaking down of hydration layer and deactivation in the medium/long term (2 weeks)
	Cationic polymer	Quaternary ammonium salts [25], [36]	>90% reduction of clinically relevant pathogens for 1 week	NA
Biofilm dispersion	Enzymes for EPS	Proteases, Polysaccharide, Hydrolases [11], [36]	Highly effective to prevent biofilm formation against *P. aeruginosa* and *S. aureus*; no bacterial resistance	Lack of *in vivo* and pre-clinical studies
	Signal interference	Acylated homoserine lactones (AHL), oligopeptide, furanosyl borate diester (AI-2), thiazolidinedione-8 (TZD-8) [36]	Prevents biofilm formation and CAUTI for 8 days	Limited efficiency against a range of pathogens that can cause CAUTI
	NO	Snitrosoglutathione (GSNO) [36], [50]	82% reduction of biofilm formation for 2 weeks	Storage for long term is a challenge; toxicity due to diffusion of nitric oxide (NO)
Bacterial interference	Benign bacterial biofilm	*Lactobacillus* species (*L. crispatus* CTV05) and *E. coli* (strain 83972) [36]	No microorganism resistance, renewable, and prophylactic	Low adherence onto silicone materials

Although all of the aforementioned coating strategies could play an important role in reducing device-associated UTI, they still need improvements and further investigations because of their associated limitations and disadvantages. For instance, loss of antimicrobial activity beyond ~2 weeks is one of the challenges that silver coated urinary catheters face. Whilst small doses are not

able to effectively address UTI, high doses can potentially cause toxicity. Notably, silver is approved by the food and drug administration (FDA) as an antimicrobial coating for urinary catheters; however, it has also been associated with tissue damage [51]. It should be noted that catheters are cost-effective devices with high demand; for any coating technology to be translated clinically, an optimal compromise between effectiveness and cost should be identified. Furthermore, devices may need to be supplied to different locations worldwide, potentially requiring storage over prolonged period of time; coatings should therefore remain active over this period before being deployed clinically. Between the abovementioned coatings, silver and hydrogels are the ones that have been most widely researched and that have gained approval for application on commercial catheters. The others would still require additional investigations *in vivo*, both pre-clinically and in human trials. CR Bard, Covidien Dover and BIOCATH® hydrogel-coated catheters are well-known silicone-based catheters that are available for clinical usage. It has also been found that combining silver and hydrogels as antimicrobial coatings can improve the antimicrobial activity of urinary catheters. Bardex® IC and Dover catheters are two examples of commercial catheters that coated with both silver and hydrogels, resulting in a decrease of catheter-associated UTI of up to 47% [36], [52].

Antimicrobial coatings that have been applied on urinary stents are shown in Table 2-2 and are categorized using the same classification reported above for urinary catheters. The communities of microorganisms implicated in catheter- and stent-associated UTIs are similar. Therefore, the antimicrobial coating strategies that have been researched on stents – and their advantages and limitations - are comparable to those used for catheters.

Table 2-2 Summary of antimicrobial coating strategies that have been implemented in urinary stents and associated advantages and disadvantages [30], [40], [51], [53], [54].

Strategy	**Type of Agent**	**Chemical Composition**	**Advantages**	**Disadvantages**
Bactericidal	Heavy metal	silver [48], [50]	Antimicrobial activity against *Pseudomonas aeruginosa, Enterococcus faecalis, Proteus mirabilis* and two strains of	Do not remain active for 2 weeks or more, May damage urothelial tissue

			Escherichia coli	
	Antibiotic	Rifampin, Ciprofloxacin, Triclosan, Gentamicin, Cefazolin, Ceftriaxone, or Tobramycin [37], [51]	Prevent UTI against *P. mirabilis, E. coli, Klebsiella pneumoniae,* and *S. aureus*	Antimicrobial resistance, Not FDA approved
	Bactericidal enzyme	Lipase B [37], [51]	prevent biofilm formation up to 16 days	Not biocompatible
	Bacteriophage	Lysogenic [37], [51]	Degradation of biofilm	Moisture sensitive, challenging storage conditions
Contact killing	AMP	Bmap-28, RRWQWR [37], [51]	Prevent encrustation and biofilm formation for 1 week	Lack of sufficient *in vivo* studies
Antifouling	Cationic polymer	polyethyleneimine (PEI) brush-like structures [52]	Prevent adhesion of *P. mirabilis* in the long term (>2 weeks)	N/A

The number of studies focusing on antimicrobial coatings for urinary stents is however lower compared to urinary catheters, thus further investigations would be required in this area (particularly in vivo). Carbothan® is an example of a commercial stent coated with silver sulfadiazine, which has been investigated for its antimicrobial activity. The clinical trial results show that this coating doesn't have a significant outcome in preventing bacterial growth in 3 weeks [51]. Biocompatibility is another challenge for urinary stents and catheters. In LbL technique adding more biocompatible constituent between bactericidal enzymes layers might help solving this issue. Biocompatible hydrogels may be one of the candidates to be used with bactericidal enzyme in LbL method.

As mentioned above, based on the similarity of UTI in urinary stents and catheters, proposed solutions for antimicrobial coatings are effective to decrease the rate of infection in both devices; However, they cannot completely address the challenge of UTI. Formation of CB under flow dynamic (urine flow), each person's body condition and problem is one the complex phenomenon occurring in human urinary system. Complexity of this process make the researcher to add simplifying assumption to their project (as an individual project cannot handle all the realistic condition) such as, investigating the UTI against one or two microorganisms, evaluating the antimicrobial coating under static flow than dynamic, or carrying on the study as an in vitro rather than in vivo due to the high expense and limited availabilities. Improving the quality of medical devices is one of the most sensitive areas in research and it needs high technology and expensive equipment based on the regulations. On the other hand, high demand for testing the medical devices make them available only for short window of time for each research based on the funding.

LbL assembly may potentially address some of these limitations; for example, silver-loaded layers could be deposited in between layers containing other antimicrobial agents, such as biocompatible polymers. This may enable greater control over the released dose and provide long lasting effects without damaging the urethral and vesical tissues. Moreover, antimicrobial resistance is a major disadvantage of antibiotics and AMPs; a LbL coating approach could mitigate this limitation by providing greater control over the release kinetics as well as enabling the elution of multiple antimicrobial compounds with synergistic action. It may also partly overcome the sensitivity of bactericidal enzymes, bacteriophages, AMPs, EPS-degrading enzymes, and NO to pH and moisture of the environment, by loading them in between less sensitive materials.

2.3 LbL assembly technique

LbL assembly is a technique for depositing multiple layers (or multilayers) coatings onto a substrate. The process involves step-by-step sequential adsorption of single layers resulting in the multilayer coating. The driving force for adsorption in electrostatic LbL assembly is electrostatic interaction between the substrate and the layers being adsorbed. Sequential adsorption of oppositely charged layers leads to charge reversal at the surface and enables electrostatic attraction of the next layer. Other forms of LbL assembly achieve adsorption via hydrogen bonding, covalent bonding, or other means. In a typical LbL assembly procedure, the substrate material is cleaned and, in some cases, treated to impart an initial electrostatic charge. Different substrate materials with different surface morphologies can be coated for various purposes. The substrate needs to chemically interact with chemical moiety that is first being deposited so that a layer adsorbs onto the surface and forms the first monolayer. Usually the interaction is electrostatic, so a suitable substrate and the first layer to be deposited have opposite charges, however other interactions such as hydrogen or covalent

bonding are also possible. Next, the substrate is submerged into an aqueous solution of the first constituent (which has opposite charge compared to the substrate) for a specific amount of time that is based on the desired layer thickness. Then, the substrate is placed in deionized water (DI) to remove residual molecules that aren't attached to its surface and to prevent cross contamination. After depositing the first layer, the substrate is submerged in an aqueous solution of the second constituent, followed by submersion in DI water. Repeating this process can provide multiple layers of the two constituents on the surface of the substrate [55]. The multilayer structure of LbL assembled coatings therefore commonly consists of repeated bilayers (BLs), in which deposition of constituent A is followed by deposition of constituent B, which is then repeated n times to produce multilayer coatings of n(AB). Coatings may also consist of tri-layers of n(ABC), quad-layers of (nABCD), or other sequences that may or may not be repeating (Figure 2-3).

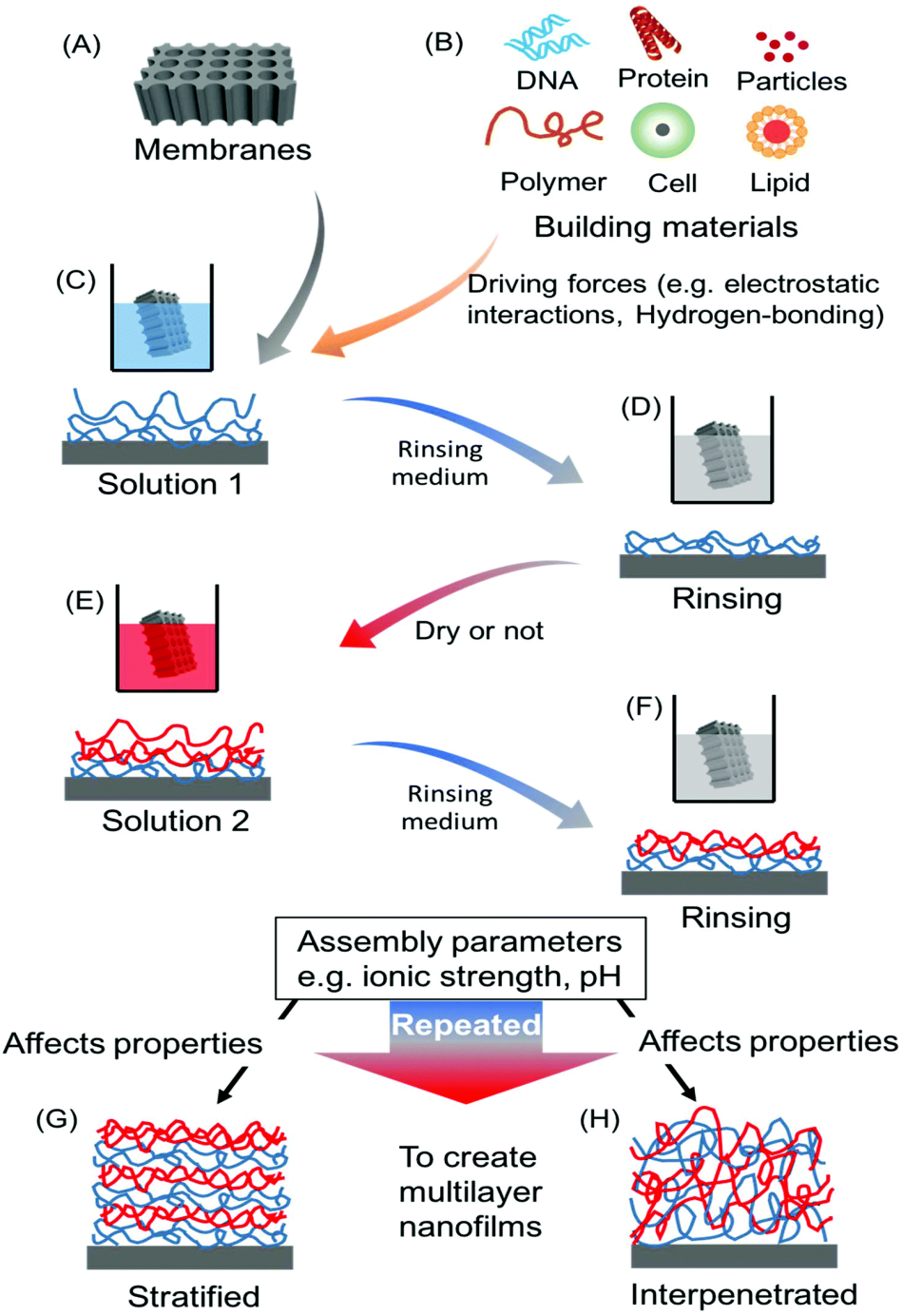

Figure 2-3 Steps of LbL assembly on the surface of a membrane including immersion, rinsing and drying [55].

Polymers, colloids, and biomolecules are constituents that are commonly used in LbL assembly of coatings on medical devices. Polyelectrolytes are one of the largest classes of constituent materials used in LbL assembly. These are polymers in which the repeating units contain an electrolyte group that dissociates and ionizes in aqueous solution. This group of compounds may be categorized as 'strong' or 'weak', based on charge. Strongly charged polyelectrolytes fully dissociate in aqueous solutions, while the degree of ionization of weakly charged polyelectrolytes is dependent on factors such as solution pH and ionic strength. As a result, the environmental conditions during LbL

assembly can affect the thickness, surface texture and other properties of the formed coating [40], [41], [44]. Also, in polyelectrolytes the pH level can dictate the conformation of polymeric chains, which include linear, branched, and star shaped. The polymer conformation in turn influences the growth rate of the coating. According to Choi et al., two linear constituents in LbL coating can lead to exponential growth with uneven surface and heterogenous morphology. Changing the structure of one or both constituents to a star shape instead leads to exponential growth, resulting in thicker coating with more uniform and smoother surface morphology. Notably, branched and star shaped chain conformations have more mobility than linear ones, and they can thus diffuse faster through the deposited layers and create thicker coatings with exponential growth rate [27]. Weak polyelectrolytes, which only partly dissociate in solution and have variable charge, exhibit this exponential growth mechanism. Poly(acrylic acid) (p(AA)), poly(allylamine hydrochloride) (p(AH)) and poly(methacrylic acid) (p(MAA)) are examples of weak polyelectrolytes that have been used in LbL assembly [56].

The contact time is the time period that a substrate is in contact with the solution of a certain compound being deposited. For some solutions (i.e. comprising weak polyelectrolytes), increasing the contact time can increase the thickness of the layer deposited. The drying time between subsequent layers can affect the consolidation of a deposited layer. All these parameters can therefore influence the architecture and mechanical properties (e.g. stiffness and elastic modulus) of a LbL coating [57].

Richardson et al. categorized the methods of performing LbL assembly into three main groups: conventional assembly (including immersive, spin, spray, fluidic, or electromagnetic assembly), unconventional assembly (including hybrid, multicomponent, stereocomplexed, lithography, or 3D printing assembly) and quasi LbL assembly (collected from traditional LbL building blocks). More details on each method is given in Table 2-3 and Figure 2-4 show the development of these LbL assembly techniques on a timeline beginning around 1970, where the immersive technique was the oldest and one of the simpler methods to implement [26].

Table 2-3 Description of conventional and unconventional LbL assembly [26].

Method of LbL assembly	**Name of assembly technique**	**Description**
conventional	immersive	Immersing the substrates into solutions of the selected material as constituents of the coating, followed by washing

	spin	Spinning the substrate for enhancing the coating process and drying
	spray	LbL film is constructed by spraying solution of material for coating on the substrate and followed by spraying water to remove excess unbound residuals
	fluidic	Polymer and washing solutions are pumped through a microchannel, and removal is carried out by a vacuum system
	electromagnetic	This method usually works for coatings which include metals by applying voltage in electrolytic cells. For applying different material as LbL coating such as polymers, enzymes, colloids and etc. the polarity of electrodes should be controlled.
unconventional	hybrid	LbL film can be fabricated by sol−gel reaction to form a liposomal membrane with a ceramic surface from inorganic−organic hybrid multilayers so-called “cerasomes”
	multicomponent	Multilayered films can be fabricated based on sequential polymerization which leads to LbL films with greater control over thickness, topology, and local chemical composition that is controllable at monomer length scales in comparison to standard interfacial polymerization
	stereocomplexed	The driving force in this method is stereocomplexation which takes place when the interaction between polymers with different tacticities overcome the interaction between polymers with the same tacticity
	lithography	This method provides patterned LbL coatings by dipping the tip of atomic force microscope into the solution of constituent (for coating) and move it close to the surface of substate. Inkjet and 3D printers are other candidates which can be used in this method to provide specific pattern as LbL assembled coating .

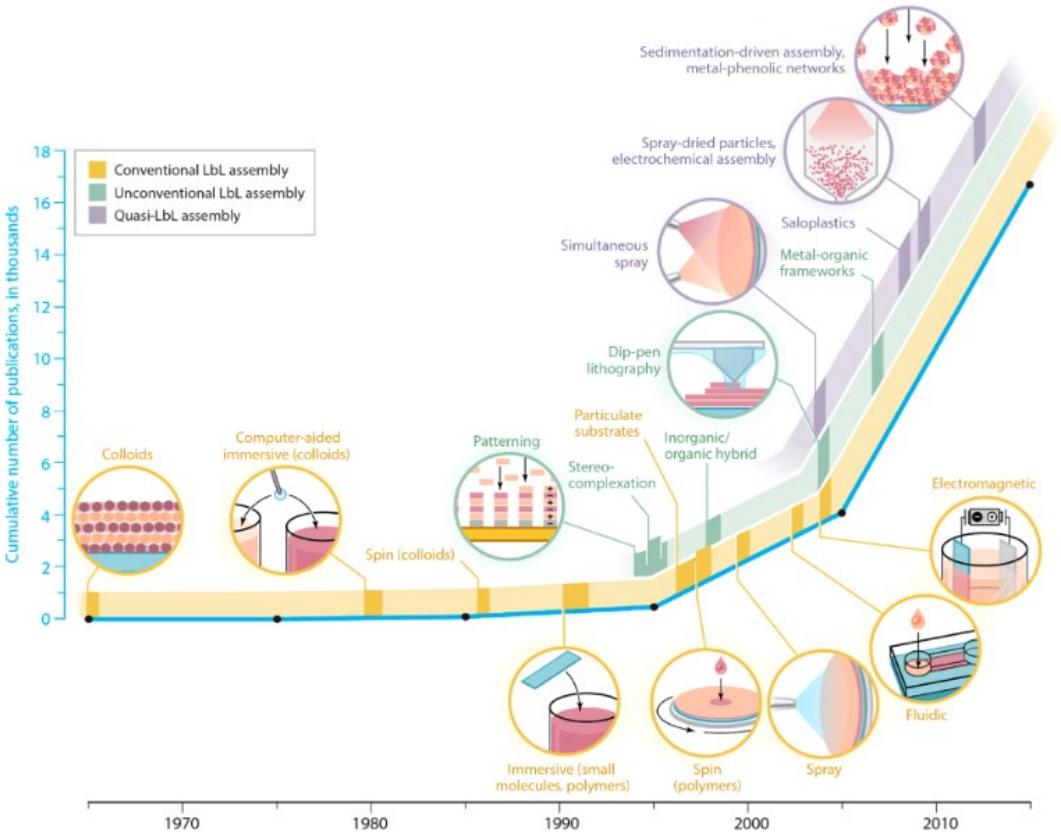

Figure 2-4 Historic development of different LbL assembly techniques since 1970. Figure reproduced from permission granted from Chem. Rev. 2016, 116, 23, 14828–14867, *Copyright © 2016, American Chemical Society* [26].

In recent decades, the LbL assembly technique has gained interest for the development of multifunctional and long-lasting anti-biofilm coatings. The final properties of a LbL coating can be tuned by varying the number of deposition cycles and material types. Antibacterial LbL films are thus one potential strategy to prevent biofilm formation and encrustation in urological devices [27], [58] which may contribute towards increasing a device's lifetime and achieving greater control over drug release kinetics, overall resulting in improved comfort for patients and a reduced burden for healthcare providers [28], [59]. Notably, in LbL assembly, the ability to deposit different layers in different combinations to form multilayer coatings means that each layer can fulfill a specific purpose once deployed in a patient's body. Some coatings are responsive to external stimuli, and can potentially change the degree of water swelling, mechanical properties, or release a drug in response to environmental conditions, such as urine pH if used on a urinary device. Despite their significant advantages, there are remaining challenges that have hindered commercial translation of LbL coatings. Compared to simpler techniques like single-step dip coating, LbL assembly is more complex with a slower rate of deposition, and therefore is likely to have a higher cost of production. There is also a lack of in vitro and in vivo studies on LbL assembled antimicrobial coatings.

2.3.1 LbL assembled materials for urinary devices

PEI and PAA are two weak polyelectrolytes that have been used in several previous studies as an antimicrobial coating [29], [60], [61]. PEI is a polycation containing an amine group that is available in both linear and branched conformations and has shown excellent bactericidal activity as a coating in medical devices. Also, it can exert both contact-killing and anti-adhesive effects on Gram-negative bacteria when applied to urinary devices. Despite these advantages, an excess dose of PEI has been shown to cause toxicity (in single layer uncontrolled coating) in mammalian cells [62], [63]. PAA is a polyanion that is capable of absorbing water and swelling to a final volume that is several times greater than its dry volume. It has demonstrated antifouling performance and the ability to prevent biofilm formation [64], [65]. The pH level plays an important role on the charge of PEI and PAA, which in turn leads to different thickness of the layers. Rubner et al. in 2000, claimed that the pH changes the level of charge in PEI from weak charge at a pH around 10 to strong at a pH around 7 [66]. On the other hand, other studies showed that PAA is weakly charged at pH of 4 and highly charged at a pH of 8 [28]. These findings have led to researchers investigating different pH levels of PEI and PAA solutions as a means to vary the charge and therefore the thickness of PEI/PAA multilayers. Commonly used pH levels for PEI/PAA multilayers are of approximately 10 for PEI (polybase) and 4 or 3.5 for PAA (polyacid). The interaction between PEI and PAA layers in named as an acid/base reaction [67]. In 2019, Ziminska et al. reported that the pH of PAA can play an important role on the thickness of the coating. They claimed that changing the pH level of a PAA solution from 4 to 8 can decrease the thickness per layer up to 79.9% [28]. Yoo et al. in 1998 concluded that highly charged polyelectrolytes have a flattened conformation and that LbL films deposited using highly charged solutions of polyelectrolytes are thinner and denser, while weakly charged polyelectrolytes have a coiled conformation, and this leads to the deposition of thicker films [68].

Poly-L-glutamic acid (PGA) and poly-L-lysine (PLL) are another polyelectrolyte pair that have shown antimicrobial behavior in LbL coatings on urinary devices [69]. They have also potential for generating LbL assemblies containing of AMPs (see Table 1) for coating of urinary catheters. Raman et al. in 2014 have investigated the antimicrobial effect of PGA and PLL multilayers loaded with β-peptide. The coating was applied to urinary catheters through a fill-and-purge, manual (immersive) technique and tested against *C. albicans*. Results showed that β-peptide-loaded coatings can prevent biofilm formation against *C. albicans* for about 17 days. The same group subsequently evaluated the effectiveness of the developed coatings on a urinary catheter deployed into a rat model. They showed that loading β-peptide on multilayers of polyelectrolytes consisting of PGA and PLL can strongly act as an antimicrobial agent against *C. albicans* [70].

Chlorhexidine (CHX) is a disinfectant that is used in medical applications; it is positively charged and can interact with the negatively charged microbial cell surface, interfering with the ability of cells to form biofilms. CHX is another candidate for incorporation in LbL coatings on urinary devices. Srisang et al. in 2019 carried out a study to evaluate bactericidal activity of layer-by-layer coatings of PAA and CHX on the surface of urinary catheters. The results of their investigation showed that a coating comprising 90 bilayers of CHX micelles/PAA on a Foley catheter (produced by dipping method) can act as an antibacterial agent against *E.coli, S. aureus* and *C. albicans* up to 6 days in an *in vitro* model, with no signs of cytotoxicity [71]. Furthermore, Srisang et al. in 2020 generated coatings of different types of CHX-loaded nanoparticles and PAA as a strategy to prevent catheter-associated UTI. Their results showed that combining 90 bilayers of CHX micelles/PAA (produced by dipping method) and 40 layers of CHX nanospheres (generated through spray coating) is effective against *E. coli* and *S. aureus in vitro*, up to 28 days. The addition of the 40 layers of CHX nanospheres on the 90 bilayers of CHX micelles/PAA caused a thickness increase from 6.87µm to 9.17 µm, while the antibacterial activity increased from 6 to 28 days [72]. Vaterrodt et al. investigated the application of polyzwitterion/enzyme (cellobiose dehydrogenase, CDH) multilayers produced by immersion LbL method. The resulting coating was designed to combine two main antimicrobial strategies at the same time (bactericidal and antifouling) on urinary catheters. Their investigation showed that the developed coating causes a 60% reduction in *S. aureus* adhesion up to 10 days [49].

Despite the number of articles on antimicrobial LbL coatings applied on urinary stents and catheters is limited in comparison to single-layer antimicrobial coatings, the mentioned findings demonstrate that there is great potential for more research on LbL coating as an effective strategy against biofilm formation and encrustation in urological devices.

As LbL assembly is an emerging method for applying antimicrobial coatings on the surface of urinary devices, the number of utilized materials are limited. Fan et al. in 2015 reported that strong/weak and weak/weak pairs of polyelectrolytes are more likely to be utilized as LbL coatings due to their chain conformation and effect on the coating's mechanical properties such as stiffness, when compared to strong/strong pairs. Weakly charged polyelectrolytes provide a coiled conformation in the polymer chain that can lead to thicker coatings. Generally, coiled conformation chains offer more free space than linear ones and, in aqueous environments, the coating layer can thus absorb more water and increase its thickness [28]. Notably, it has been observed that thicker coatings have greater antimicrobial activity than thinner ones, as bacteria are less capable of sensing the underlying substrate surface. Moreover, these polyelectrolytes present high chain mobility, which has been associated with reduced attachment of microorganism over a surface [73], and their pH responsiveness may enable synergistic effects [31], [74].

Chitosan is a weak polyelectrolyte and have been used in antimicrobial coating on the surface of urological devices. According to the literature Chitosan can play an important role as both bactericidal and antifouling agent in LbL assembled coatings. Heparin, poly(ethyleneterephthalate) (PET), polymethylmethacrylate (PMMA), collagen, PAA, hyaluronan, and silver are other components that have been used with Chitosan in LbL assembled coating to increase the antimicrobial activity against *E. coli* [40], [75], [76]

2.3.2 Bactericidal LbL coatings

Bactericidal coatings include those releasing heavy metals (such as silver and copper), bactericidal enzymes, and antibiotics. Silver nanoparticles and nanoclusters have been incorporated into surface coatings and have shown high antimicrobial efficiency [8], [9]. For example, Jenny A et al. reported that loading silver nanoparticles in PAH/PAA multilayers using the immersive technique (at a solution pH of around 3.5) produces coatings with antimicrobial activity against *E. coli* [77]. *E. coli* is one of the microorganism that can cause UTI, therefore LbL assembly of these silver-containing PAH and PAA coatings could be an effective strategy for use on urinary devices. Additionally, Kruk et al. deposited multilayers of PEI, poly(sodium 4-styrenesulfonate) (PSS) and silver nanoparticles (AGNPs) with different bilayer and quadlayer structures, including $(PEI/AgNPs)_{1-5}$, $(PEI/PSS)_5$, and $PEI/AgNPs/(PEI/PSS)_n$, using an immersive LbL assembly. Their study showed that $(PEI/AgNPs)_{1-5}$ were more effective against biofilm formation *(E.coli)* than $(PEI/PSS)_5$, and that $PEI/AgNPs/(PEI/PSS)_4$ had greater antimicrobial activity than thinner samples ($n<4$). In general, silver-polyelectrolyte coatings have been effective against some of the bacteria that can cause UTI [78] and therefore are promising for coatings on urinary devices.

Bactericidal LbL assembled multilayer systems have been developed that contain and elute antibiotic drugs. Coatings containing bactericidal enzymes, which kill bacteria through the production of antimicrobial oxidative enzymes, have been used as highly active antibacterial materials for catheter coating. K. Ivanova et al. deposited multilayers of acylase (bactericidal enzyme) and PEI on the surface of silicone made urinary catheters utilizing immersive method to provide LbL assembled coating. The coating showed antimicrobial activity against *P. aeruginosa,* demonstrating potential for bactericidal enzymes in LbL assembled antimicrobial coatings on urinary devices. However, the production and purification process of these enzymes is much more expensive compared to the costs associated with the manufacturing of silver or antibiotics coated materials [79]. One requirement for urinary devices is to keep the costs low due to their high demand, and although antimicrobial enzymes have shown beneficial results, they may be less clinically translatable due to their high cost.

2.4 Effect of surface stiffness on antimicrobial activity

There are different hypotheses on how surface stiffness affects biofilm formation. A number of studies have claimed that substrate stiffness should be increased to reduce bacterial adhesion, while others concluded that softer surface coatings should be employed to achieve the same outcome. Polydimethylsiloxane (PDMS) is a transparent silicone elastomer that is commonly used in laboratory research and is representative of materials often employed to manufacture urinary stents and ureteral catheters. Song et al. in 2014 carried out a study to evaluate whether the stiffness of PDMS affects biofilm formation. The Young's modulus of PDMS samples varied from 0.1 to 2.6 MPa and the species of microorganisms employed were *E. coli* and *P. aeruginosa*. The outcomes from this study showed that by increasing the stiffness of PDMS, cell attachment and growth decreased for both microorganisms [80]. Additionally, Valentin et al. concluded that the viscoelastic behavior of PDMS can play an important role on bacterial adhesion in the presence of dynamic flow. They showed that adhesion of *E. coli* to a PDMS surface was 50% lower in the stiffest sample compared to the softest one, upon exposure to a flow rate of 100 µL/min for 30 min. Also, movement of bacteria over the surface of stiffer PDMS was observed by time-lapse microscopy, whilst it could not be detected in the soft sample. Furthermore, results showed that most of the bacteria which adhered to the softer PDMS sample remained on the surface, while a large proportion of those on the stiffer sample (about 60%) detached [23]. In contrast to these results for PDMS, different conclusions have been drawn concerning hydrogel polymer coatings. Previous studies claimed that hydrogel coatings should be relatively soft to prevent bacterial adhesion. Kolewe et al. in 2015 evaluated bacterial adhesion on the surface of hydrogels having different mechanical properties. They employed poly (ethylene glycol) dimethacrylate (PEGDMA) samples that were divided into three groups based on their Young's modulus: soft (44.05 – 308.5 kPa), intermediate (1495 – 2877 kPa), and stiff (5152 – 6489 kPa). The microorganisms which were used in this study were *E. coli* and *S. aureus*. Results showed that *E. coli* adhesion to the surface of soft PEGDMA was 52% and 82% lower when compared to intermediate and stiff samples. The results for *S. aureus* followed the same pattern; the adhesion of the bacteria was reduced by 62% and 79% on the soft sample in comparison to the intermediate and stiff ones [81]. Additionally, they investigated whether the thickness and stiffness of PEG hydrogels affect bacterial adhesion. They produced samples that were thin (15 µm), medium (40 µm), and thick (150 µm), with Young's modulus that were classified as soft (20 kPa), intermediate (300 kPa), and stiff (1000 kPa). It was concluded that biofilm formation and bacterial adhesion (of *E. coli and S. aureus*) were the lowest when the thicker and softer hydrogel coating was employed [17].

Bacterial adhesion resistant LbL systems include hydrophilic antifouling coatings, such as those incorporating zwitterionic polymers, PEG, PAA, poly(acrylamide) (PAAm), and ethylcellulose. The

stiffness of LbL assemblies can also influence the adhesion of bacteria on a surface. For example, J. A. Lichter et al. in 2009 assembled PAH and PAA to fabricate LbL films at different pH values to evaluate various stiffness levels of the films. They reported that bacterial attachment was increased with an increase in elastic modulus from 1 MPa to 100 MPa when changing the pH during assembly from 2 to 6.5 [77]. Anti-adhesion LbL assembled coatings are ecofriendly antibacterial solutions with low cytotoxicity. However, their antibacterial efficacy and performance lifetime need to be further assessed both *in vitro* and *in vivo* [4].

2.5 Aims and objectives of this project

As mentioned above, single layer antimicrobial coatings have a number of disadvantages and LbL coating techniques have the potential for addressing these. PEI/PAA multilayer coatings assembled using a LbL method showed promising antimicrobial activity in recent studies [29], [82]. However, there is a lack of investigations regarding the mechanisms that lead to the antimicrobial activity of these coatings, including on the effect of the last layer's composition [83], [84], coating thickness and surface stiffness. This project will therefore provide a broader characterization of PEI/PAA multilayer coatings for application on urinary devices to prevent UTI [29]. The ability of PEI/PAA multilayer coatings to prevent biofilm formation has already been studied. However, there are still open questions about the underlying mechanisms of action. The milestones to achieve the main aim are detecting the coating on the surface and measuring the thickness, detecting the chemical bonds of LbL coating to confirm the deposition of PEI/PAA BLs on the surface of substrate, characterizing the stiffness of the coating and investigating the antimicrobial activity of applied coating in different time periods. Additionally, in LbL assembly techniques, different numbers of constituents can be used and the addition of a third component to multilayers of PEI/PAA could extend the antimicrobial activity of the coating over a longer period of time. Chitosan has been used as an antibiofilm coating on the surface of urinary stents [85] and its degradability makes it an interesting constituent to be used between PEI/PAA multilayers. Chitosan was combined with expensive biopolymers - such as hyaluronan - in previous work [40], [75], [82]. However, highly expensive coatings are the last choice for healthcare providers when it comes to the acquisition of urinary devices. On the other hand, in a few studies chitosan has been combined with PAA [31], [76], which encouraged us to prepare LbL assembled coatings including PEI, PAA and chitosan, as a more cost-effective biodegradable coating strategy. We hypothesized that depositing degradable layers between PEI/PAA multi BLs could promote the peeling off of the old multi layers of PEI/PAA from the surface and potentially improve the antimicrobial activity of the coating for a longer period by shedding biofilm or fouling from the surface.

Chapter 3 Materials and methods

3.1 Depositing BLs of PEI/PAA on the surface of PDMS

According to the literature review, PEI and PAA have been widely studied in LbL assembled coatings for their antimicrobial properties. They are also commercially available at relatively low cost (£85.30 for 100ml of PEI and £58.10 for 100 ml of PAA from Sigma Aldrich with the product number (PN) of 408727 and 416002) and so were deemed potentially suitable for application onto urinary devices and selected for further investigation in this project. The immersive LbL technique has been used to apply layers of coating on the surface of PDMS and the coated samples were characterized to evaluate their mechanical and biological behavior. Branched PEI and PAA were purchased from Sigma Aldrich with M_W = 25,000 and average M_w = 250,000, respectively. Hydrochloric acid (HCl) with PN 10478470 and sodium hydroxide (NaOH) with the PN of 15274864 were ordered from Fisher Scientific for the purpose of tuning the pH of PEI and PAA solutions. PDMS monomer and curing agent were purchased as SYLGARD® 184 pack from Sigma Aldrich (PN: 761036). PDMS was prepared by mixing the monomer and curing agent at a weight ratio of 10:1 , followed by degassing using a vacuum desiccator and curing for 24 hours at 65 ℃ in an oven [86]. The thickness of prepared PDMS samples were 2mm. A hydrogen peroxide solution (H_2O_2, 15% from Sigma Aldrich (PN: 1.08600)) was used to clean the surface of the PDMS cast by soaking for 15 minutes. Then, the cast was rinsed with deionized water, and dried with a stream of compressed air.

For LbL assembly of coatings on the surface of PDMS, solutions were prepared of 1 weight percent (wt.%) PEI with pH of 10 and 1 wt.% PAA with pH of 4. pH of the solutions was measured by Fisherbrand™ accumet™ AB150 pH Benchtop Meters. Solutions of HCl (0.1 mol/L (M)) and NaOH (0.1 M) were used for adjusting the pH of PEI and PAA, respectively [67], [87]. 0.1 M of HCl was prepared by diluting 9.85 g of 37 wt.% HCl solution in DI water up to a total solution volume of 1 L, and 0.1 M NaOH was prepared by diluting 40 g of NaOH in DI water up to a total solution volume of 1 L. Before applying the coating, the surface of PDMS casts were cleaned by removing any residues, oils, or contamination and activated for attachment of the first layer of PEI by exposure to oxygen plasma [88] (2.6 litre plasma lab system from Zepto) for 30 seconds. The plasma activated PDMS was immersed in the PEI solution for 5 minutes, immersed for 1.5 minutes in DI water (3 steps of 30 seconds in 3 different DI water reservoirs, to remove unbound excess PEI) and dried with a stream of compressed air. Subsequently, it was immersed in the PAA solution for 5 minutes, immersed for 1.5 minutes in DI water (3 steps of 30 seconds in 3 different DI water reservoirs, to remove unbound excess PAA) and dried with compressed air to generate one BL of PEI/PAA on the surface of PDMS [67]. According to the literature, the immersing time in DI water reported as 1 step

between immersing the substrate into PEI and PAA solutions. However, in this study this was done three times to decrease the chance of cross contamination between PEI and PAA solutions. By repeating this procedure, the number of BLs, and therefore the overall coating thickness, could be increased (Figure 3-1). At the end of the coating process, the sample was placed in an oven (65 ℃) for 24 hours to dry.

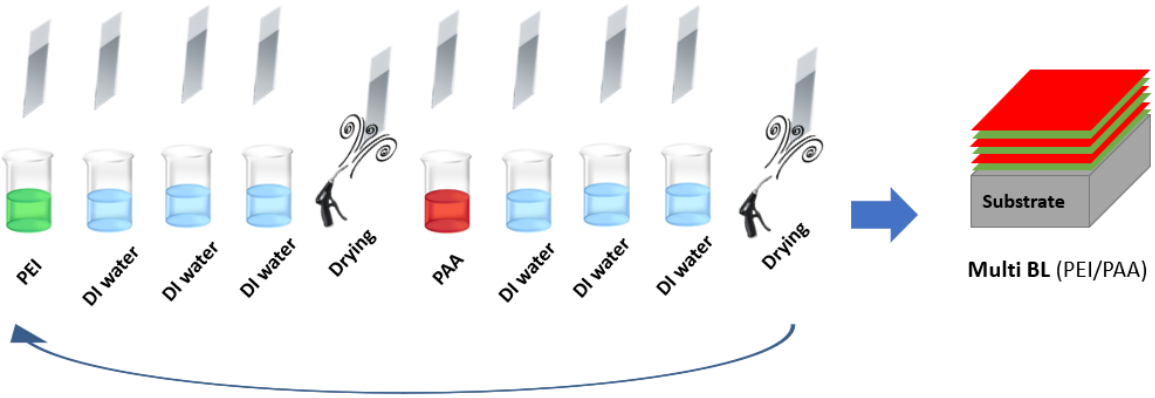

Figure 3-1 summary of steps required to apply multi BLs of PEI/PAA on the surface of PDMS. These include surface immersion in PEI, 3 immersing in DI water steps and using a stream of compressed air drying, immersion in PAA, 3 immersing in DI water steps and using a stream of compressed air drying.

3.2 Cell culturing in static condition

The antimicrobial activity of PEI/PAA coatings was investigated using *P. aeruginosa* (PAO1) which is a microorganism that can cause UTI and was ordered from Thistle Scientific [89]. A fresh solution of 2% Virkon (Fisher Scientific with PN of 12338667) in 250 mL DI water was prepared and kept for no longer than 5 days. The work area was cleaned with 70% ethanol (Merck with the PN: 459836) prior to use. Agar plates were prepared by adding 40 gr of tryptic soy agar (ordered from Sigma Aldrich with the PN of 1.04323) to 1 L of DI water and was poured to petri dishes after being sterilized at 121 ℃ for 15 minutes. At the end the agar plate incubated in incubator with the temperature of 37 ℃ overnight. An overnight culture was produced by using a sterile inoculating loop to select three identical bacterial colonies from an agar plate, to inoculate 5 mL of growth medium in a sterile Falcon tube which was then incubated at 37 °C. After 24 hours, confirmation of growth in the overnight culture was determined by its turbidity [90]. After confirmation of *P. aeruginosa* growth, the turbid overnight culture was diluted 1/100 by volume in sterile Lysogeny broth (LB) purchased from Merck (PN: L3027). On the other hand, 24 well plates (from Fisher Scientific with PN of 10387523) were filled with 7 mm thick layers of PDMS cured in each well and were coated with 5, 10, 15, 20, 25 and 50 BLs of PEI/PAA coating, deposited using LbL assembly as

described in second paragraph of this chapter . The composition of the final layer was varied between PEI and PAA . *P. aeruginosa* was added to samples (1/100 by volume in LB) and incubated at 37 ℃ in ambient atmosphere for 2 different time scales (1 day and 7 days). Subsequently, 200 µl of the 1/100 suspension was pipetted on to the surface of coated PDMS in each well. Concerning the well plate that was incubated for 7 days, every day the media was pipetted out gently and fresh LB (200 µl) was added to each well. After taking the well plates out of the incubator, the planktonic suspension which contains single bacteria from the surface of each cell was drawn up slowly, to avoid disruption of the biofilm and was discarded into 2% Virkon to prevent contamination of the working area.

3.3 Cell culturing on urinary catheter under dynamic conditions

After overnight culture of *P. aeruginosa* in a Falcon tube, 50 ml of fresh LB and 500 µl of *P. aeruginosa* suspension (1/100 by volume) were added to an empty sterile bottle to replicate remained volume of urine in the bladder after urination [85]. Then, pieces of uncoated and 50 BLs coated urinary catheter (Dover, 20 French (Fr), 100% silicone) with the length of 2 cm (20 Fr catheter has outer diameter of 6.7 mm) was immersed in the mentioned solution and the bottle was placed in a water bath (Techne-10 A) at 37 ℃ for 1 hour to allow interaction of *P. aeruginosa* with the catheter. After 1 hour, fresh LB was pumped at a flow rate of 0.7 ml/min (using an Ismatec Reglo ICC Digital Pump, 4-Channel, 8-Roller) into the bottle that contained the catheter through the tubes that connected the bottles to each other. The liquid level of the bottle which contained catheter was maintained by pumping LB out into a waste bottle containing 2% Virkon solution at the same rate of 0.7 ml/min [48]. The setup is shown in Figure 3-2 and Figure 3-3. This process was carried out for a total time of either 1 day or 7 days, after which the catheter was removed from the bottle. Then the thickness of coating on the surface of catheter and optical density (OD) of stained samples with crystal violet was measured. Also, the sample were imaged with fluorescent microscopy to view the coverage area of the sample with live and dead bacteria.

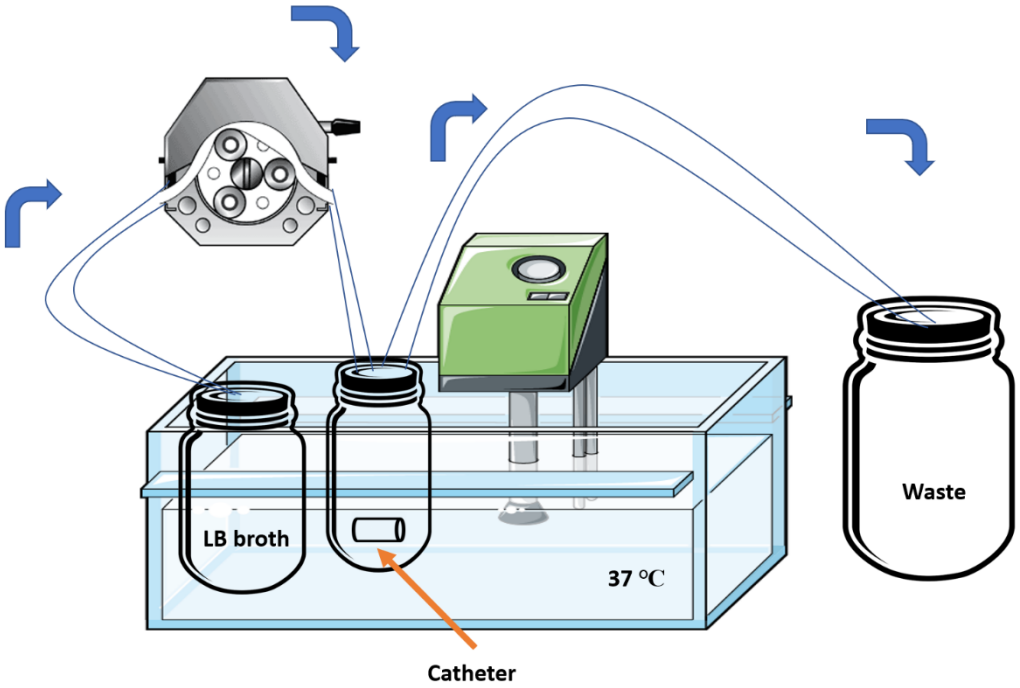

Figure 3-2 Schematic of dynamic set up for testing antimicrobial behaviour of uncoated and coated catheter, including peristaltic pump, water bath, bottles containing fresh LB, catheter and waste. Blue arrows are showing the circulation of fresh LB n the system.

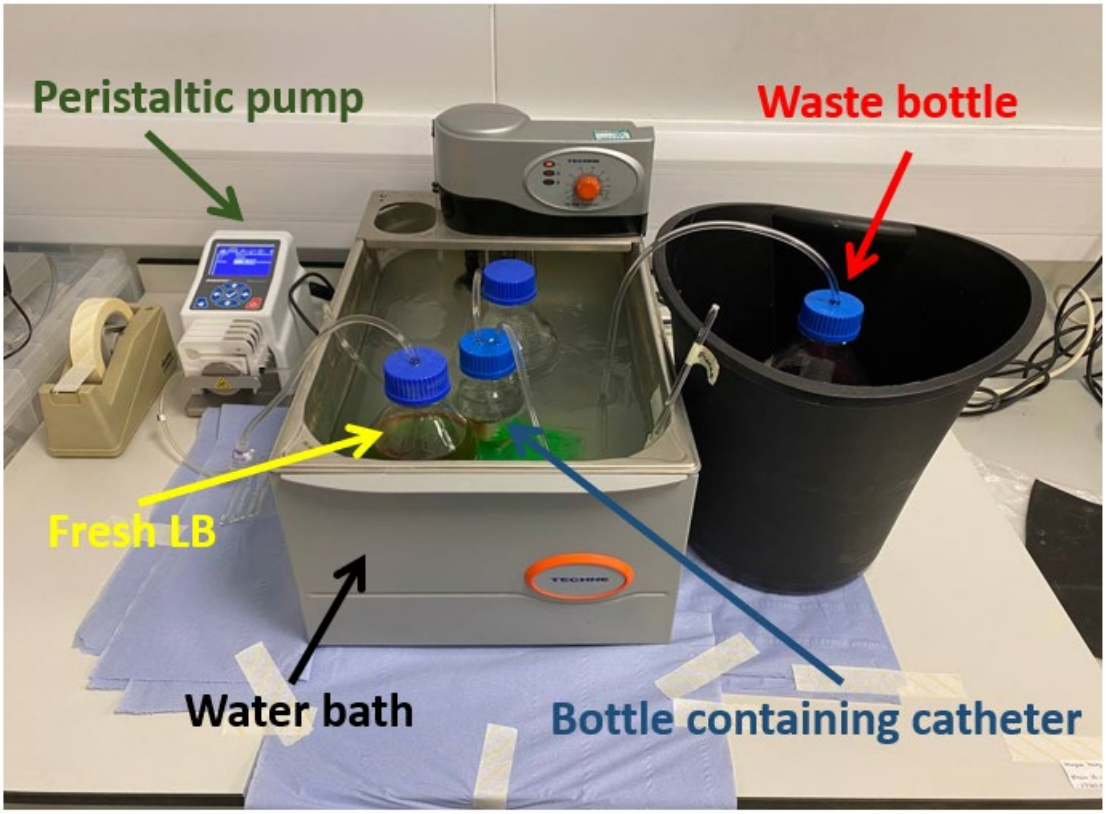

Figure 3-3 Set up of testing antimicrobial behaviour of uncoated and coated catheter under dynamic flow (0.7 ml/min). Peristaltic pump provides the dynamic flow between bottles through the tubes that connecting the bottles together.

3.4 Multilayer coating including 3 constituents

Chitosan is a biodegradable natural polymer and a candidate material for inclusion as a third layer between multi BLs of PEI/PAA. Chitosan was purchased from Sigma Aldrich (PN: 448869) in low molecular weight. 1% mass per volume (m/v) chitosan solution with pH of 5 and 1 wt% PAA with pH of 4 were prepared [29], and 50 BLs of chitosan/PAA were applied on the surface of PDMS with the same protocol used for generating PEI/PAA multi BLs. Also, the degradable chitosan was sandwiched between PEI/PAA multilayers to investigate its degradation when embedded within non-degradable multi BLs. Sandwiched coatings were produced with 5 BLs of PEI/PAA, 50 BLs of Chitosan/PAA, and 5 BLs of PEI/PAA at the surface, denoted as '(PEI/PAA)5(Chitosan/PAA)50(PEI/PAA)5', and also with 50 BLs of PEI/PAA at the surface, denoted as '(PEI/PAA)5(Chitosan/PAA)50(PEI/PAA)50'.

3.5 Methods of characterization

To confirm deposition of the PEI/PAA coatings onto PDMS substrates, two characterization methods have been used:

- Scanning electron microscopy (SEM)
- Raman spectroscopy

Samples of PEI/PAA coatings with 5, 10, 15, 20, 25, and 50 BLs were imaged using SEM to have detailed images of uncoated and coated PDMS surfaces for thickness measurement. Prior to SEM imaging, all samples were cross sectioned using a surgical blade (ordered from Fisher Scientific) and gold coated using an Agar Auto Sputter Coater - AGB7341 machine for 20 seconds to make the samples conductive and eligible for SEM imaging (Figure 3-3 3-3). For each coating, 3 samples were prepared for thickness measurements and the thickness of each sample was measured from 3 different locations along the surface (right edge, middle and left edge). The ruler feature in JSM software was used to measure the thickness of top surface on the substate with different roughness and auto focused was used during imaging. The coatings were applied on the surface of 1×1 cm squares of PDMS sheet with the thickness of 2 mm and cross sectioned from the middle for SEM imaging.

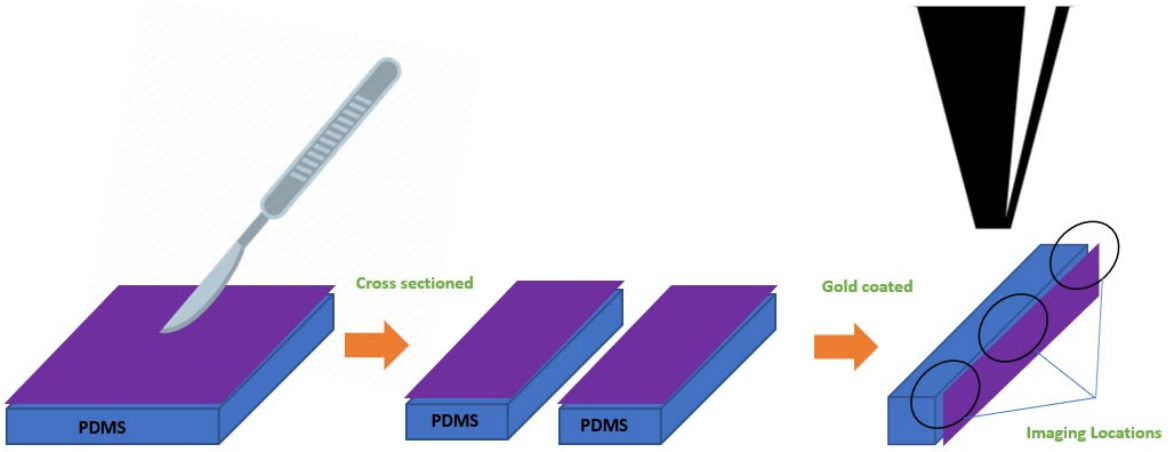

Figure 3-4 steps of preparing coated samples for SEM imaging including cross sectioning, gold coating and imaging.

After confirming the presence of the coating on the surface of PDMS and thickness measurement, Raman spectroscopy was used to detect chemical bonds of PEI/PAA coating to approve the successful deposition of PEI/PAA on PDMS substrate. Renishaw inVia confocal Raman microscope with a 784 nm laser module was used in this study for characterization of uncoated and coated samples. For each coating, 3 samples were prepared for characterization and spectroscopy was characterized on 3 different locations along the surface. The coatings were applied on the surface of 1×1 cm squares of PDMS sheet with the thickness of 2 mm.

Surface stiffness was assessed for the uncoated and coated samples after confirming the presence of the coating on the surface of PDMS substrate. The mechanical stiffness of the surface was tested using a nanoindentation machine (Nanovantage system Micromaterials) with a 500 µm radius spherical tip to assess the reduced modulus (E_r) of PEI/PAA coatings on PDMS substrates, which takes into account the Young's modulus of the diamond indenter and of the specimen. Equation 1 illustrates how the reduced modulus was calculated from nanoindentation tests [91]. The parameter values needed are E_i , E_s, υ_i and υ_s . E_i is the Young's modulus of the indenter with a value of 1141 GPa for diamond indenters, E_s is the Young's modulus of the specimen, υ_i is the Poisson's ratio of the indenter (0.07) and υ_s is the Poisson's ratio of the specimen which commonly was assumed 0.45 for PDMS and other soft materials [92].

$$\frac{1}{E_r} = \frac{(1-\vartheta_i{}^2)}{E_i} + \frac{(1-\vartheta_s{}^2)}{E_s} \quad (1)$$

Prior to nanoindentation, hydrated samples were soaked in phosphate-buffer saline (PBS) for 24 hours. Uncoated PDMS, and PDMS coated with 5, 10, 15, 20, 25, and 50 BLs were tested at depths of 2-28 µm according to nanoindentation machine limit at different random points on the surface.

The reduced modulus was measured at least for 3 samples of each coating (5-50 BLs) in 3 random locations on the surface with the distance of 500 µm. The coatings were applied on the surface of 1×1 cm squares of PDMS sheet with the thickness of 2 mm.

3.6 Staining of the formed biofilm on the surface of uncoated and coated samples

To stain the biofilm formed on the surface of coated samples, 150 µl of crystal violet solution (1%, aqueous solution purchased from Sigma Aldrich with PN of C0775) was added to each well containing biofilm and was left in contact with the biofilm for 15-20 minutes at room temperature. After staining, wells were washed with 200 µl of water to remove excess stain. This process was repeated until the solution ran clear (usually 3 to 4 washes). Subsequently, a 30% acetic acid solution was prepared by adding 15 ml of pure acetic acid (Merck with the PN of 1.60305) to 35 ml of DI water in a 50 ml Falcon tube. 150 µl of diluted acetic acid was added to each well containing biofilm and left for a minimum of 20 minutes. 100 µl of liquid from each well with crystal violet was then transferred to a new plate (non-sterile plates) together with one sample of 100 µl of clear 30% acetic acid to serve as a baseline for plate reading. The OD at 584 nm (purple colour of crystal violet) were read by a FLUOstar Omega plate reader to measure the amount of attached crystal violet to formed biofilm. Lower number in OD shows the lower amount of biofilm formation.

3.7 Imaging the live and dead bacteria on the surface of coated samples

To investigate the antimicrobial activity of the developed coatings, fluorescence microscopy images of uncoated and coated PDMS samples were acquired to obtain more in-depth information about live and dead bacteria as staining the biofilm with crystal violet has limitation in dividing live and dead bacteria and visualizing the surface coverage area with biofilm. After incubating *P. aeruginosa* on the surface of uncoated and coated PDMS samples in well plates, the remaining planktonic suspension was drawn up slowly from each well, to avoid disruption of the biofilm, and was discarded into 2% Virkon. Then the remained biofilm was stained using a mixture of 10 µL SYTO 9 (Fisher Scientific, PN: 10237582) and 120 µL Propidium Iodide (PI) (Sigma Aldrich, PN: P4170) in 20 ml DI water for 10 minutes; samples were protected from light using a lid of well plate and a tissue on top to cover the samples [50]. After 10 minutes, the stain was pipetted out and the sample was transferred into a Ibidi dish (µ-Dish 35 mm, high Glass Bottom from Ibidi) and assessed by fluorescent microscopy (EVOS M5000 from Thermo Fisher Scientific). Samples were viewed at the magnifications of 10x and 20x and images were taken by a gain of 150, light intensity of 1.8, brightness of 0.5 and an exposure time of 90 ms. SYTO 9 is a green, fluorescent

nucleic acid stain which has been widely used in fluorescence microscopy to detect live bacteria and extra cellular matrix (ECM) [93]. The excitation and emission wavelengths for SYTO 9 are 483 and 500 nm, respectively. PI is another fluorescent nucleic acid stain that has a fluorescence emission maximum at 617 nm and excitation maximum in 536 nm which appears red in color [94]. The combination of these two dyes can show live and dead bacteria in fluorescent microscopy and assess the surface coverage of formed biofilm on uncoated and coated samples.

3.8 Chitosan degradation testing

Lysozymes are a class of enzymes which are present in human urine at a typical concentration of 0.1 μg/ml [95]. The degradation rate of chitosan in the presence of 1 mg/ml lysozymes has been previously reported to be significant (98% of film degraded) over a period of 3 days [96]. Chitosan/PAA and Chitosan/PEI/PAA containing coated samples were placed into a lysozyme solution (Sigma Aldrich, PN: 1.05281) at a concentration of 1 mg/ml for 1, 2 and 7 days, in an incubator at a temperature of 37℃. The thickness reduction of the coating was subsequently investigated. In order to achieve this, samples were cross sectioned after degradation, returned half of the specimen to solution for further degradation testing, and inspected the other half to assess thickness loss. The cross-sectioned surface was therefore the centre of the specimen during degradation and so lysozyme would have needed to diffuse through the top layers to access layers of chitosan embedded below. To investigate the thickness of degraded coating, SEM images were taken from the right edge, middle, and left edge of the sample with the same protocol for the samples without chitosan (gold coated and cross sectioned with a blade).

3.9 Statistical analysis

The statistical tests on data from staining the formed biofilm with crystal violet was performed and plotted by Origin software using Kruskal-Wallis ANOVA to compare the results for multiple independent samples. This non-parametric method was used due to the small number of repeats for each sample (3 times).

For analysing the coverage area of formed biofilm on the surface of samples, ImageJ software was used by following Image > Adjust > Color Threshold to specify the area of calculation. Then Analyze particle feature (size: 0 – infinity, Circularity: 0 – 1, Show: Outlines) was used to calculate the coverage area.

Chapter 4 Results and discussions

4.1 Dried coating morphology and thickness

The main aim of SEM imaging in this project was to characterize the morphology and thickness of the coating on the surface of PDMS substrates. Figure 4-1 is taken from a cross section of 3 PDMS samples that were coated with 20 BLs of PEI/PAA and it can be seen that the morphology of the top surface shows a clear difference after LbL assembly, indicating that a PEI/PAA coating has been deposited. The top surface shows the PEI/PAA BLs of coating. These appear as a rougher surface in comparison to the PDMS which can be seen below the PEI/PAA as a smoother surface layer. After depositing each layer of PEI or PAA on the surface of PDMS, the coating was dried by a stream of compressed air. However, further loss of moisture may have occurred when oven drying the samples, which may have increased roughness due to volumetric contraction. SEM images show that the coatings appeared well adhered on the surface of PDMS as there were no apparent gaps between the coating and substrate. Even during the cross sectioning required to prepare the samples for SEM imaging, the attachment of coating on PDMS was not affected and remained intact. Throughout this section, the coating thickness values are presented as an average of at least 3 measurements taken at the middle and edges of 3 different coated samples after drying.

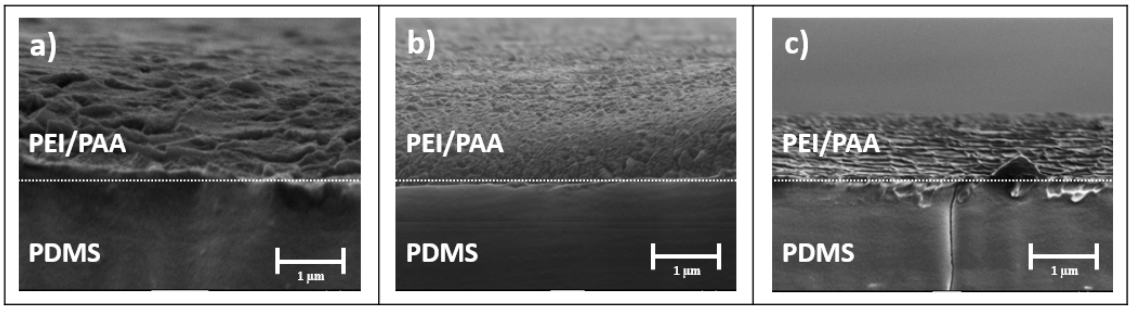

Figure 4-1 SEM image of 20 PEI/PAA BLs coated PDMS a) sample 1, b) sample 2 and c) sample 3 as three independent repeats.

SEM images of 5 BLs coated PDMS from three independent samples (Figure A-1, in appendix A) confirmed the presence of the coating on the PDMS substrate, and the average of nine thickness measurements (three per specimen) with standard deviation was 0.99 ± 0.36 µm after drying. According to the images, it can be seen that the coating is deposited uniformly on the surface of PDMS. Figure 4-2 is one of the SEM images of 5 PEI/PAA BLs coated PDMS samples and shows the presence of coating on the substrate.

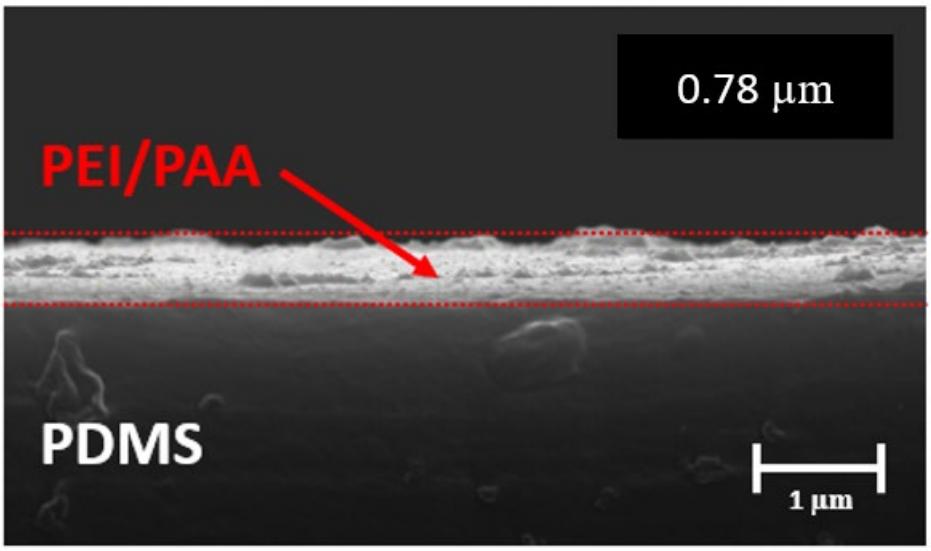

Figure 4-2 SEM image of 5 PEI/PAA BLs coated PDMS. The number on the top right shows the thickness of coating which is highlighted by the two red lines.

The same procedure was performed to measure the thickness of 10 BLs coated PDMS from three repeated samples and the average of nine thickness measurements (three per specimen) with standard deviation was 1.88 ± 0.42 µm after drying (Figure A-2, in appendix A) while confirming presence of the coating on the surface of PDMS. Figure 4-3 shows the thickness of 1.79 µm for 10 PEI/PAA BLs coated PDMS samples and different roughness of coating and substrate.

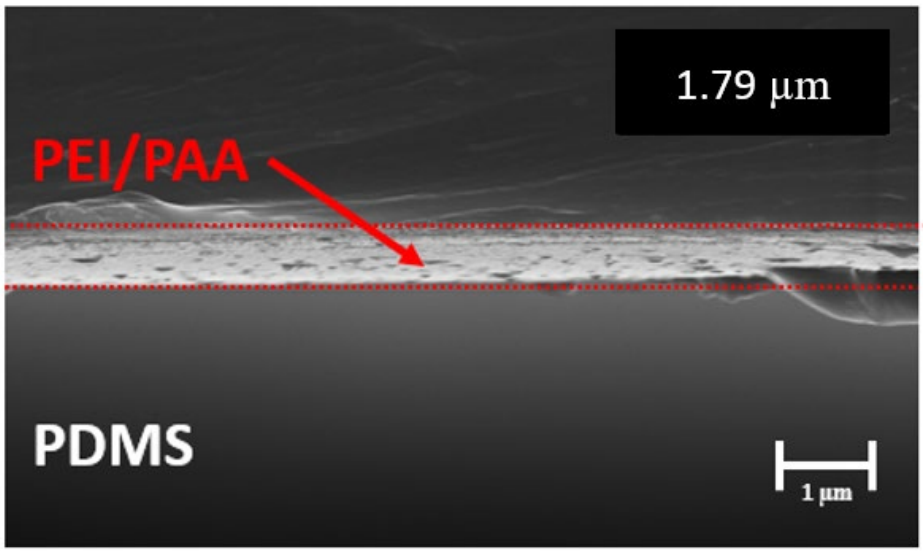

Figure 4-3 SEM image of 10 PEI/PAA BLs coated PDMS. The number in image shows the thickness of coating which is highlighted by the two red lines.

Figure 4-4 shows the SEM images from 15 PEI/PAA BLs coated PDMS and confirms the presence of coating on the substrate with the thickness of 2.46 µm. More SEM images of 15 BLs coated PDMS were taken from three repeated samples (Figure A-3, in appendix A) and the average of nine thickness measurements (three per specimen) with standard deviation was 2.37 ± 0.33 µm after drying.

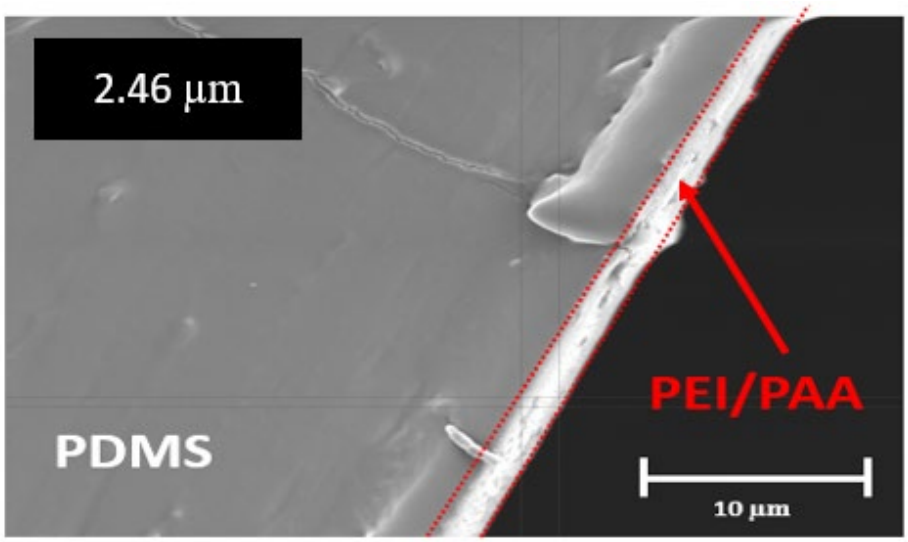

Figure 4-4 SEM image of 15 PEI/PAA BLs coated PDMS. The number in image shows the thickness of coating which is highlighted by the two red lines.

Following the same protocol for the thickness measurement of 20 BLs coated sample, SEM images confirmed the presence of the coating with the thickness 3.10 ± 0.81 µm after drying. Figure A-4, in appendix A is the result of nine thickness measurements (three per specimen). Figure 4-5 shows the thickness of 3.25 µm for 20 BLs coated PDMS and shows the presence of coating on the substrate.

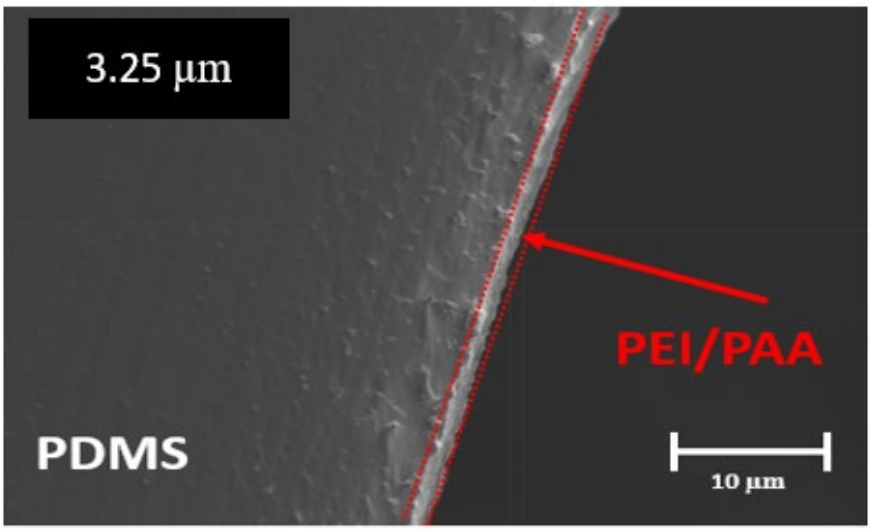

Figure 4-5 SEM image of 20 BLs coated PDMS. The number in image shows the thickness of coating which is highlighted by the two red lines.

SEM images of 25 BLs coated PDMS showed the average of nine thickness measurements (three per specimen) with standard deviation was 5.74 ± 1.76 µm after drying (Figure A-5, in appendix A). All the images confirmed the presence of the coating on the substrate. Figure 4-6 is one of the SEM images from 25 PEI/PAA BLs coated PDMS and shows the presence and uniform deposition of coating on the substrate.

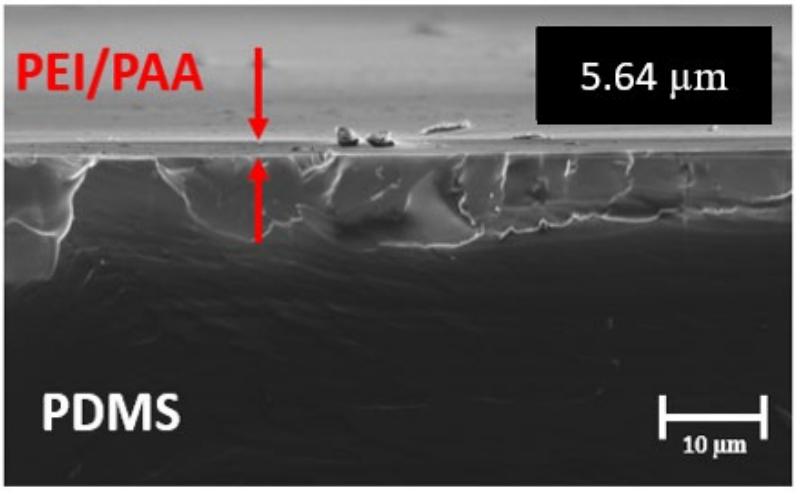

Figure 4-6 SEM image of 25 PEI/PAA BLs coated PDMS. The number in image shows the thickness of coating which is highlighted by the two red arrows.

By increasing the number of BLs to 50, the thickness of the coating reached to an average of 16.13 ± 2.93 µm after drying in SEM images. The results of nine thickness measurements (three per specimen) from three repeated samples is shown in Figure A-6, in appendix A confirmed the presence of the coating on PDMS substrate. Figure 4-7 is one of the SEM images from 50 PEI/PAA BLs coated PDMS and shows the presence with the thickness of 18.75 µm.

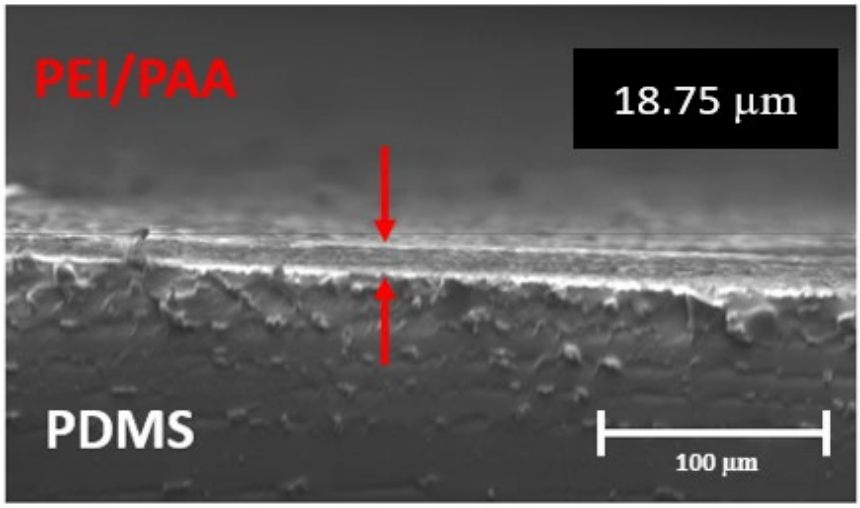

Figure 4-7 SEM image of 50 PEI/PAA BLs coated PDMS. The number in image shows the thickness of coating which is highlighted by the two red arrows.

Table 4-1 and Figure 4-8 show all the thicknesses of applied coatings, ranging from 5 to 50 BLs. The coating is uniformly deposited in all of the images on the surface of the substrate and thickness per number of BL appears to follow an exponential growth. There are different mechanisms that can cause the observed trend, “in and out diffusion” and chain mobility. After depositing the first BL of PEI/PAA on the substrate, by immersing the PDMS into the PEI and PAA solutions, the outer charged layer (positive or negative) of coating interacts with another constituent and forms a multi BLs of

PEI/PAA. Additionally, excess PEI and PAA can cross electrostatic energy barrier on the surface of the coating and diffuse into the coating layers (diffusion in) which were known as free chain. On the other hand, by increasing the diffusion of free PEI or PAA in the coating, the chemical potential of the coating increases and it can continue up to the point that the chemical potential of free PEI or PAA in the coating becomes equal to the chemical potential of the solution that the substrate is immersed in. Following this step, by immersing the substrate inro DI water, free PEI or PAA can diffuse out of the coating by overcoming the electrostatic barrier (diffusion out). However, reduction of free PEI or PAA in the coating followed by reduction of chemical potential, makes it harder for all of the free chains to diffuse out. The remaining free PEI or PAA into the coating can thus form a new complex of PEI/PAA BL by being immersed in opposite solutions during deposition of the multilayer coating and lead to an exponential growth of the coating by increasing the number of BLs [97]. Furthermore, pH plays an important role in the electrostatic charge of polyelectrolytes, which can affect structure and ionization of the polymer chain. In this project, PEI (at pH 10) and PAA (at pH 4) are both weakly charged and have coiled structures which provide more space for diffusion of free PEI or PAAs [98]. In comparison to the investigation of Yang et al. [67], the thickness of 20 BLs of PEI/PAA coated silicone at the same pH conditions was close to 20 PEI/PAA BLs (within 8% or 2.9 μm) coated PDMS in this project. For each coating, thickness measurements were carried out at 3 different locations on the surface of each sample (also, there were 3 repeated samples manufactured for each number of BLs). The maximum standard deviation of 26% was observed for 5 BLs coated samples, and is indicative of the expected repeatability. The variability observed for different locations within a specimen was similar to the variability between different specimens, which suggests that spatial variations are dominant and repeatable over different implementations of the coating deposition processes.

Table 4-1 thickness (μm) of 5, 10, 15, 20, 25 and 50 PEI/PAA BLs coated samples. The sample number and measurement location (left, middle, right) are specified for each thickness measurement.

	1-left	1-mid	1-rt	2-left	2-mid	2-rt	3-left	3-mid	3-rt	avg
5 BLs	1.09	0.77	0.78	0.90	0.80	0.70	1.43	1.43	1.01	0.99
10 BLs	2.10	1.87	1.57	2.12	1.35	1.80	2.18	1.87	2.13	1.88
15 BLs	2.14	2.46	2.51	2.44	2.36	2.26	2.26	2.78	2.11	2.37

20 BLs	2.21	3.31	2.93	3.97	3.83	3.75	2.53	3.09	2.26	3.10
25 BLs	5.23	5.01	5.23	5.01	7.74	6.54	6.97	4.22	5.69	5.74
50 BLs	14.65	13.21	15.79	18.75	18.89	15.49	16.59	18.75	13.02	16.13

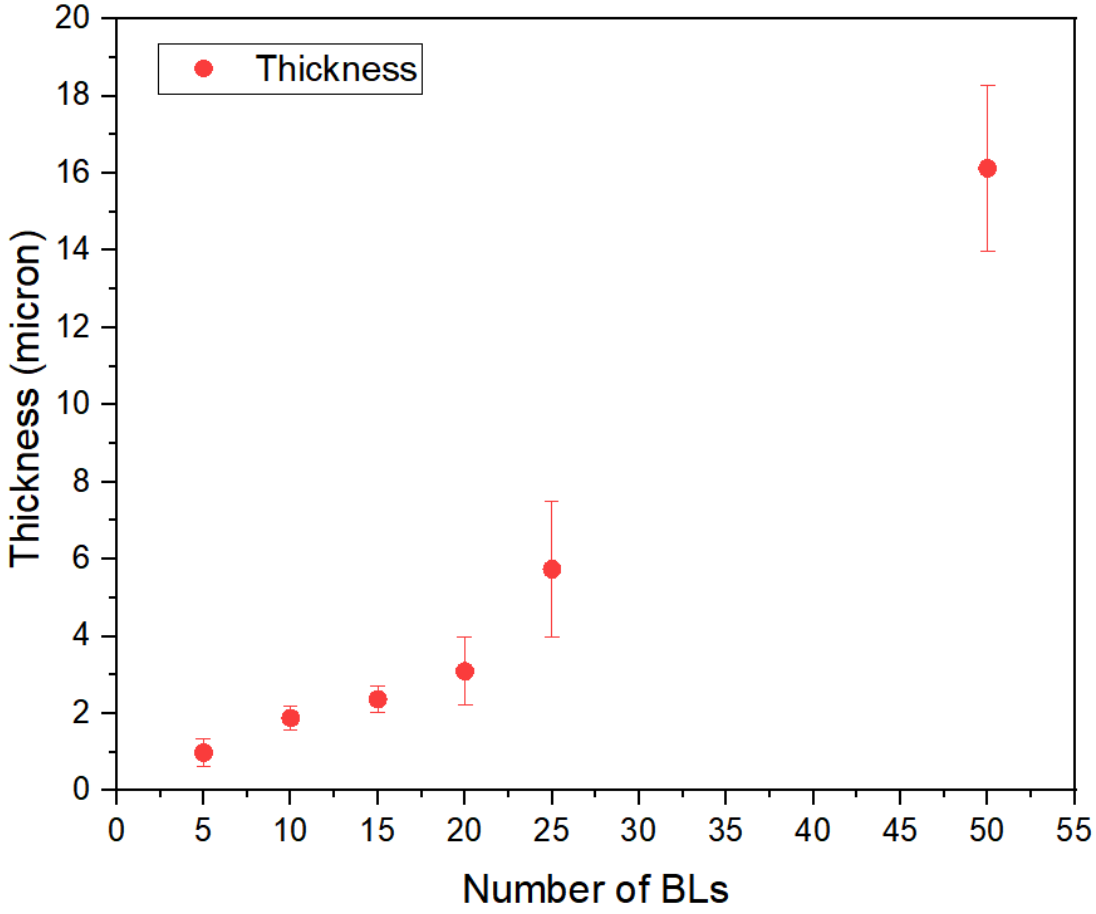

Figure 4-8 average thickness of 5, 10, 15, 20, 25 and 50 BLs of PEI/PAA on the PDMS substrate. Red circles show average value for each thickness measurements (3 measurements for each sample) and the error bars show the minimum and maximum of measured thicknesses.

4.2 Chemical composition of coating

To investigate the chemical bonds on the coated surfaces and to detect PEI/PAA multilayers, Raman spectroscopy was used. Figure 4-9 shows the Raman shift for uncoated PDMS, as well as 5, 10, 15, 20, 25 and 50 PEI/PAA BLs coated PDMS. For Uncoated PDMS and 5-25 BLs coated samples the Raman shift only showed the peaks relating to pure PDMS and was not able to detect the coating on the substrate. Presence of main peaks at 492, 618 and 712 cm^{-1} are signs for stretching Si-O-Si and stretching Si-CH_3 respectively and relate to PDMS. However, for 50 BLs coated PDMS the

presence of a stretching peak at 900-1000 (cm^{-1}) and the absence of a peak at 1700 (cm^{-1}) relates to C-COO^- and indicates deposition of PAA. Also, the presence of a peak at 1500-1600 (cm^{-1}) indicates presence of NH_3^+ and the deposition of PEI. Another peak at 1400-1500 (cm^{-1}) shows the presence of the main chain of PEI and PAA (CH_2). The results of this study show the similar results to Fan et al. study regarding multilayers of PEI/PAA LbL assembled coating [73]. Detecting the chemical bonds relating to the deposition of PEI/PAA BLs on the surface of PDMS in Raman spectroscopy and detecting the morphology of coating on the surface of PDMS substrate. Between all of the samples, the chemical bonds of PEI/PAA were detected for the 50 BLs coated sample due to the Raman spectroscopy depth (<10 µm) and the coating should have a certain thickness (more than 10 µm) to be detected. For other coated samples (5-25 BLs of PEI/PAA) the coating was not thick enough for Raman microscope (≤ 5 µm) and the substrate was affecting the spectrum, while for the 50 BLs coated sample the thickness was around 16 µm and the Raman microscope could detect the chemical bonds of it. The Raman shift of 50 BLs coated PDMS were measured for at least 3 samples and compared with uncoated PDMS, as shown in Figure 4-10

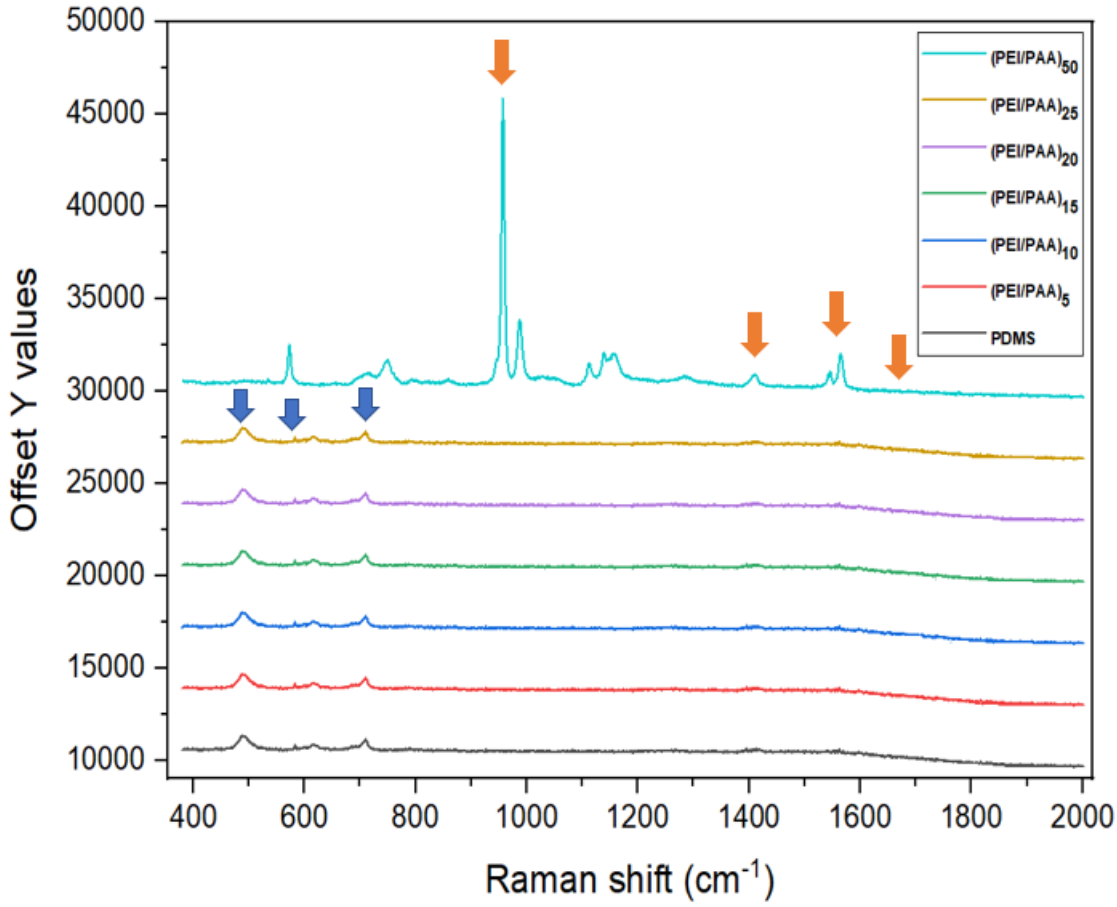

Figure 4-9 Raman shifts of uncoated PDMS and samples that were coated by 5, 10, 15, 20, 25 and 50 BL of PEI/PAA.

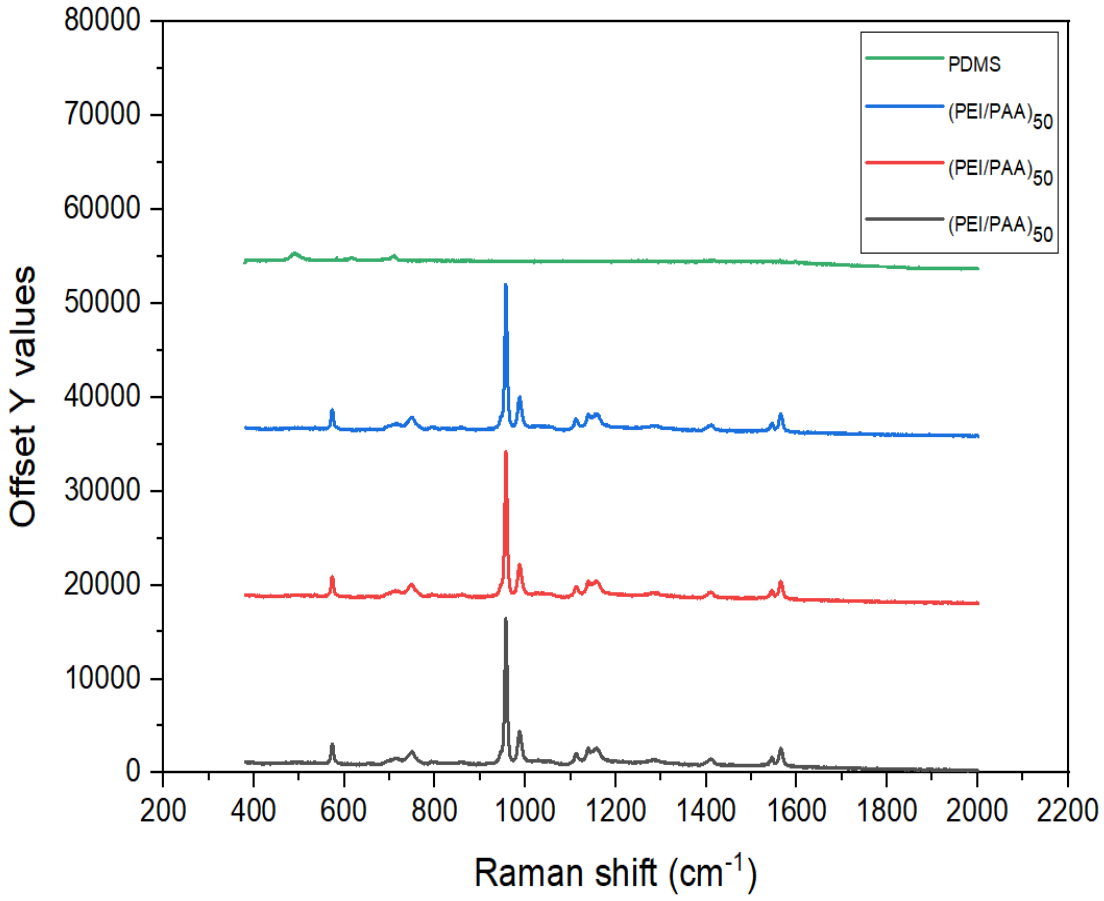

Figure 4-10 Raman shifts of uncoated PDMS and 3 samples that were coated by 50 BLs of PEI/PAA.

4.3 Mechanical properties of coating

After confirming the presence of PEI/PAA coatings on the surface of PDMS, the stiffness of the surface was tested by nanoindentation method. According to Kolewe et al. [81], the viscoelastic behaviour of surfaces plays an important role in antimicrobial activity. The reduced modulus (obtained from nanoindentation) is a measure of the stiffness of the surface and a component of the viscoelastic behaviour. In their work, they hypothesised that bacteria can sense the stiffness of the surface and attach more strongly to stiffer materials. By applying hydrogel coating on PDMS and placing it in a water-rich environment (body fluid or culturing media), the coating can absorb water and expand, while it does not allow the bacteria to sense the stiff substrate and leads to reduced biofilm formation. Also, Kolewe et al. asserted that fluctuations of polymer chains in hydrogels can release air bubbles which prevent bacterial attachment on the coated surface [17].

The reduced modulus was measured for at least 3 samples of each coating (5-50 BLs) at 3 random locations on the surface, with a distance of 500 μm between locations. Also, the indentation depths were varied from 2 to 28 μm for each sample and 3 measurements were taken for each indentation depth for each sample. Figure 4-11 shows the average reduced modulus for PDMS with and without

coatings, with increasing number of BLs and therefore increasing coating thickness. The average of multiple indentation depths (2-28 μm) is given for one sample of each coating thickness. The uncoated PDMS had the highest reduced modulus of 1.99 ± 0.03 MPa and the results were close (2.61 ± 0.021 MPa) to the reported stiffness of PDMS with the same ratio of curing agent and resin, measured by nanoindentation [99]. Also, the value of stiffness for 100% silicone elastomer used to make the urinary catheter studied in this project (1.8 MPa) [45] was close to the stiffness of the PDMS prepared in this project. The average reduced modulus (averaged over all indent locations and all indent depths) for coated samples decreased as the coating thickness increased. The high standard deviation for coated samples results from variation in reduced modulus with changing indentation depth. All the samples were soaked in PBS for 24 hours before the test to mimic the condition of the coated catheter while it is in the body and swollen.

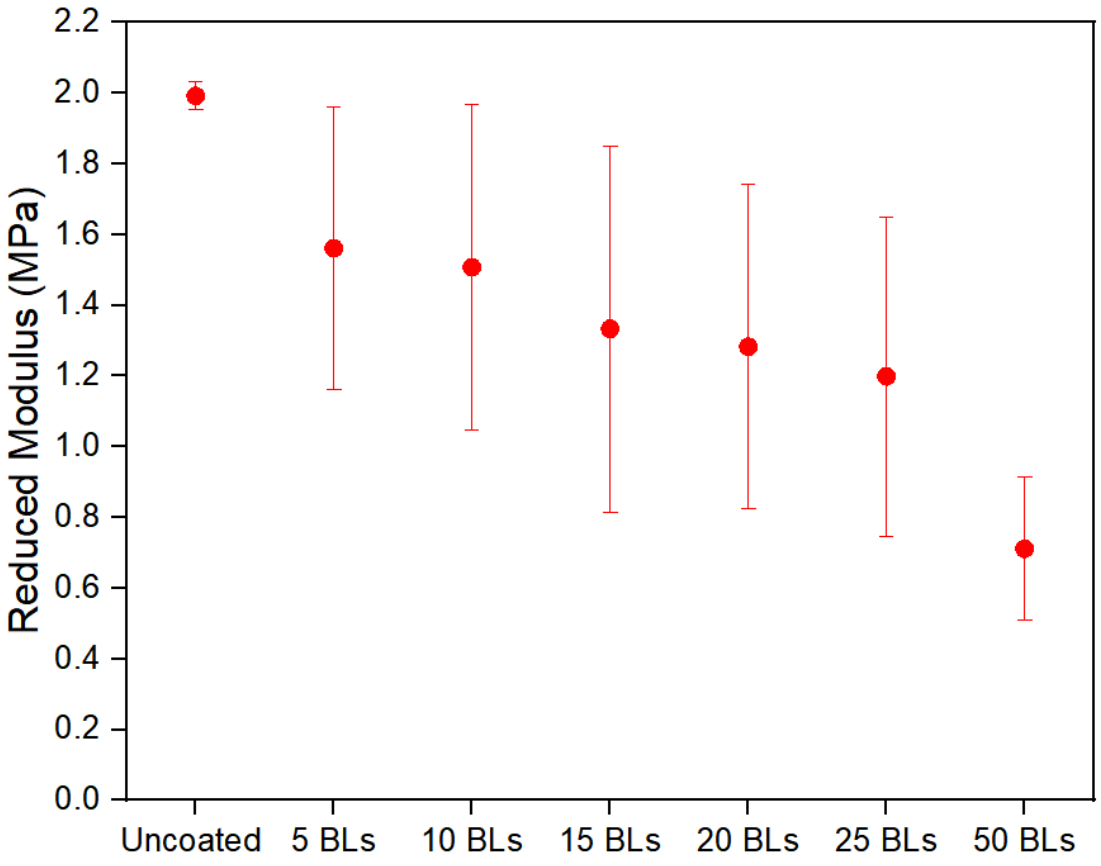

Figure 4-11 Reduced modulus of uncoated and coated PDMS with 5, 10, 15, 20, 25 and 50 BLs of PEI/PAA. Red circles show average values, and the error bars show minimum and maximum values for each sample. At least 3 measurements were taken for each average.

The effect of indentation depth on the value of surface stiffness is shown in Figure 4-12, which shows that the reduced modulus of PEI/PAA ranges from ~0.5 to 1.0 MPa at shallow indentation depths of 2 μm. As indentation depth increased, the reduced modulus increased. Coatings of 5 and

10 PEI/PAA BLs exhibited a sharp transition in reduced modulus (between 2-4 μm and 4-6 μm, respectively). This is consistent with the indenter reaching the interface between these thinner coatings and the PDMS substrate, and a mechanical response that was heavily influenced by the properties of the PDMS substrate. At the largest indentation depth of 28 μm, the reduced modulus of 5 and 10 PEI/PAA BL coatings reached ~1.8 MPa, close to the reduced modulus of uncoated PDMS. Thicker coatings did not exhibit such sharp transitions in reduced modulus. The thickest 50 BLs PEI/PAA coatings only reached a maximum reduced modulus of 0.8 MPa and exhibited no clear transition in mechanical response, suggesting that the maximum indentation depth did not reach the interface between the coating and the PDMS substrate. Although the thickness of the PEI/PAA coatings when swelled in PBS is not known, the average dry thickness of 50 PEI/PAA BLs was 16.13 μm, which suggests that the thickness of the swelled coating was likely greater that the largest indentation depth of 28 μm. According to nanoindentation results, the thickness of hydrated coatings was estimated as 2-4 μm for 5 BLs, 4-6 μm for 10 BLs, 6-12 μm for 15 BLs, 8-12 μm for 20 BLs, 8-14 μm for 25 BLs, and >28 μm for 50 BLs. By comparing these values with the thickness of coatings in dry environment, the swelling ratio is estimated to be around 2.5 (Figure 4-13).

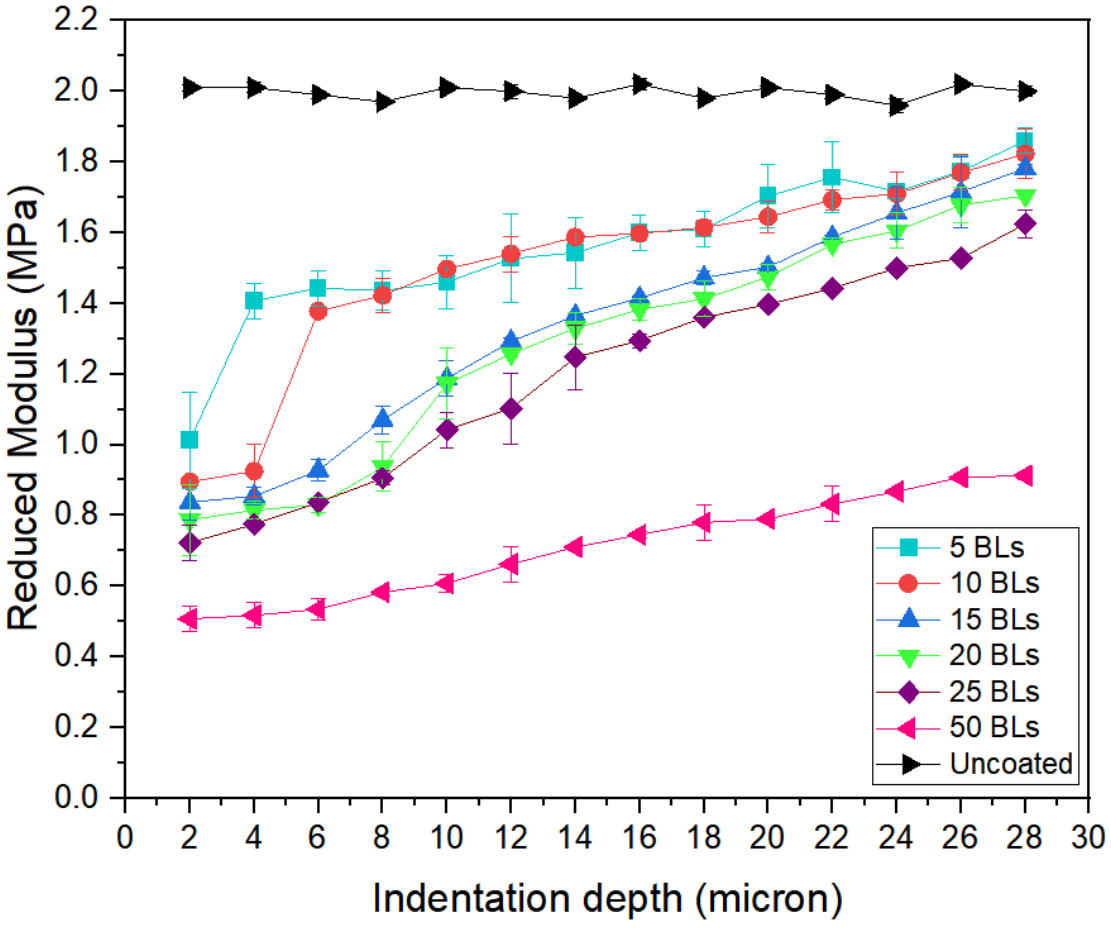

Figure 4-12 Reduced modulus of coated samples by different indentation depth for uncoated PDMS and 5, 10, 15, 15, 20, 25 and 50 BLs coated samples. Each value is an average of at least 3

measurements for a single specimen and error bars indicate the range of minimum and maximum values.

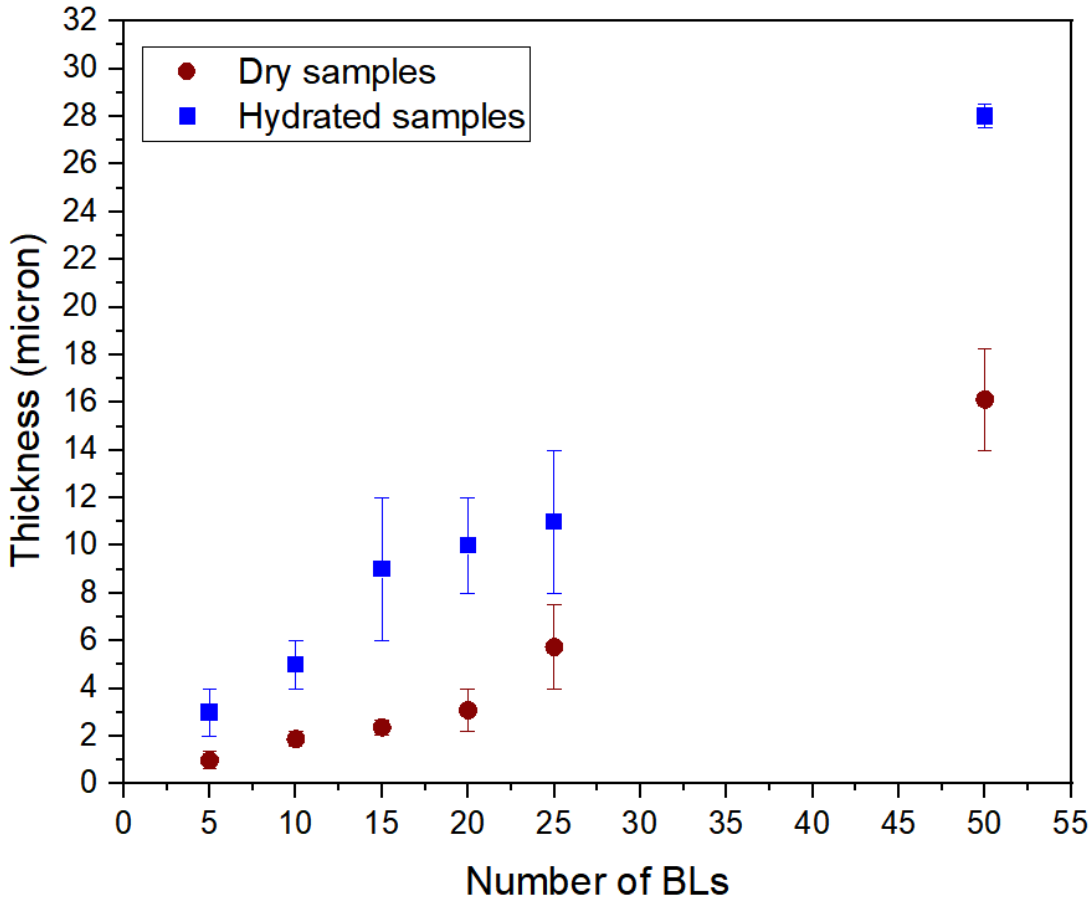

Figure 4-13 Average thickness of 5, 10, 15, 20, 25 and 50 BLs (dry and hydrated) of PEI/PAA on the PDMS substrate. Blue squares and red circles show the average value for each measurement and the error bars show the minimum and maximum of measured thicknesses. At least 3 measurements were performed for each coating.

4.3.1 Presence of the coating in nanoindentation tests

To confirm the presence of the coating in nanoindentation tests and to investigate the thickness of coated samples, two of them (50 BLs coated PDMS samples) were dried in the oven with a temperature of 65 ℃ for 24 hours after being tested by nanoindentation (in wet condition). The samples were cross-sectioned, and then the SEM images were acquired as shown in Figure 4-14 and Figure 4-15.

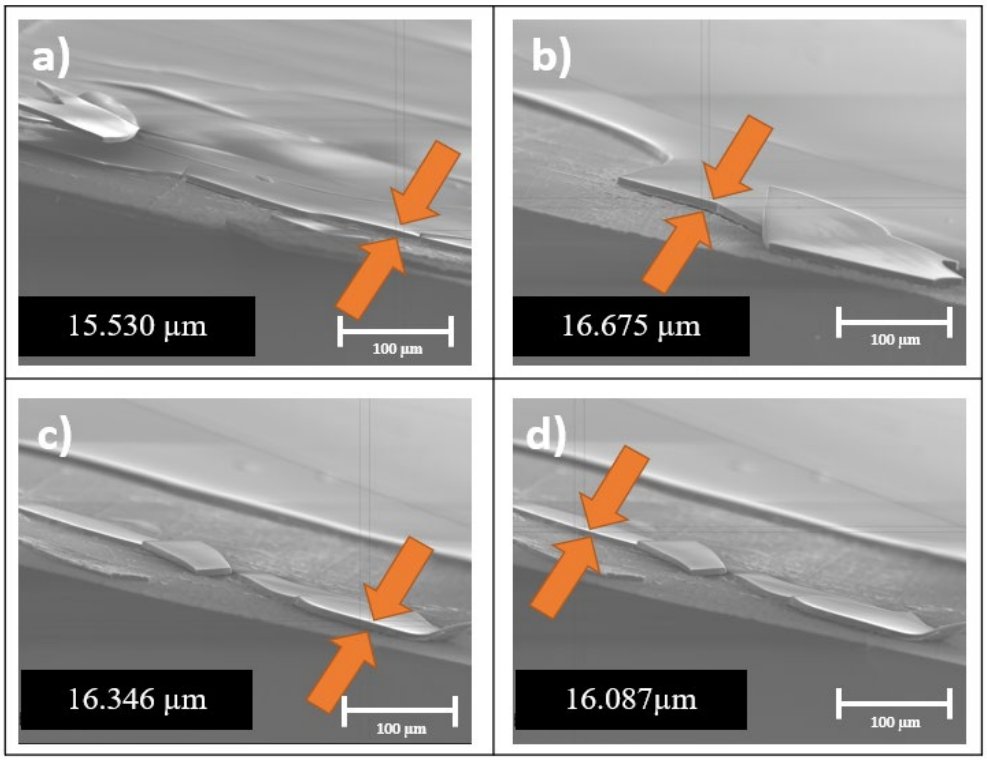

Figure 4-14 SEM images of a sample from a) left edge, b) right edge, c) and d) from the middle of sample 1 (50 BLs coated). The distance between two orange arrows shows the thickness of coating.

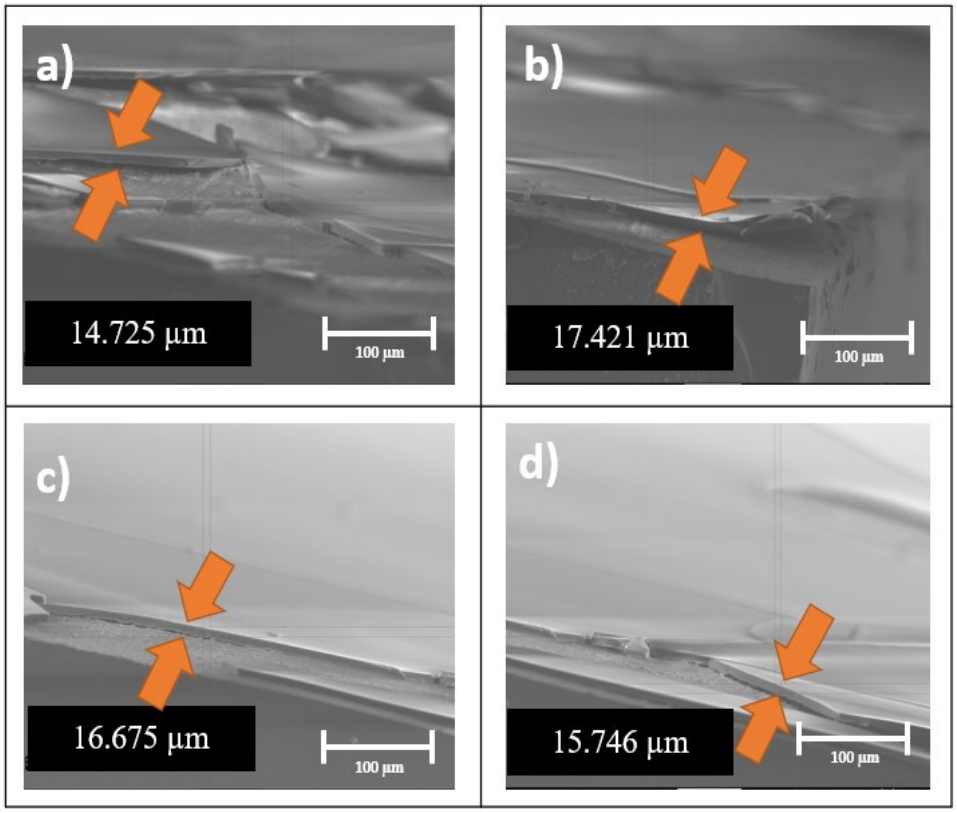

Figure 4-15 SEM images of a sample from a) left edge, b) right edge, c) and d) from the middle of sample 2 (50 BLs coated). Distance between two orange arrows show the thickness of coating.

By comparing the SEM images of coated samples before and after nanoindentation, it can be seen that cross sectioning the samples for imaging does not cause any damage to the coating, which implies nanoindentation was the cause of this damage (the coating peeled off in different sections of the surface). Also, the coating thickness (average of 16.15 µm) was similar to SEM images of 50 BLs coated samples in dry conditions before nanoindentation (average 16.13 µm). The dry thickness of 50 BLs coatings does not seem to have been affected by the repeated drying (after deposition), rehydration (for wet nanoindentation testing), and then re-drying (for SEM). The coating also shows signs of localised damage, which may have occurred during nanoindentation.

4.4 Antimicrobial activity of PEI/PAA multilayer coatings

The antimicrobial activity of PEI/PAA coatings was investigated against *P. aeruginosa*, which is known to be a common contributing cause of UTIs [100]–[102].

4.4.1 Characterizing the amount of formed biomass on the surface of samples

The uncoated and 5-25 BLs coated samples were inoculated with *P. aeruginosa* and incubated for 1 day and then stained by crystal violet to investigate the antibiofilm activity of the coatings. Based on this initial study, it was observed that by increasing the number of BLs the amount absorbance ($OD_{584\ nm}$) was decreased (Figure 4-16). Significant difference (with lowest $p < 0.001$) in the absorbance was observed between uncoated PDMS and coatings with 10 BLs or more. Though statistically significant, the difference in $OD_{584\ nm}$ was very small in comparison to uncoated PDMS for 5 BLs and 10 BLs (0.85% and 1%, respectively). The 25 BLs coating caused the greatest reduction in biomass, i.e.by 28.56% compared with uncoated PDMS.

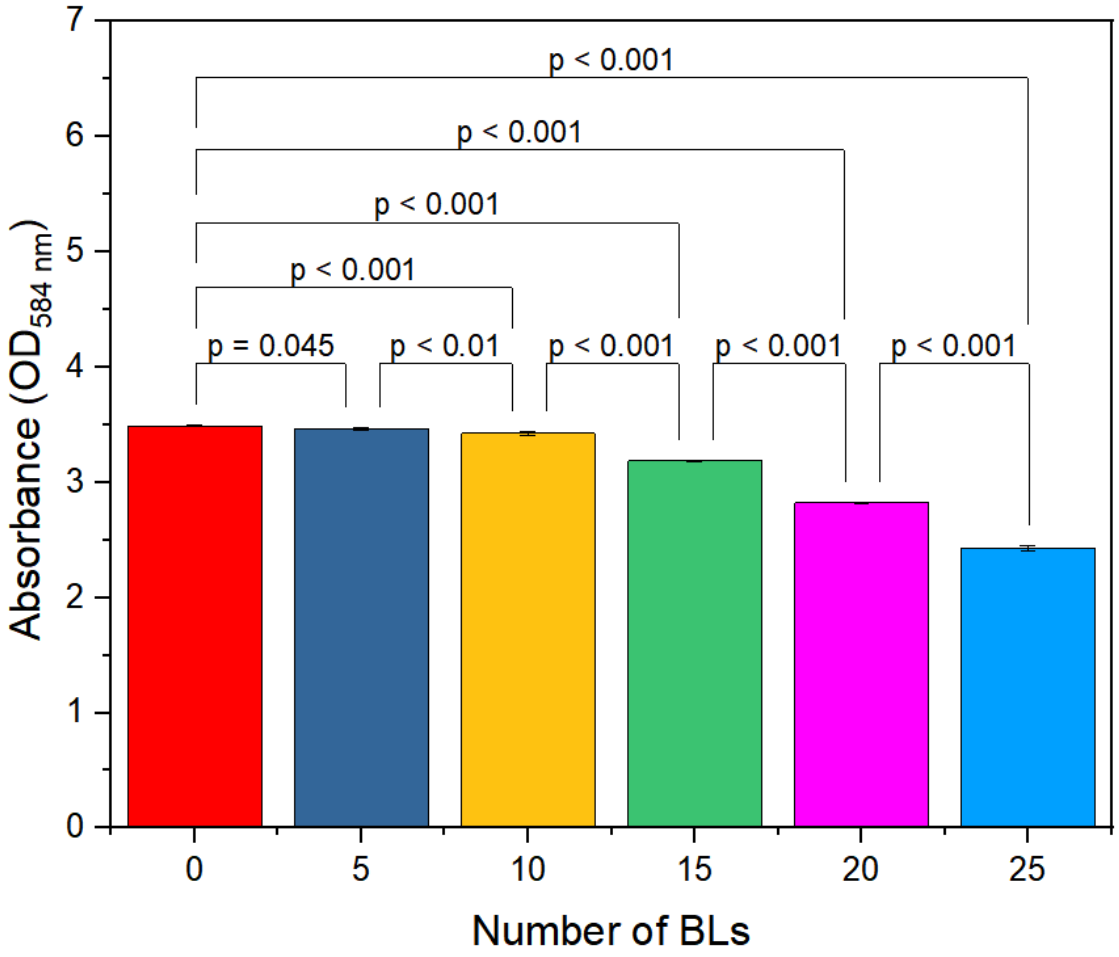

Figure 4-16 Absorbance ($OD_{584\ nm}$) measured on the surface of uncoated and 5, 10, 15, 20 and 25 BLs coated samples stained with crystal violet after 1 day incubation of *P. aeruginosa*. Bars represent average values of at least 3 measurements for one sample of each coating, and error bars correspond to the range of minimum and maximum values. p values were calculated by Origin software, using non-parametric, Kruskal-Wallis ANOVA.

To assess the degree to which crystal violet can stain the coating and PDMS materials in the absence of biofilm, uncoated and coated PDMS with 5, 10, 15, 20 and 25 BLs of PEI/PAA (without bacterial culturing) were stained with crystal violet using the same protocol as for samples incubated with bacteria. The results in Figure 4-17 shows that the range of values for samples without bacteria (0.225 to 0.491) is significantly smaller than samples with bacteria cultured (2.43 to 3.49), indicating that crystal violet only weakly interacts with PDMS and the coating. The largest value of absorbance for samples without bacteria is 0.491 for the 25BL coating, compared to 0.225 for uncoated PDMS. This higher background $OD_{584\ nm}$ from the 25BLs coating indicates that the reduction in biomass from bacterial culture is even greater than the difference in Figure 4-16 indicates.

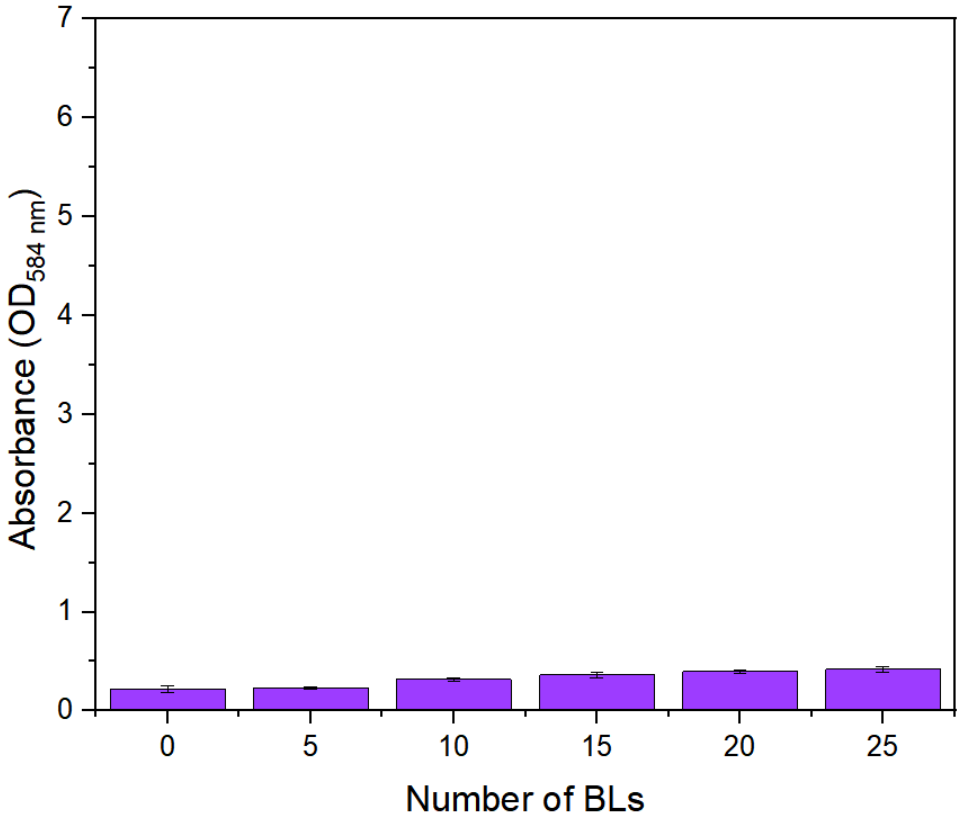

Figure 4-17 Comparing the amount of crystal violet on uncoated and 5, 10, 15, 20 and 25 BLs coated samples which were not inoculated with bacteria. Bars present average value of at least 3 measurements for one sample of each coating, and error bars bound the range of minimum and maximum values.

Further studies of biofilm formation assessed the absorbance ($OD_{584\ nm}$) after 1 day and after longer incubation of 7 days. 25 BLs coatings were studied because of the largest decrease in $OD_{584\ nm}$ at 1 day, and thicker 50 BLs coatings were also studied to assess whether further decreases would result. Additionally, the composition of the last layer was tested to investigate antibiofilm behaviour of either PEI or PAA as the last layer of coating (Figure 4-18 and Figure 4-19). The results of staining the samples with crystal violet for 25 BLs coated sample with the last layer of PEI and PAA showed the values of 2.3 and 2.57, respectively after 1 day of incubation. By increasing the incubation time to 7 days the same values reached to 2.74 and 3.47, respectively. The same assessment was carried out for the 50 BLs coated samples and the values of crystal violet staining were 1.47 and 1.62 for the samples with the last layer of PEI and PAA, respectively after 1 day of incubation. Also, the same values were reached to 1.5 and 1.97 after 7 days of incubate for the samples with the last layer of PEI and PAA, respectively. In general, it can be seen that the values of crystal violet for the samples with the last layer of PAA were greater than the values for the samples with the last layer of PEI for both incubation times (1 day and 7 days). The reason behind this occurrence can be surface charge. It has been evidenced that positively charged hydrogels can damage the bacterial membrane and

prevent biofilm formation [103]. PEI carries positive charge and presence of it as the last layer of coating can reduce the biofilm formation as a bactericidal agent. Furthermore, negatively charged hydrogels (like PAA) can play as antifouling agent and prevent bacterial attachment on the surface of negative substrates. However, recent research showed that flagella part of *P. aeruginosa* can attach to negatively charged materials while it cannot show the same behaviour for positively charged surfaces [103]. The crystal violet staining results for both 25 and 50 BLs coated samples followed the same behaviour and PEI as the last layer showed less amount of formed biofilm on the coating than PAA. These results can be due to attachment of flagella part of *P. aeruginosa* to PAA that they do not have the same chance with PEI. Also, the amount of formed biofilm after 7 days increased for both samples which need other characterizing method to clarify whether the number is for live or dead bacteria.

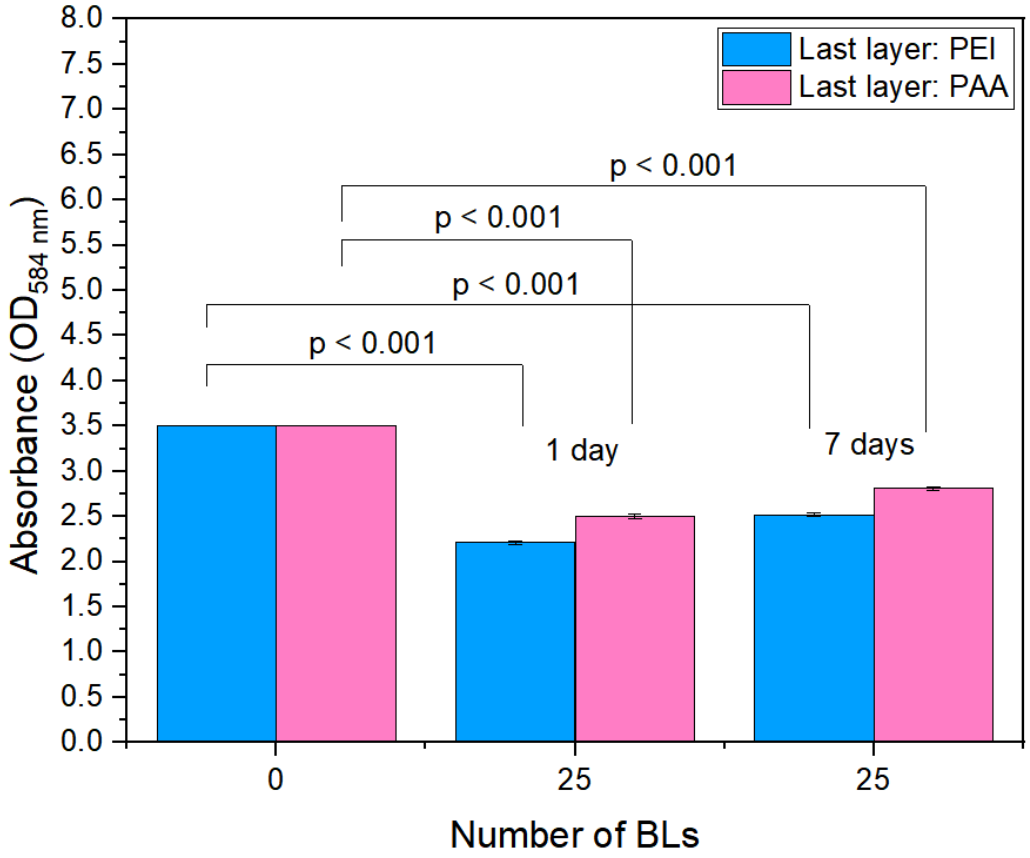

Figure 4-18 Comparing the amount of crystal violet on uncoated and 25 BLs coated samples for 1 day and 7 days of incubation for both last layer of PEI and PAA. Bars present average value of at least 3 measurements for one sample of each coating, and error bars bound the range of minimum and maximum values. p values were calculated by Origin software, using non-parametric, Kruskal-

Wallis ANOVA.

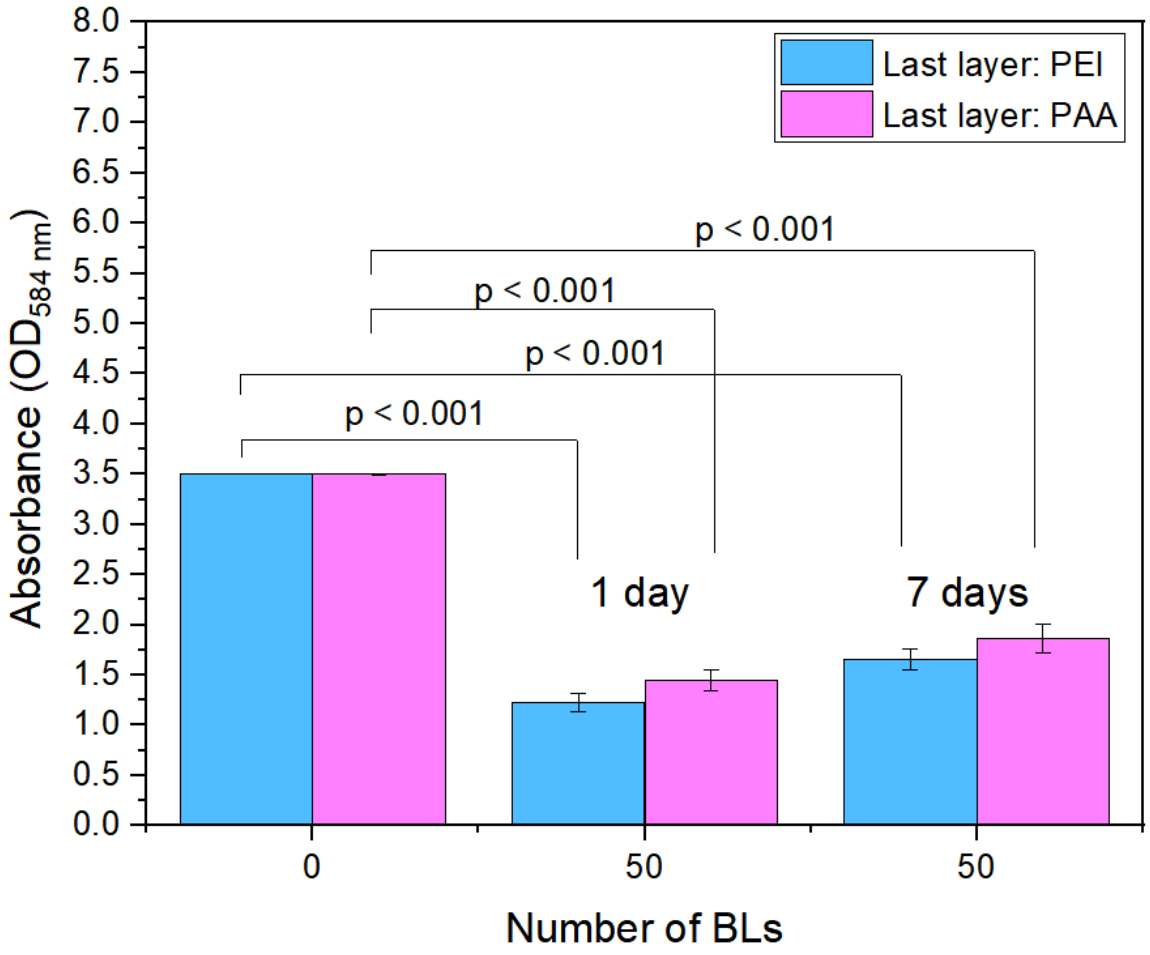

Figure 4-19 comparing the amount of crystal violet on uncoated and 50 BLs coated samples for 1 day and 7 days of incubation for both last layer of PEI and PAA. Bars present average value of at least 3 measurements for one sample of each coating, and error bars bound the range of minimum and maximum values. p values were calculated by Origin software, using non-parametric, Kruskal-Wallis ANOVA.

4.4.2 Fluorescence microscopy of uncoated and PEI/PAA coated PDMS

Although staining the biofilm with crystal violet can show the effect of coatings on biofilm formation, it does not give details about coverage area on the surface of uncoated and coated samples. Fluorescent microscopy is a method that provides detailed images of the samples to assess the surface coverage area with formed biofilm [50]. The composite images show combined green (live) and red (dead) wavelengths, indicating the proportion of live and dead bacteria on each surface. Images after incubation times for both 1 day and 7 days incubation of *P. aeruginosa* on the surface of uncoated PDMS in Figure 4-20 and Figure 4-21, respectively appear to show biofilms populated by live cells (continuous green patches). After 1 day of incubation on the surface of all samples *P. aeruginosa* were observed in green color, while the same behavior was observed for the samples which were incubated for 7 days . Also, the overlap of live and dead bacteria appeared in

bright yellow color in Figure 4-21 which means that the membrane of *P. aeruginosa* is damaged. Although the red spots appeared on the surface of PDMS (sample 2) after 7 days of incubation, the majority of samples surface were covered with formed biofilm of *P. aeruginosa* and the uncoated PDMS was not showed any resistance against biofilm formation.

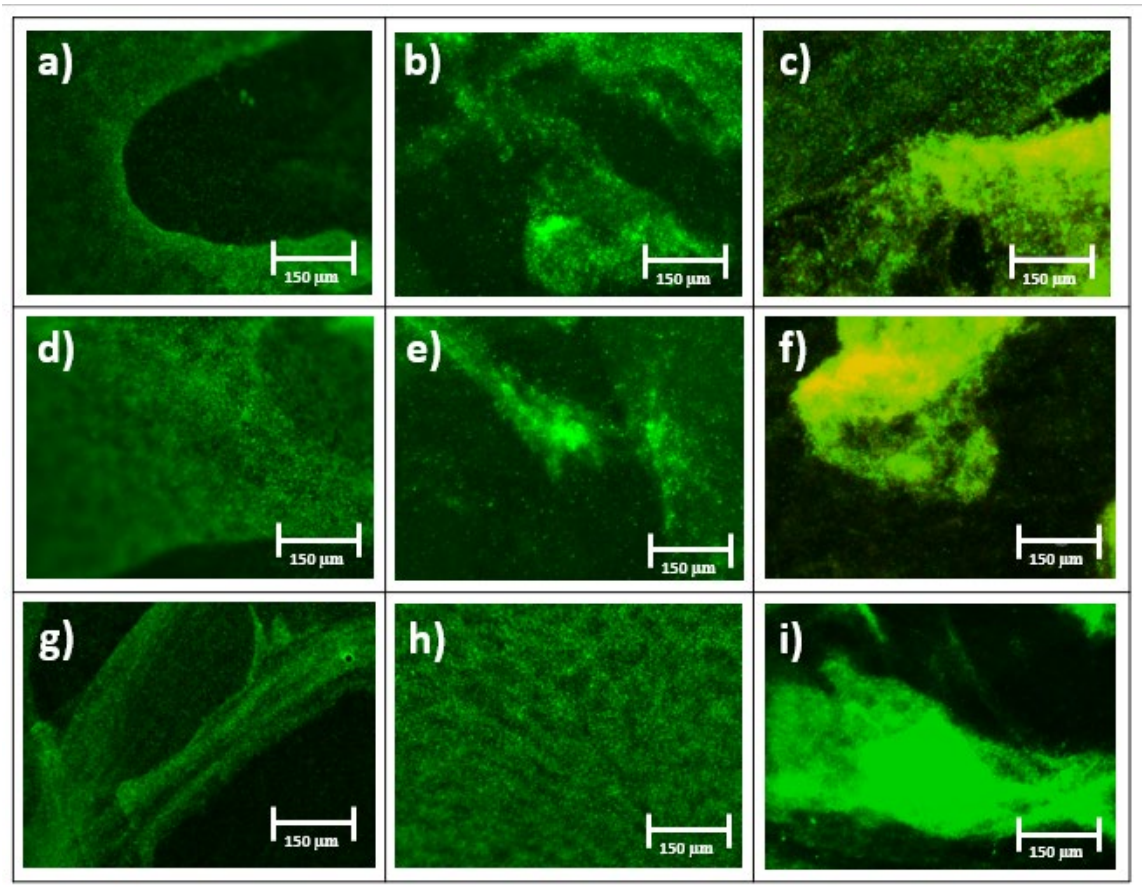

Figure 4-20 Fluorescent images of *P. aeruginosa* stained with SYTO9/PI after 1 day incubation on uncoated PDMS a) left corner, b) middle, c) right corner of sample 1, d) left corner, e) middle, f) right corner of sample 2, g) left corner, h) middle and i) left corner of sample 3.

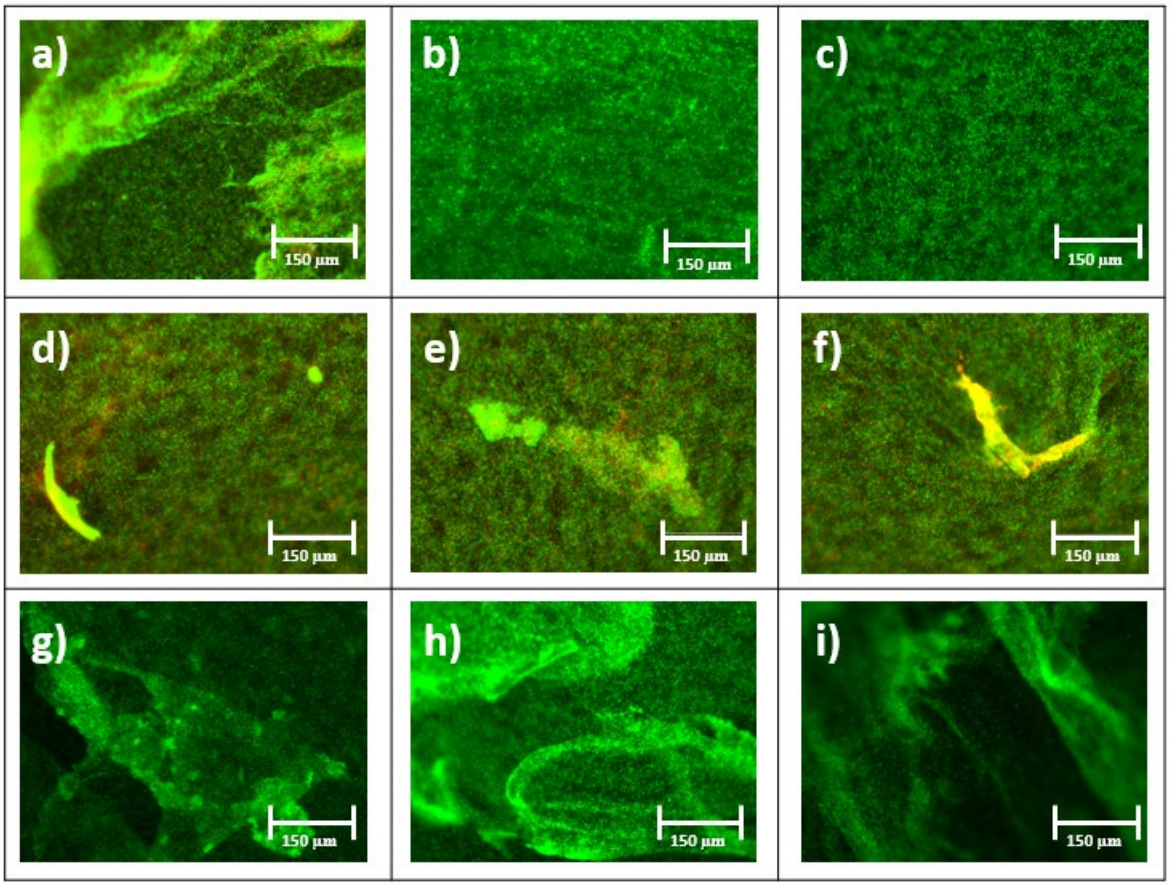

Figure 4-21 Fluorescent images of *P. aeruginosa* stained with SYTO9/P after 7 days incubation on uncoated PDMS a) left corner, b) middle, c) right corner of sample 1, d) left corner, e) middle, f) right corner of sample 2, g) left corner, h) middle and i) left corner of sample 3.

The results of fluorescent microscopy for 25 and 50 BLs coated samples after 1 day and 7 days incubation times are shown in the figures below. In 25 BLs coated PDMS, the majority of *P. aeruginosa* on the surface were shown in red spots (dead bacteria) after 1 day of incubation both for last layers of PEI and PAA in comparison to uncoated samples (Figure 4-22 and Figure 4-23). Additionally, for coated samples with the last layer of PAA the smaller, more fragmented biofilm (patches) were observed than PEI which shows antifouling activity of PAA on the surface. Both PEI and PAA polymers in the coating had a branched structure and according to the literature, dynamic motion of polymeric side chains in wet environment can prevent bacterial adhesion to the surface. Also, polymer brushes (branches of main chain) can disturb the bacterial membrane, damage them and decrease the biofilm formation [104].

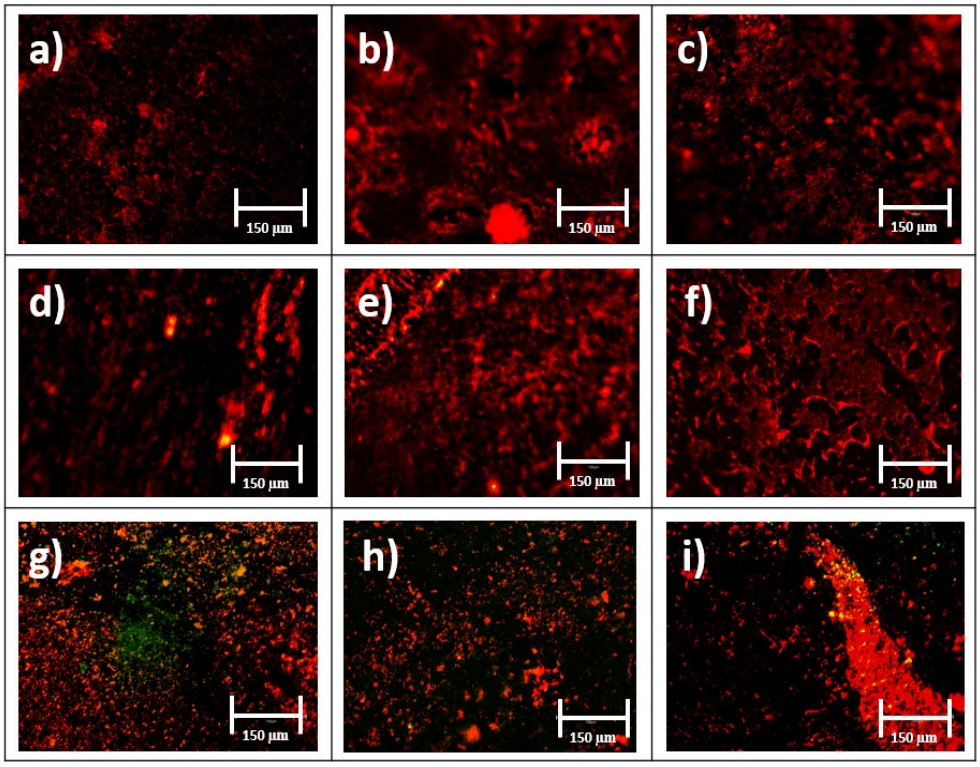

Figure 4-22 Fluorescent images of *P. aeruginosa* stained with SYTO9/PI after 1 day incubation on 25 BLs (last layer PEI) coated a) left corner, b) middle, c) right corner of sample 1, d) left corner, e) middle, f) right corner of sample 2, g) left corner, h) middle and i) left corner of sample 3.

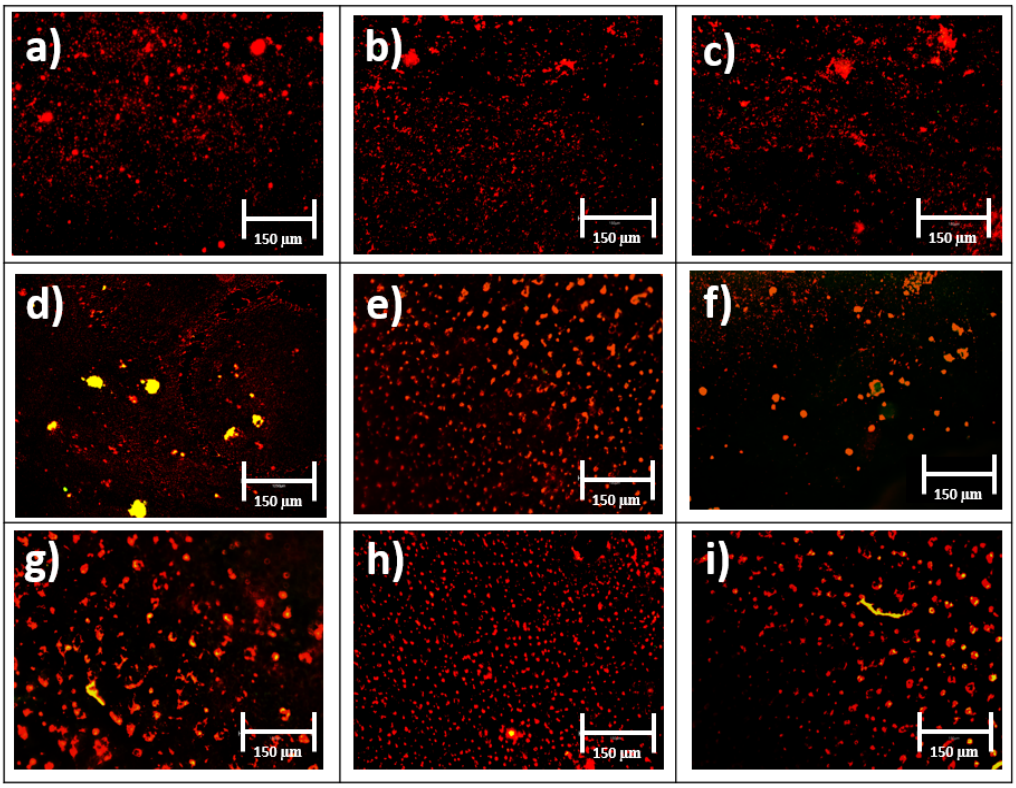

Figure 4-23 Fluorescent images of *P. aeruginosa* stained with SYTO9/PI after 1 day incubation on 25 BLs (last layer PAA) coated a) left corner, b) middle, c) right corner of sample 1, d) left corner, e) middle, f) right corner of sample 2, g) left corner, h) middle and i) left corner of sample 3.

To investigate the antimicrobial activity of 25 BLs coated sample over a longer period, the incubation time was increased to 7 days. It can be seen that still the majority of patches on the surface were in red or yellow colour (dead or damaged) with greater area of coverage. However, the number of green patches were appeared on the surface of samples for both 25 BLs coated composition (Figure 4-24 and Figure 4-25) which shows a group of the *P. aeruginosa* were grown on the surface in comparison to the results for 1 day of incubation. This may be due to the contamination of the coating surface with dead bacteria, which might prevent the live bacteria from direct contact with the coating and act to shield from the coating antimicrobial effects exhibited over durations shorter durations of 1 day.

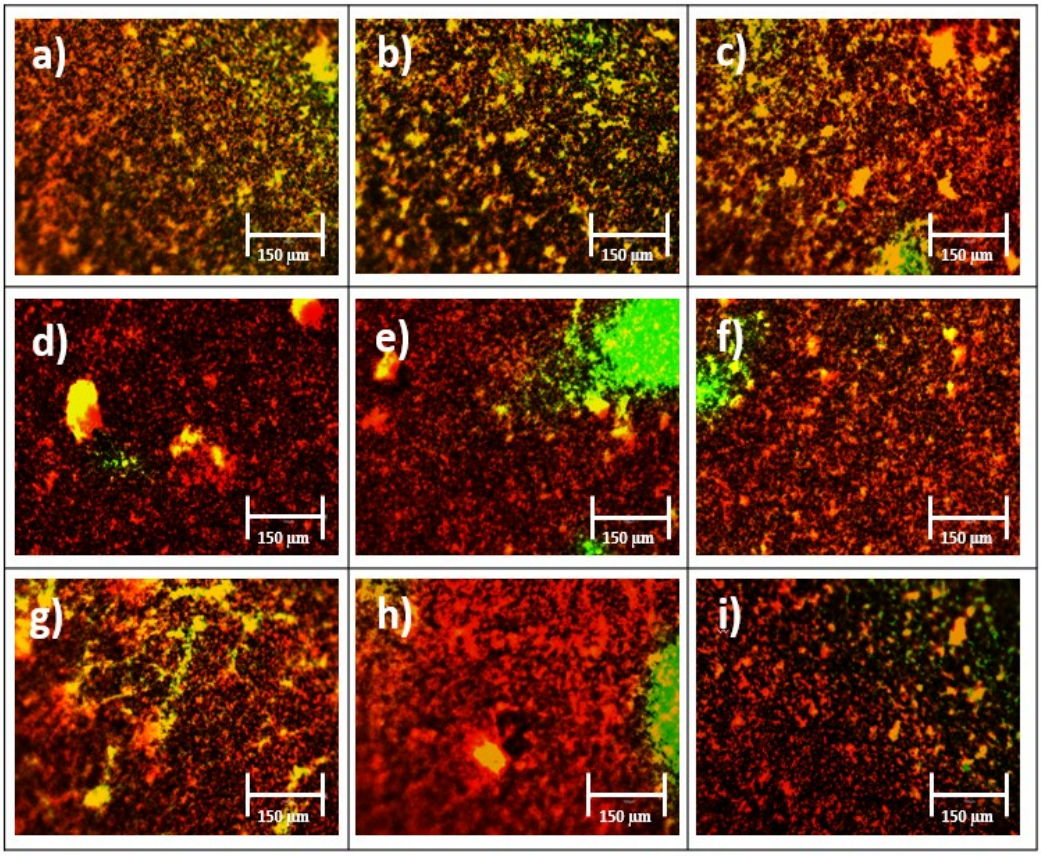

Figure 4-24 Fluorescent images of *P. aeruginosa* stained with SYTO9/PI after 7 days incubation on 25 BL (last layer PEI) coated a) left corner, b) middle, c) right corner of sample 1, d) left corner, e) middle, f) right corner of sample 2, g) left corner, h) middle and i) left corner of sample 3.

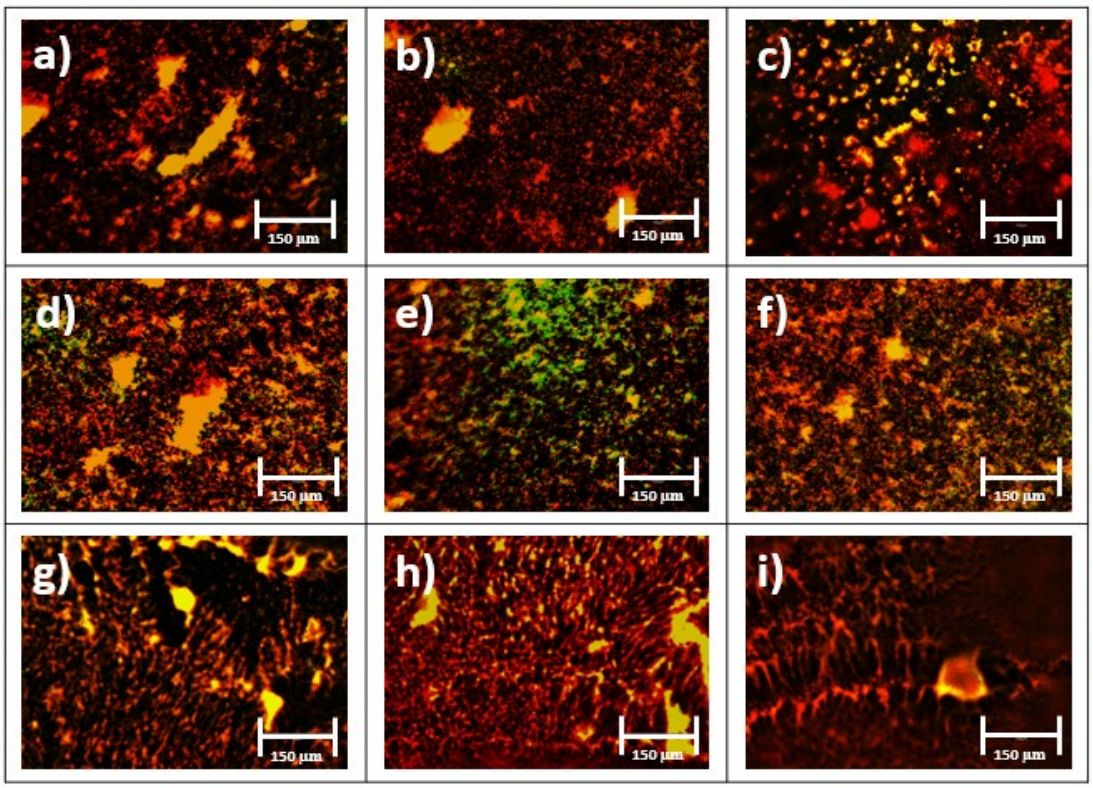

Figure 4-25 Fluorescent images of *P. aeruginosa* stained with SYTO9/PI after 7 days incubation on 25 BLs (last layer PAA) coated a) left corner, b) middle, c) right corner of sample 1, d) left corner, e) middle, f) right corner of sample 2, g) left corner, h) middle and i) left corner of sample 3.

To compare the antimicrobial activity, the same procedure was conducted for 50 BLs coated sample. After 1 day of incubation, for both last layers of PEI and PAA, the number of detectable bacteria on the surface of sample were significantly lower compared with uncoated and 25 BLs coated PDMS (Figure 4-26 and Figure 4-27). Also, the samples with the last layer of PAA showed the same behaviour (smaller, more patches) while the samples with the last layer of PEI showed fewer patches on their surface. In general, the number of green patches for both sample compositions were significantly low in comparison to uncoated and 25 BLs coated samples. By increasing the incubation time for 7 days, the number of red and yellow spots were increased for both sample compositions (dead or damaged) shown in Figure 4-28 and Figure 4-29, However, still the surface coverage area was significantly low in comparison to uncoated and 25 BLs coated samples.

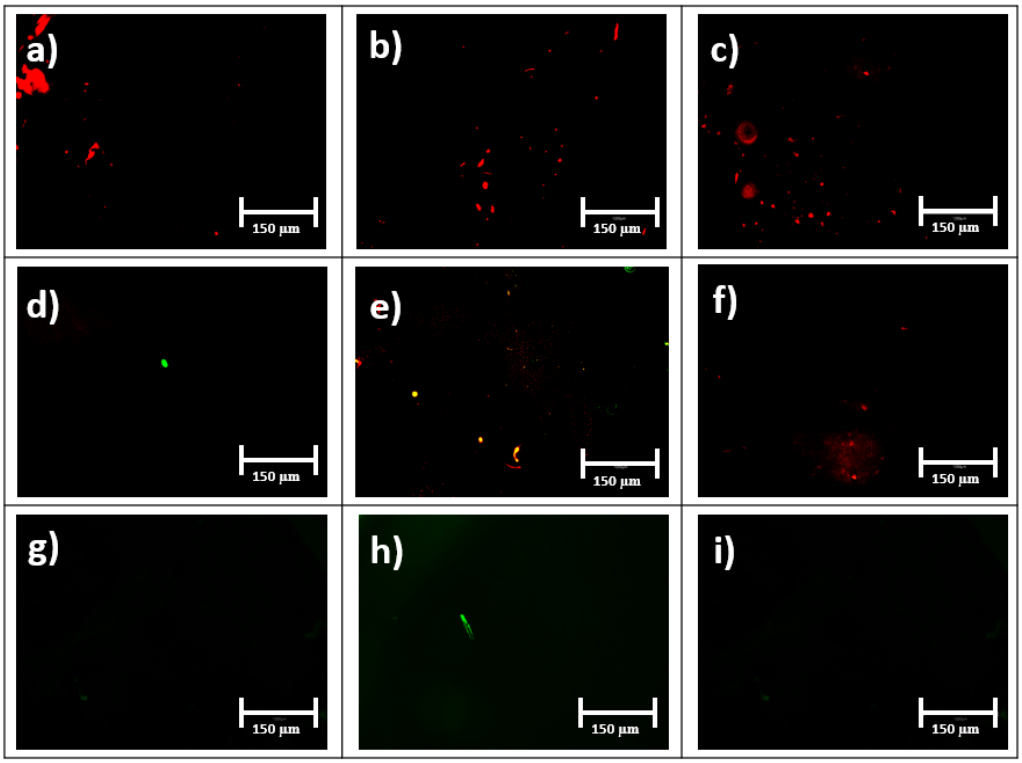

Figure 4-26 Fluorescent images of *P. aeruginosa* stained with SYTO9/PI after 1 day incubation on 50 BLs (last layer PEI) coated a) left corner, b) middle, c) right corner of sample 1, d) left corner, e) middle, f) right corner of sample 2, g) left corner, h) middle and i) left corner of sample 3.

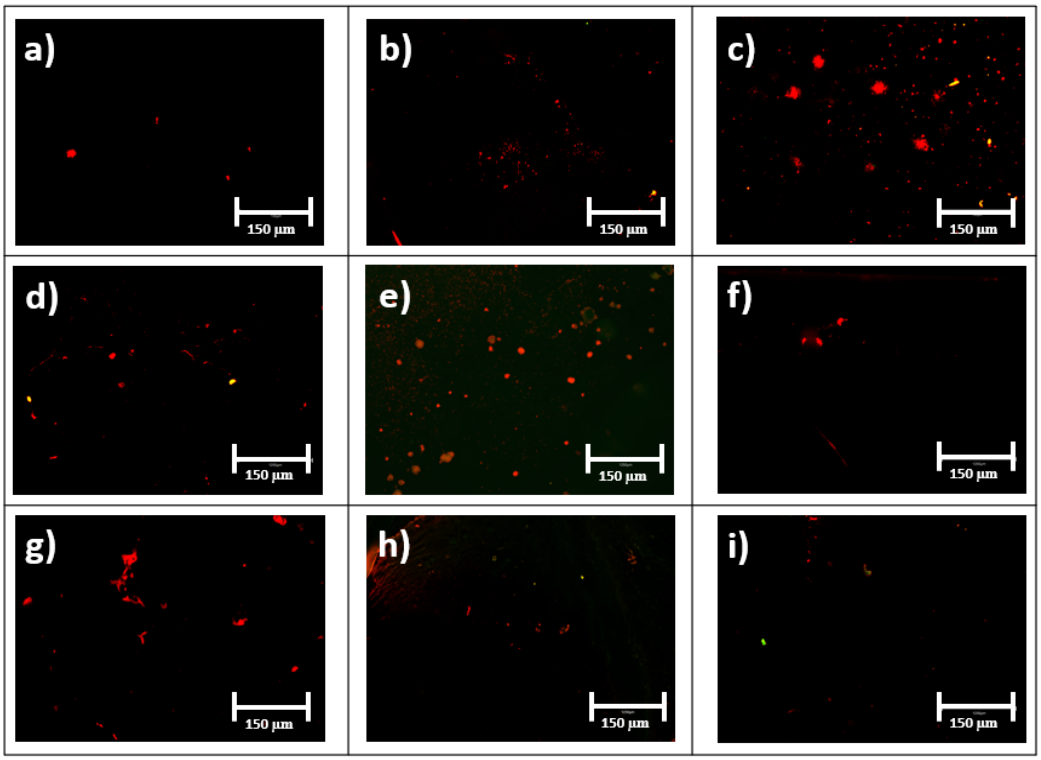

Figure 4-27 Fluorescent images of *P. aeruginosa* stained with SYTO9/PI after 1 day incubation on 50 BLs (last layer PAA) coated a) left corner, b) middle, c) right corner of sample 1, d) left corner, e) middle, f) right corner of sample 2, g) left corner, h) middle and i) left corner of sample 3.

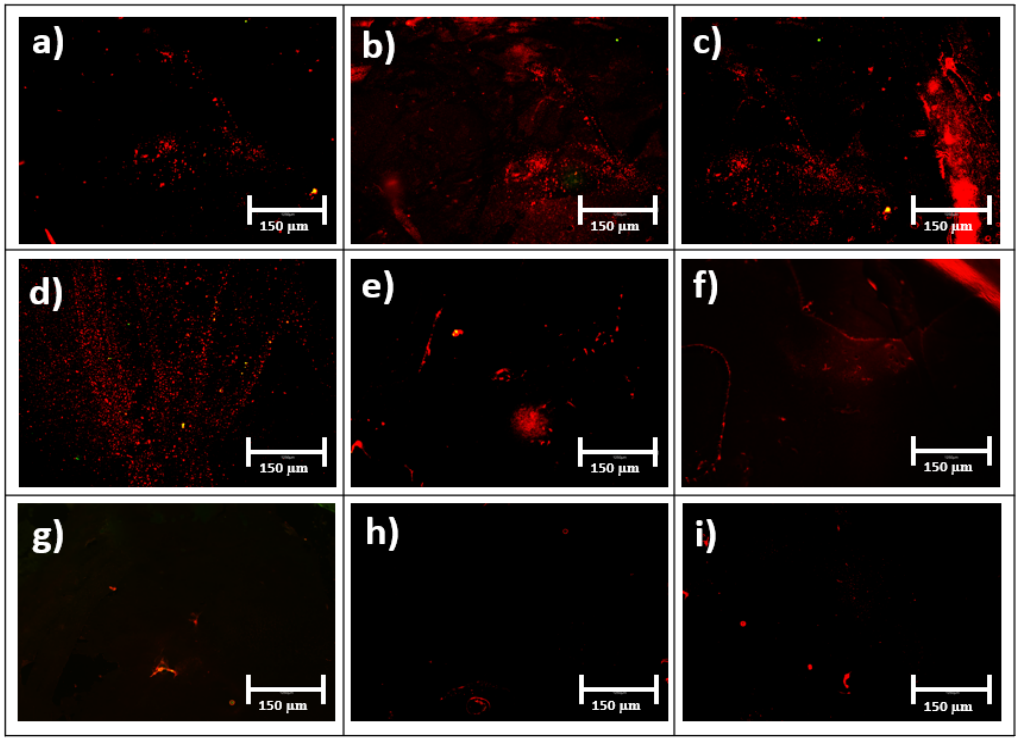

Figure 4-28 Fluorescent images of *P. aeruginosa* stained with SYTO9/PI after 7 days incubation on 50 BLs (last layer PEI) coated a) left corner, b) middle, c) right corner of sample 1, d) left corner, e) middle, f) right corner of sample 2, g) left corner, h) middle and i) left corner of sample 3.

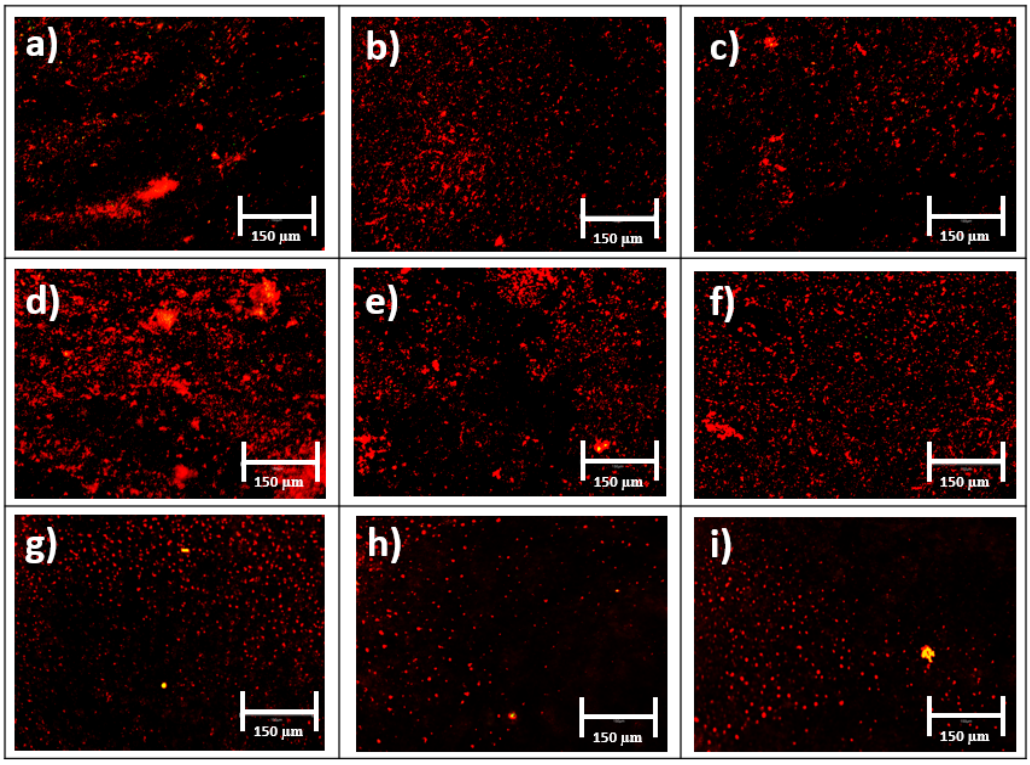

Figure 4-29 Fluorescent images of *P. aeruginosa* stained with SYTO9/PI after 7 days incubation on 50 BLs (last layer PAA) coated a) left corner, b) middle, c) right corner of sample 1, d) left corner, e) middle, f) right corner of sample 2, g) left corner, h) middle and i) left corner of sample 3.

After comparing the fluorescent microscopy images of proposed coating, it can be seen that the thickness of the coating is one of the elements that can affect the antimicrobial activity. According to the literature, in multilayers of PEI and PAA, the NH^{3+} in ionized PEI interacts with COO^- in ionized PAA through electrostatic interactions and form cross linked network structure, while the interaction of NH_2 and COOH groups can lead to the formation of hydrogen bonds between PEI and PAA and formation of second cross linked structure in multilayers of PEI/PAA coating [84]. These two phenomena can create double crosslinked networks in polymeric chain of PEI and PAA which improves resistance of coating from peeling off the surface. Also, formed crosslinks prevent PEI and PAA to be released in the media and cause cytotoxicity toward bladder cells [29]. Following the thickness of PEI/PAA multilayer coatings it can be seen that up to 20 BLs the coating thickness is smaller or similar in size to *P. aeruginosa*, a rod shape microorganism with the size of 1-5 µm long and 0.5-1 µm wide [105] and the coating were not able to prevent biofilm formation. For 25 BLs coated sample, the thickness of coating in dry conditions is around 6 µm and by absorbing water it expands and can be bigger than *P. aeruginosa.* This reason can explain the significant antibiofilm activity of 25 PEI/PAA BLs coated PDMS for 1 day, however, small group of P. aeruginosa could grow on the surface of samples for 7 days of incubation and it seemed that the thickness of coating was not thick enough to prevent biofilm formation while single bacteria were accumulated and in bigger size. 50 BLs coated sample showed continuous antimicrobial activity up to 7 days. By inoculating *P. aeruginosa* on coated samples, a great number of them are in contact with the coating and the results show that the thickness of coating should reach to a critical value to have antibiofilm activity. According to our observations, at least the thickness of applied coating should not be less than size of the microorganism that allows the bacteria to only sense the soft coating than stiff substrate. Also, the reduced modulus assessment results with different indentation depth showed that for thinner coatings, substate can affect more on the stiffness of the surface than thicker coating. Uncoated, 25 and 50 BLs coated PDMS samples without exposure to bacteria of *P. aeruginosa* were stained with SYTO9/PI mixture and imaged by fluorescent imaging (same protocol for samples in contact with bacteria) to assess if the coating or PDMS absorb any fluorescent dye. Figure 4-30 shows that uncoated and coated PDMS samples do not absorb any florescent dye and only in 75 µm scale image a small amount of dye was detected which can be a residual on the surface. These results confirmed that green and red parts in previous fluorescent images related to live and dead bacteria, rather than staining of the coatings or PDMS.

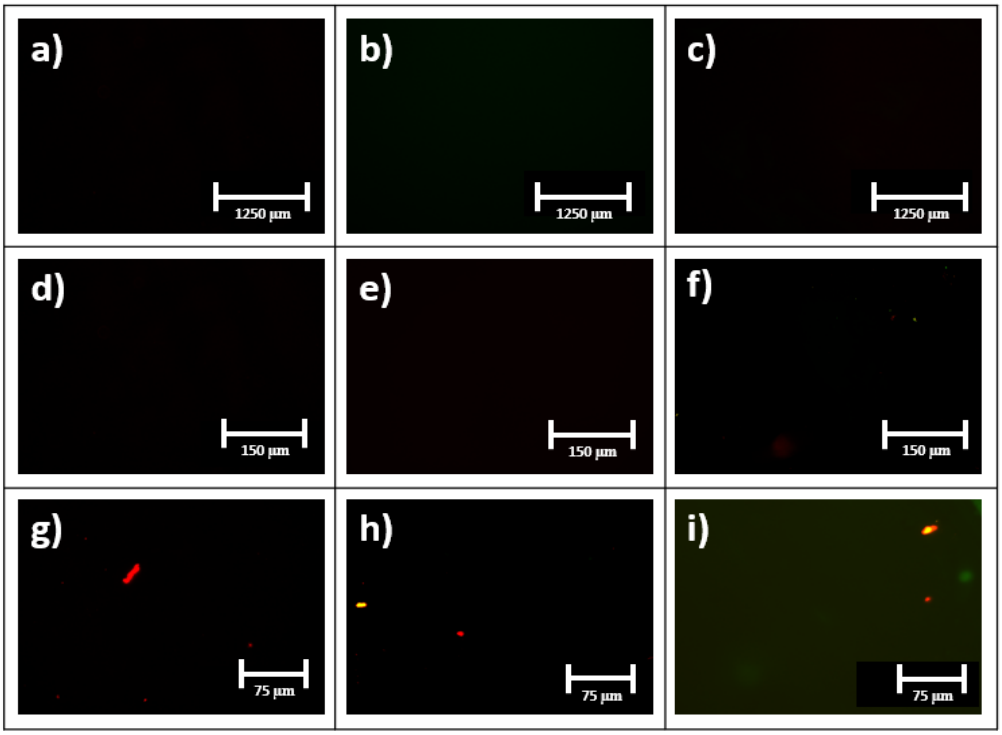

Figure 4-30 Fluorescent images of uncoated PDMS in a) 1250, d) 150, g) 75 µm scale, 25 PEI/PAA BLs coated PDMS b) 1250, e) 150, h) 75 µm scale, 50 PEI/PAA BLs coated PDMS c) 1250, f) 150 and i) 75 µm scale stained with SYTO9/PI.

The coverage area of the surface by formed biofilm was calculated in Fiji ImageJ software by using analyze particle setting to investigate the antibiofilm activity. The images in this section show a square of 6×6 mm in the center of each sample which was prepared with the diameter of 1 cm. Figure 4-31 and Figure 4-32 show that the majority of uncoated PDMS surface was covered with formed biofilm (91.94 ± 2 % in 1 day and 95.13 ± 1 % in 7 days).

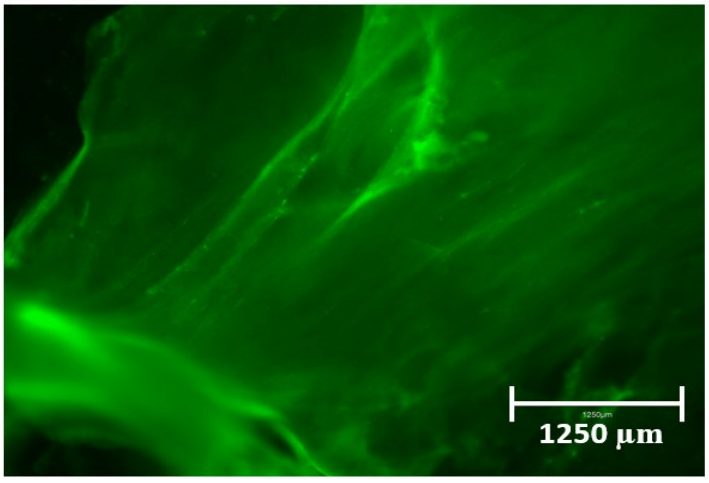

Figure 4-31 Covered area of formed biofilm on uncoated PDMS after 1 day of incubation time captured by fluorescent microscopy. Sample was stained with SYTO9/PI and coverage area is processed with Fiji ImageJ.

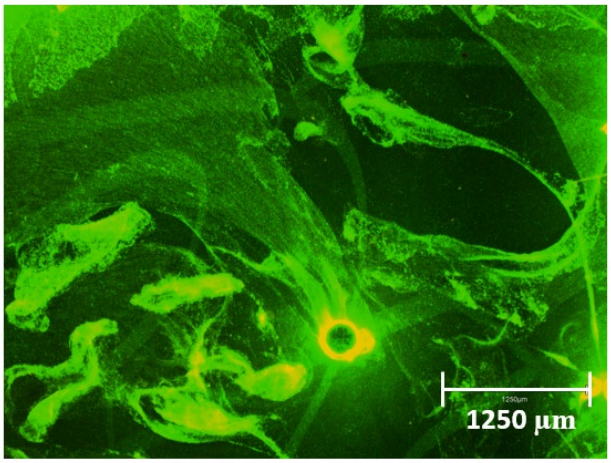

Figure 4-32 Covered area of formed biofilm on uncoated PDMS after 7 days of incubation time captured by fluorescent microscopy. Sample was stained with SYTO9/PI and coverage area is processed with Fiji ImageJ.

The same test was carried out for the 25 BLs coated sample with different last layer composition (PEI or PAA) for 2 different incubation times (1 day and 7 days). The coverage area of formed biofilm after 1 day of incubation reached to around 36.81 ± 0.5 % when the last layer of the coating was PEI and 45.88 ± 0.6 % when the last layer was PAA. In comparison to uncoated sample, the biofilm coverage area decreased significantly (from 91.94%) for both composition of last layer and the coating showed antibiofilm activity for 1 day (Figure 4-33 and Figure 4-34). By increasing the incubation time to 7 days the biofilm coverage area increased to around 50.53 ± 4 % and 52.48 ± 3 % for last layer composition of PEI and PAA, respectively (Figure 4-35 and Figure 4-36). Although, after 7 days the amount of formed biofilm increased on 25 BLs coated sample for both compositions, still the numbers are lower than uncoated samples which was reached 95.13 % after 7 days.

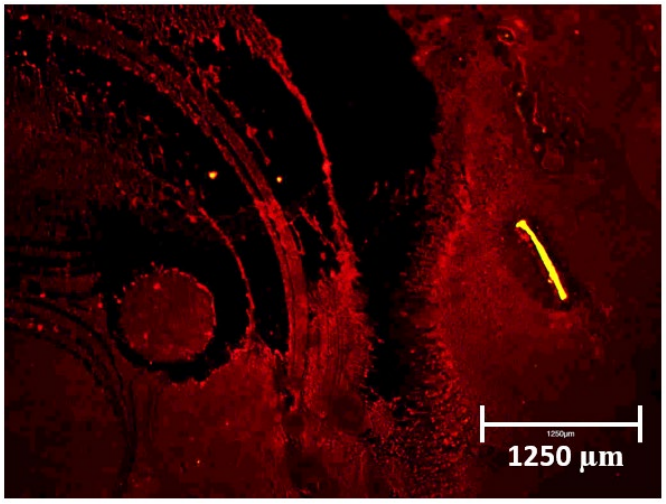

Figure 4-33 Covered area of formed biofilm on 25 BLs coated PDMS (last layer: PEI) after 1 day of incubation time captured by fluorescent microscopy. Sample was stained with SYTO9/PI and coverage area is processed with Fiji ImageJ.

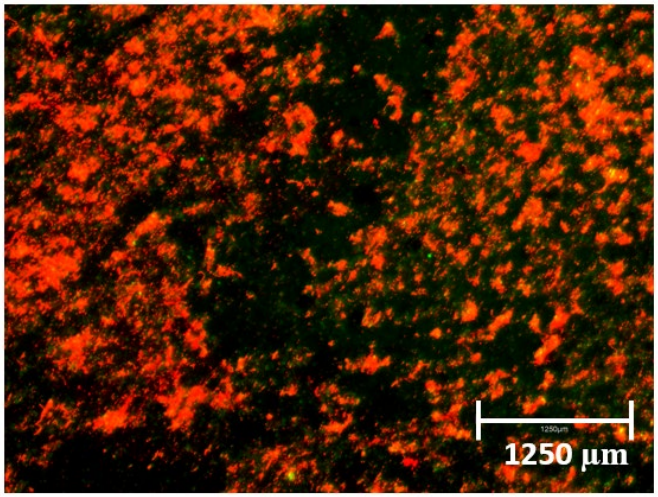

Figure 4-34 Covered area of formed biofilm on 25 BL coated PDMS (last layer: PAA) after 1 day of incubation time captured by fluorescent microscopy. Sample was stained with SYTO9/PI and coverage area is processed with Fiji ImageJ.

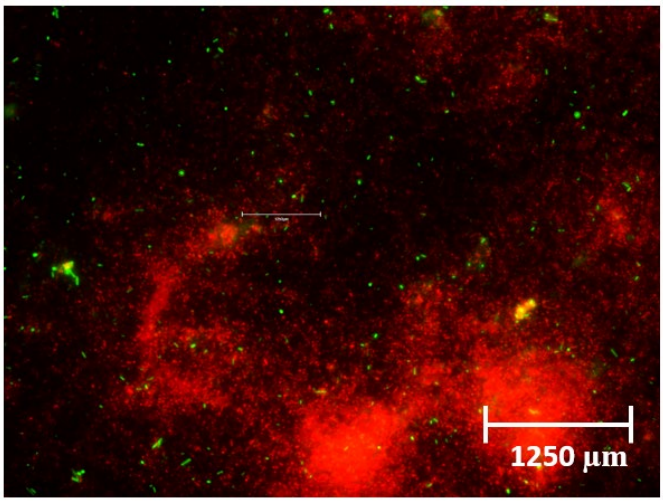

Figure 4-35 Covered area of formed biofilm on 25 BLs coated PDMS (last layer: PEI) after 7 days of incubation time captured by fluorescent microscopy. Sample was stained with SYTO9/PI and coverage area is processed with Fiji ImageJ.

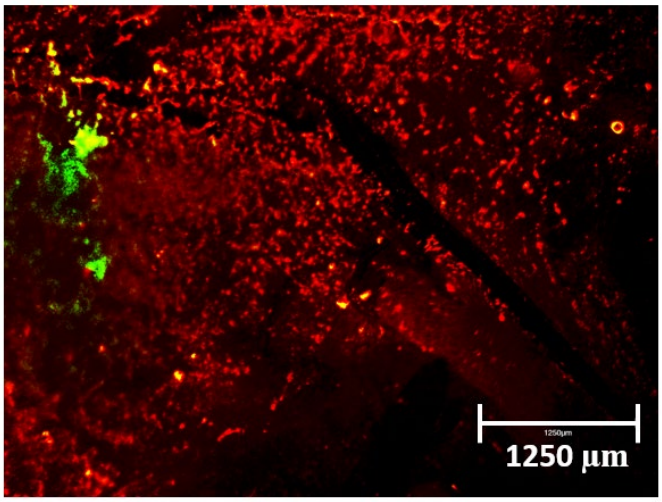

Figure 4-36 Covered area of formed biofilm on 25 BLs coated PDMS (last layer: PAA) after 7 days of incubation time captured by fluorescent microscopy. Sample was stained with SYTO9/PI and coverage area is processed with Fiji ImageJ.

The same investigation was carried out for 50 BLs coated PDMS and the coverage area of formed biofilm after 1 day of incubation reached to around 0.58 ± 0.7 % when the last layer of the coating was PEI and 0.71 ± 0.3 % when the last layer was PAA. The large drop in amount of formed biofilm on the surface of 50 BLs coated sample compared to uncoated and 25 BLs coated samples shows the good efficacy antibiofilm activity of the coating (Figure 4-37 and Figure 4-38). By increasing the incubation time to 7 days, the biofilm coverage area reached to around 5.94 ± 1 % and 14.46 ± 2 % for last layer composition of PEI and PAA, respectively (Figure 4-39 and Figure 4-40). 50 PEI/PAA BLs coated sample showed the highest antibiofilm activity against *P. aeruginosa* up to 7 days. Figure 4-41 shows the percentage of formed biofilm on the surface of mentioned samples above.

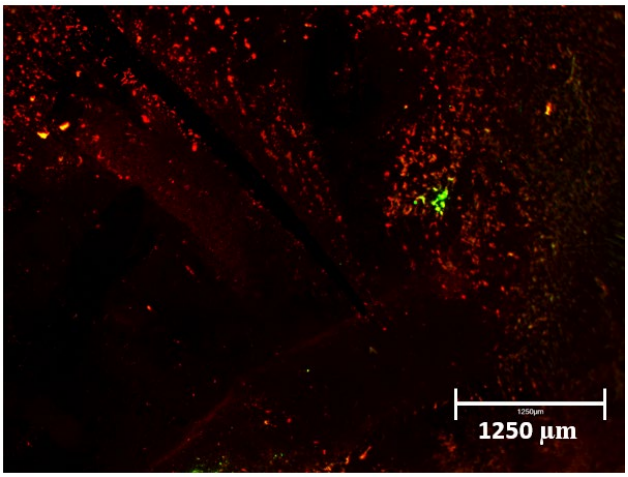

Figure 4-37 Covered area of formed biofilm on 50 BLs coated PDMS (last layer: PEI) after 1 day of incubation time captured by fluorescent microscopy. Sample was stained with SYTO9/PI and coverage area is processed with Fiji ImageJ.

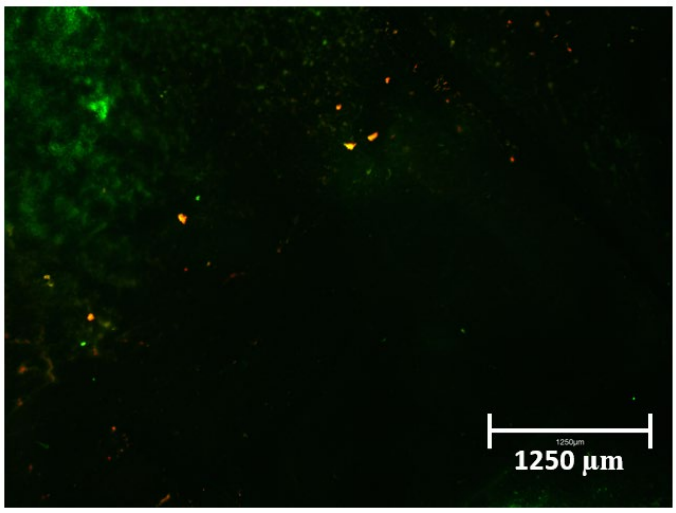

Figure 4-38 Covered area of formed biofilm on 50 BLs coated PDMS (last layer: PAA) after 1 day of incubation time captured by fluorescent microscopy. Sample was stained with SYTO9/PI and coverage area is processed with Fiji ImageJ.

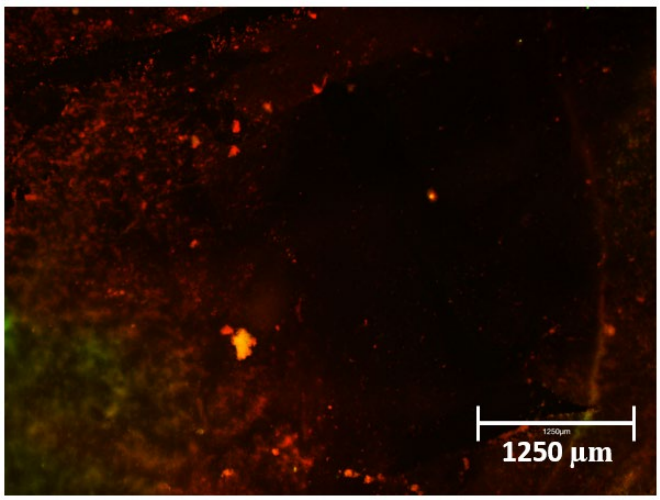

Figure 4-39 Covered area of formed biofilm on 50 BLs coated PDMS (last layer: PEI) after 7 days of incubation time captured by fluorescent microscopy. Sample was stained with SYTO9/PI and coverage area is processed with Fiji ImageJ.

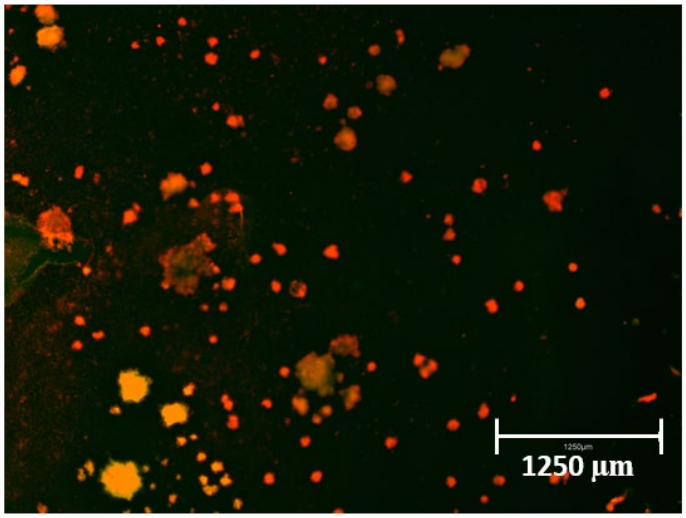

Figure 4-40 Covered area of formed biofilm on 50 BLs coated PDMS (last layer: PAA) after 7 days of incubation time captured by fluorescent microscopy. Sample was stained with SYTO9/PI and coverage area is processed with Fiji ImageJ.

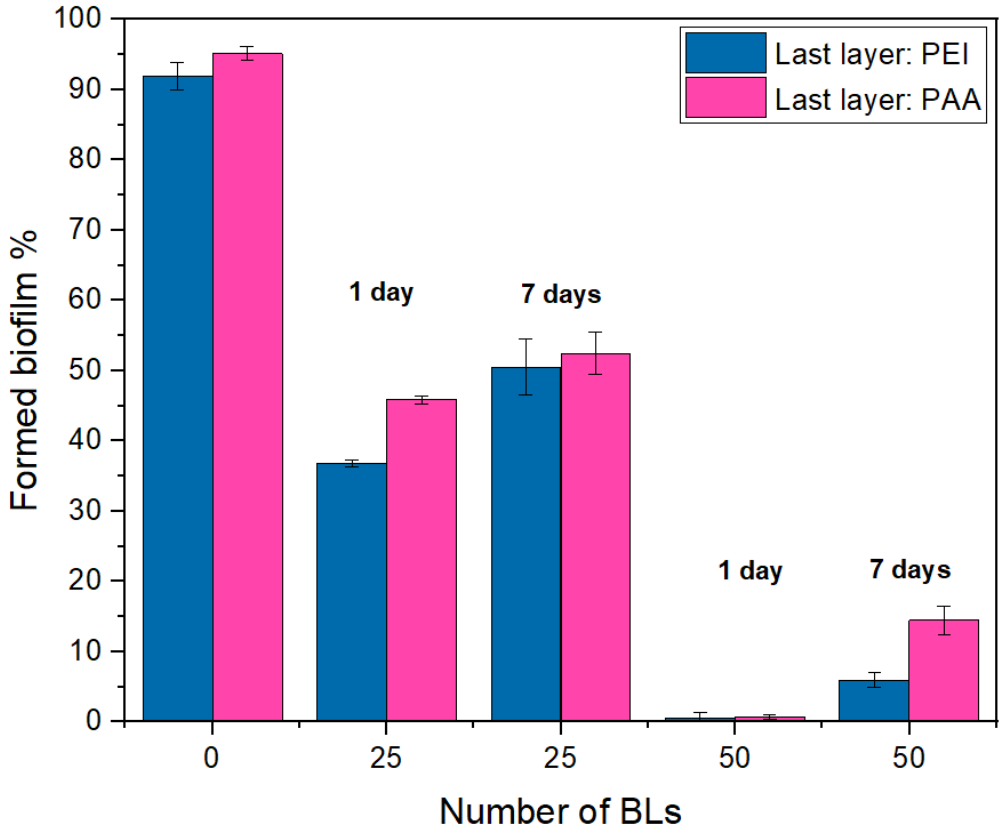

Figure 4-41 Percentage of formed biofilm on the surface on uncoated, 25 BLs and 50 BLs coated PDMS surface with last layer of PEI and PAA after 1 day and 7 days of incubation. Error bars show the minimum and maximum of each value and each bar shows the average value of 3 measurements for each coating.

4.4.3 Characterizing antimicrobial activity of the coating on urinary catheter under dynamic flow

After observing the significant antibiofilm activity of 50 BLs PEI/PAA coated samples on PDMS, the same procedure was repeated to deposit the LbL assembled coating on a piece of catheter (Dover, size of 20 Fr , 100% silicone) under dynamic flow to investigate the biofilm formation in realistic circumstance.

The volume of bladder in human adults (older than 15 years old) is approximately 300-400 ml and the urination can happen up to 8 times a day [106]. Also, post-void residual volume for both sex should be around 50 ml that defines as remain amount of urine in bladder after urination [107]. According to Manikandan et al., the flow rate in 20 Fr Dover catheter is 24 ml/sec as an average. However, the peristaltic pump cannot provide this flow rate to investigate the biofilm formation [108]. Nzakizwanayo et al. investigated a standard Foley catheter (14 Fr Bard all silicone) scaling against *P. mirabilis* with flow rate of 0.7 ml/min and observed the complete blockage and developed biofilm in 18-24 and 10 hours, respectively [109]. In the work in this thesis, 50 ml of fresh LB were

added to 500 µl (1/100 by volume) of overnight grown *P. aeruginosa* in a bottle and placed in a water bath with the temperature of 37°C for 1 hour to let *P. aeruginosa* inoculation on the catheter [34]. Then fresh LB were transferred (flow rate of 0.7 ml/min) to the bottle which contained the catheter and bacteria through tubes that connects them together. The media was next transferred from the bottle with the catheter to another container with 2% Virkon solution to prevent contamination. This process was carried out to investigate the biofilm formation of *P. aeruginosa* for 1 day and 7 days under these dynamic conditions representative of the bladder.

4.4.4 Thickness of coating on the surface of catheter

To detect 50 BLs of PEI/PAA coating on the surface of catheter, 2 coated samples were investigated with SEM imaging (Figure 4-41). The average thickness and standard deviation of the coating on the lumen of a segmented catheter was 18.09 ± 3.51 µm which is close to the average thickness of 50 BLs coatings on flat PDMS (16.13 µm).

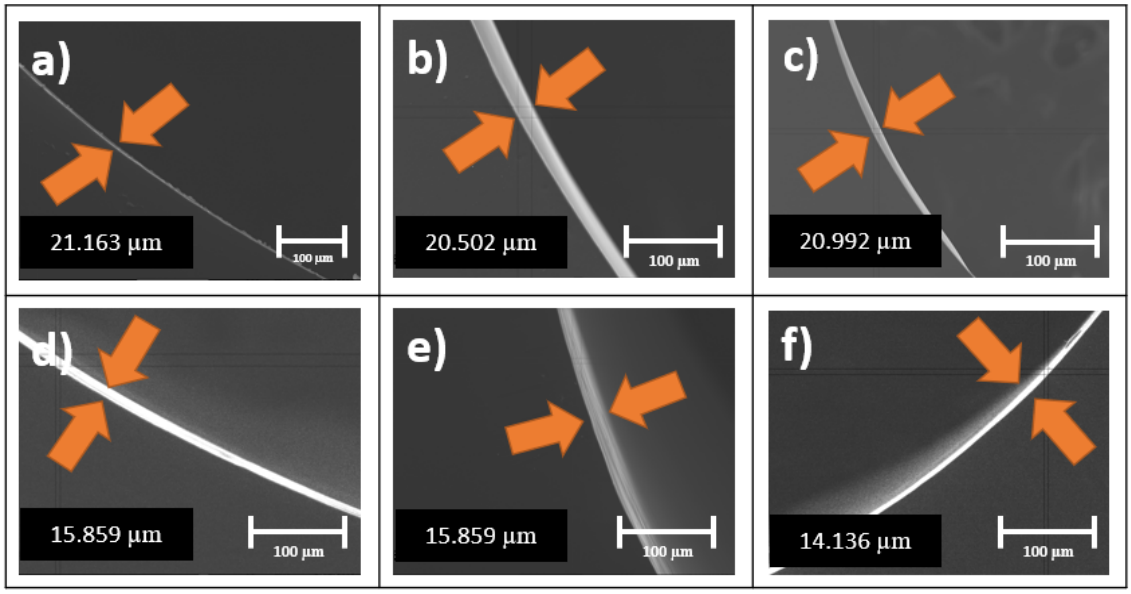

Figure 4-42 SEM images of 50 BLs coated catheter a) top edge, b) middle, c) bottom edge of sample 1, d) top edge, e) middle, f) bottom edge of sample 2. The number in each image shows the thickness of coating between the 2 orange arrows.

4.4.5 Staining the formed biofilm on 50 BLs PEI/PAA coated catheter

Following the same protocol for staining the multi BLs of PEI/PAA on the surface of PDMS, the uncoated and 50 BLs coated catheter were stained with crystal violet and the amount of formed biofilm were investigated. Results show that the same amount of formed *P. aeruginosa* biofilm on uncoated catheter is the same as uncoated PDMS (absorbance of 3.49). The coated catheters had less biofilm with either the last layers as PEI or as PAA when compared to the uncoated PDMS (around 15%) and the absorbance reached to 0.73 and 1.12 for 50 BLs coated sample with the last

layer of PEI and PAA, respectively after 1 day of incubation. By increasing the incubation time to 7 days absorbance number reached to average of 0.84 and 1.27 for the samples with the last layer of PEI and PAA, respectively. Figure 4-42 shows absorbance (OD_{584nm}) on the surface of coated and uncoated catheter.

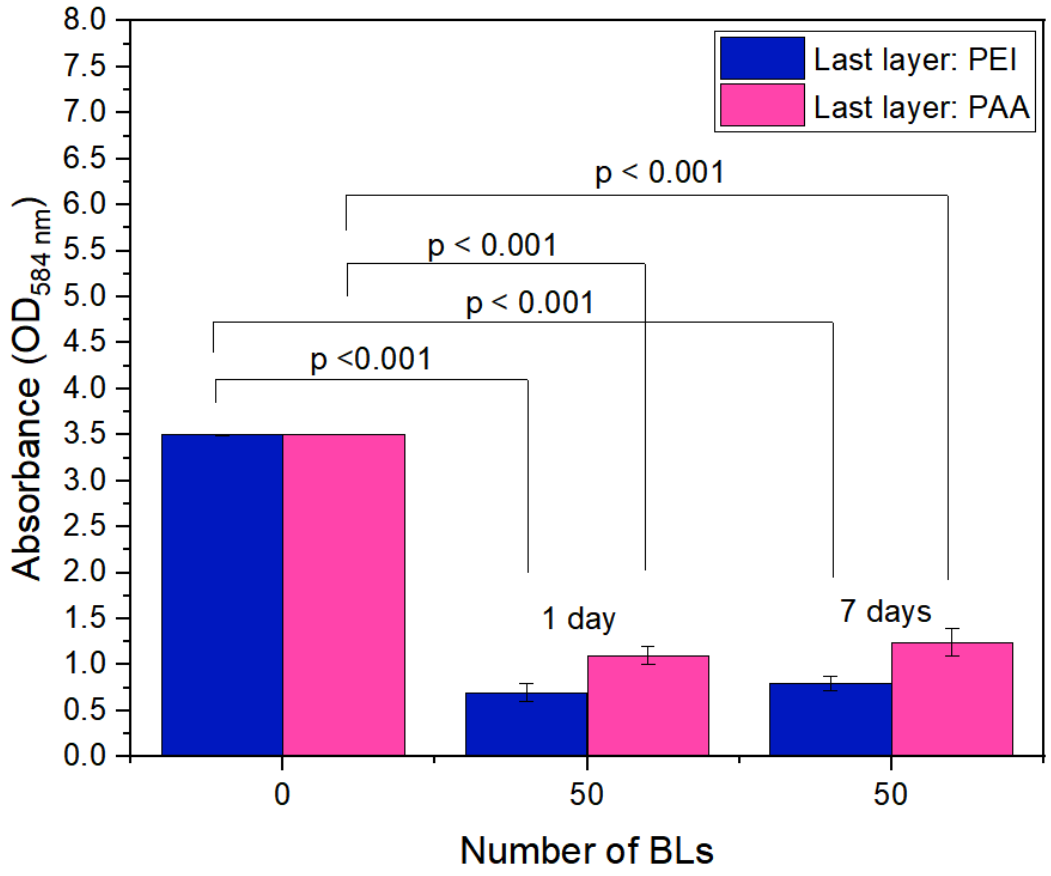

Figure 4-43 Comparing the amount of crystal violet on uncoated and 50 BLs coated catheter for 1 day and 7 days of incubation for both last layer of PEI and PAA. Bars present average value of at least 3 measurements for one sample of each coating, and error bars bound the range of minimum and maximum values. p values were calculated by Origin software, using non-parametric, Kruskal-Wallis ANOVA.

4.4.6 Fluorescent microscopy of 50 PEI/PAA BLs coated catheter

The uncoated catheter (incubated for 1 day and 7 days) was investigated by fluorescent microscopy to assess the surface coverage. As can be seen in Figure 4-43 and Figure 4-44, the majority of catheter surface is covered with formed biofilm and which are detectable in green patches and shows the accumulation of bacteria. Also, rod shape live *P. aeruginosa* covered the surface of uncoated catheter for both incubation time. Red spots were rarely seen in on uncoated catheter after 1 day of incubation, while there was no sign of red spots after 7 days.

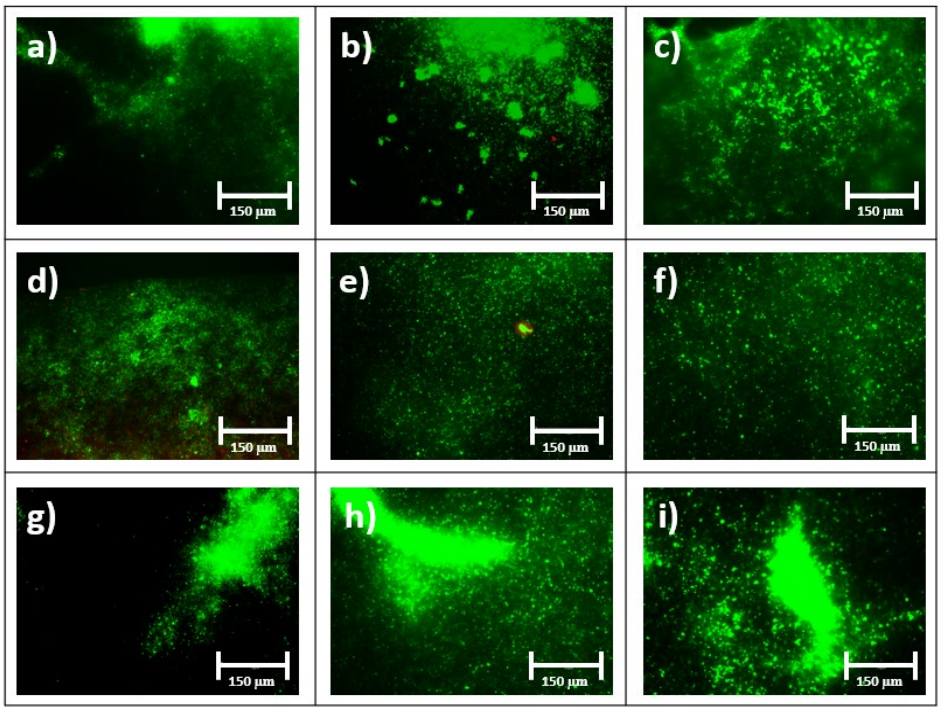

Figure 4-44 Fluorescent images *P. aeruginosa* stained with SYTO9/PI after 1 day incubation on uncoated catheter a) left corner, b) middle, c) right corner of sample 1, d) left corner, e) middle, f) right corner of sample 2, g) left corner, h) middle and i) left corner of sample 3.

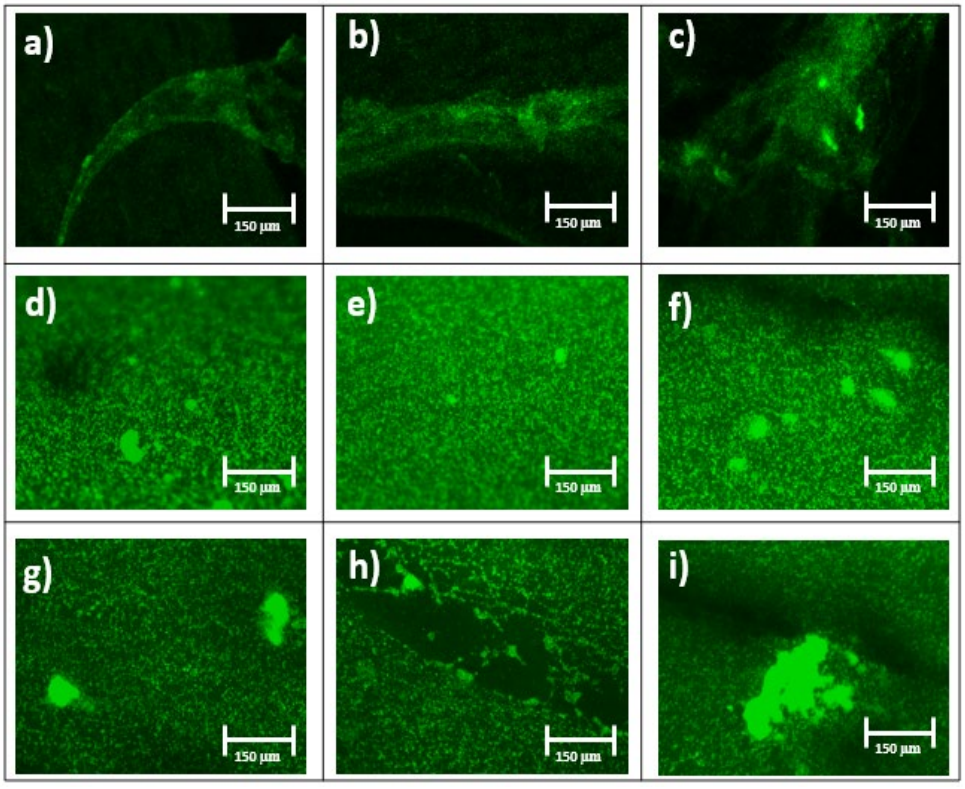

Figure 4-45 Fluorescent images *P. aeruginosa* stained with SYTO9/PI after 7 days incubation on uncoated catheter a) left corner, b) middle, c) right corner of sample 1, d) left corner, e) middle, f) right corner of sample 2, g) left corner, h) middle and i) left corner of sample 3.

The 50 BLs coated catheter showed a very small amount of formed biofilm on its surface and fluorescent microscopy confirmed the presence of dead bacteria on the coated catheter. After 1 day of incubation the majority of surface were shown in black color (no live or dead bacteria) and the rest of surface covered in red spots for both last layer compositions. Although after 7 days of incaution the formed biofilm area increased for both samples with the last layer of PEI and PAA, still biofilms were shown in red colour (dead bacteria). 50 BLs coated catheter showed significant antimicrobial activity up to 7 days under dynamic flow with flow rate of 0.7 ml/min (Figure 4-45, Figure 4-46, Figure 4-47 and Figure 4-48).

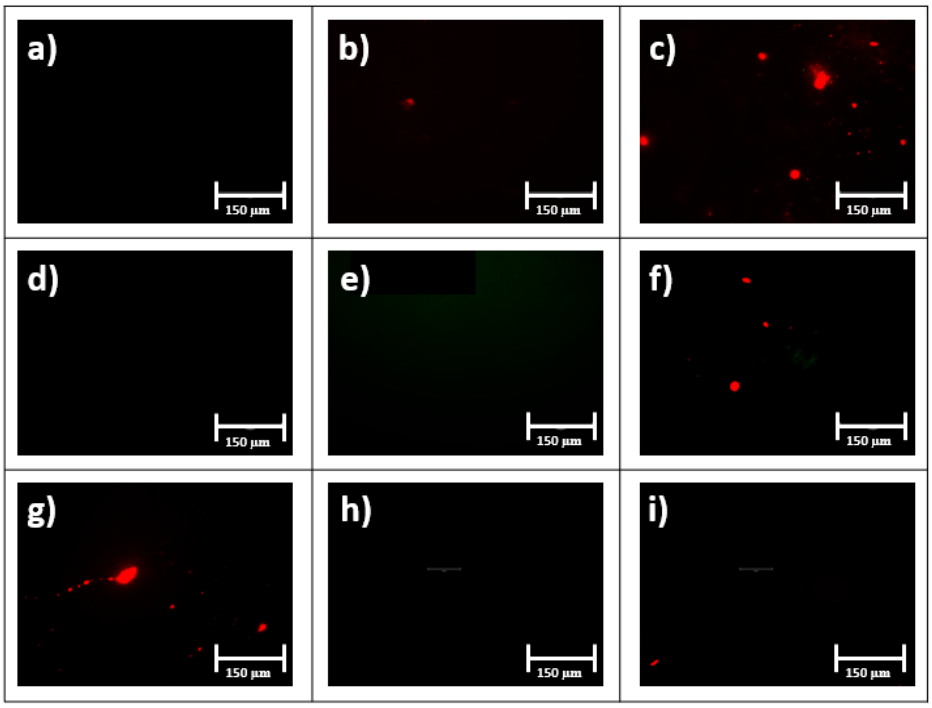

Figure 4-46 Fluorescent images P. aeruginosa stained with SYTO9/PI after 1 day incubation on 50 BLs (last layer PEI) coated catheter a) left corner, b) middle, c) right corner of sample 1, d) left corner, e) middle, f) right corner of sample 2, g) left corner, h) middle and i) left corner of sample 3.

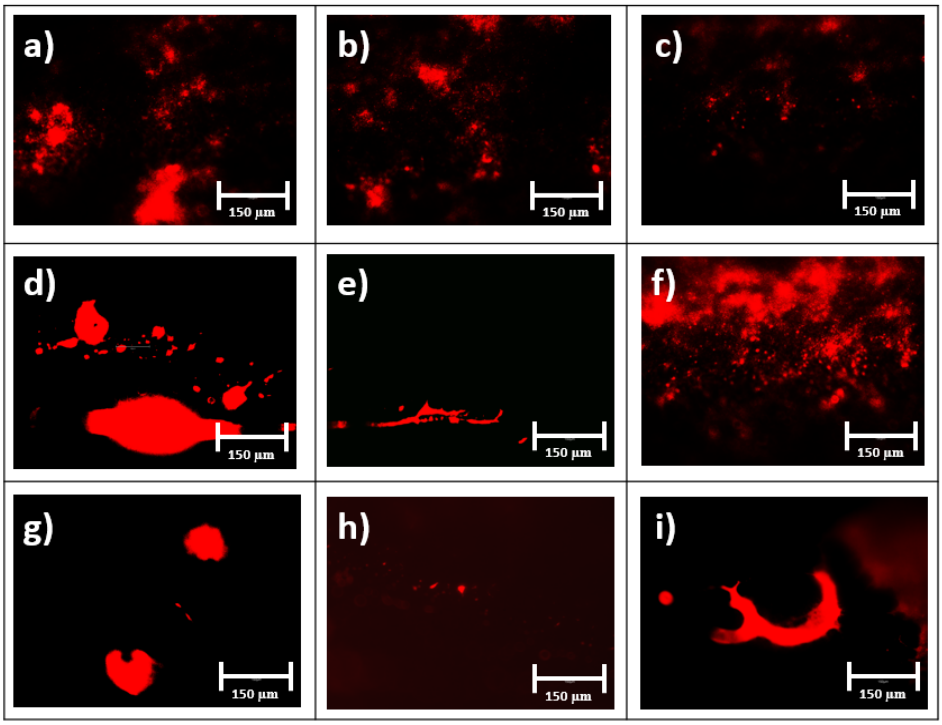

Figure 4-47 Fluorescent images P. aeruginosa stained with SYTO9/PI after 7 days incubation on 50 BLs (last layer PEI) coated catheter a) left corner, b) middle, c) right corner of sample 1, d) left corner, e) middle, f) right corner of sample 2, g) left corner, h) middle and i) left corner of sample 3.

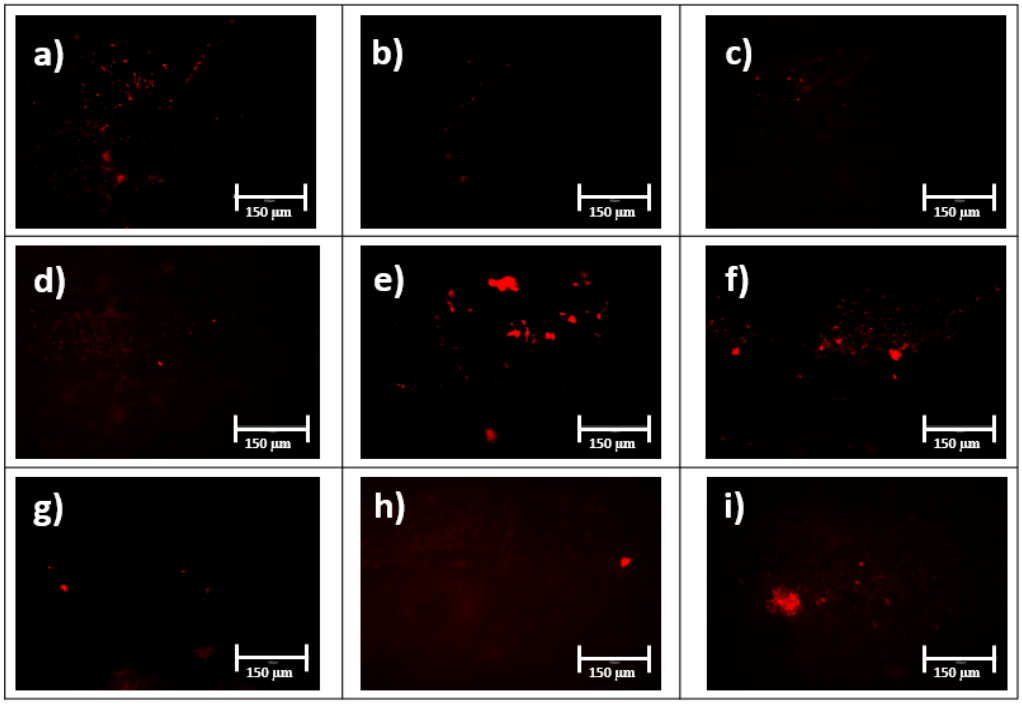

Figure 4-48 Fluorescent images P. aeruginosa stained with SYTO9/PI after 1 day incubation on 50 BLs (last layer PAA) coated catheter a) left corner, b) middle, c) right corner of sample 1, d) left corner, e) middle, f) right corner of sample 2, g) left corner, h) middle and i) left corner of sample 3.

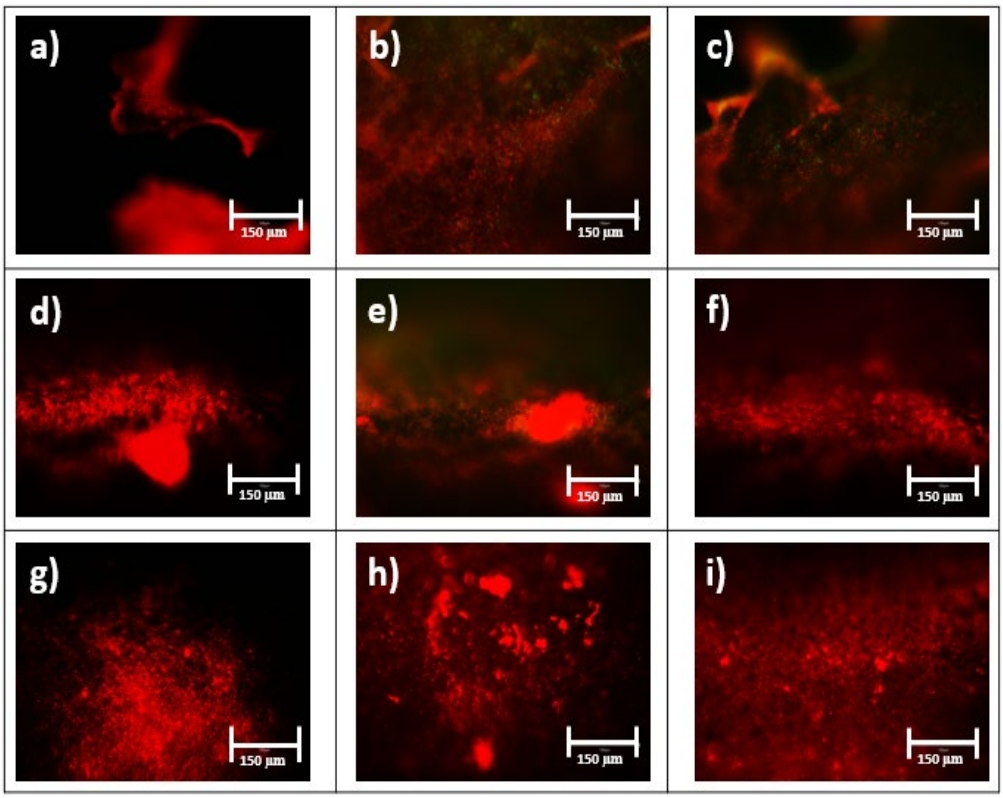

Figure 4-49 Fluorescent images P. aeruginosa stained with SYTO9/PI after 1 week incubation on 50 BLs (last layer PAA) coated catheter a) left corner, b) middle, c) right corner of sample 1, d) left corner, e) middle, f) right corner of sample 2, g) left corner, h) middle and i) left corner of sample 3.

To make sure that used *P. aeruginosa* was active in planktonic form within the dynamic flow system and the coating is responsible for preventing attachment and biofilm formation, a small amount of media was taken out and was investigated with fluorescent microscopy. Results showed that *P. aeruginosa* biofilms were present in the media which 50 BLs PEI/PAA coated catheter was placed (Figure 4-49Figure 4-49). However, the amount of attached bacteria on the surface of coated catheter was significantly lower than uncoated one and even the attached ones were damaged. These results were confirmed the antibiofilm activity of 50 BLs coated catheter in presence of *P. aeruginosa.*

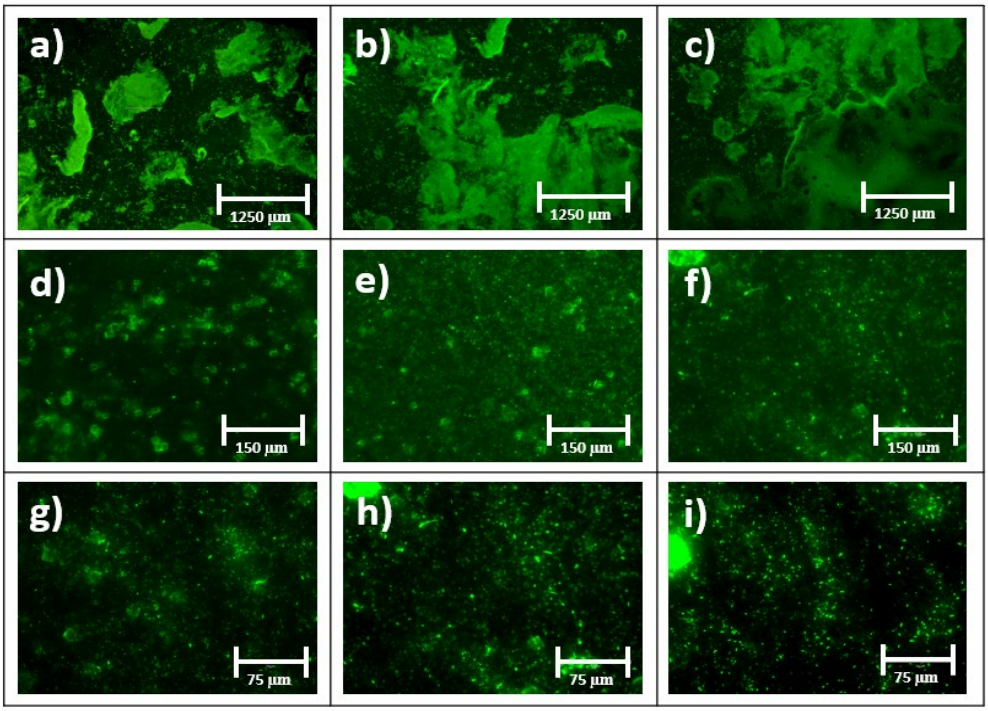

Figure 4-50 Fluorescent images *P. aeruginosa* stained with SYTO9/PI of media in which 50 BLs coated catheter was placed a), b), c) at lower magnification, d, e), f) at higher magnification, g), h) and i) at higher magnification.

The results of antibiofilm activity for 50 BLs coated PDMS samples and the same coatings on silicone rubber catheter pieces were close to each other and both significantly reduced biofilm formation. This similarity in coating performance between two different substrates can be attributed the similar composition and stiffness of substrates (stiffness of 1.8 MPa expected for silicone rubber [45] and stiffness of prepared PDMS measured as 1.99 MPa).

4.5 Chitosan/PAA multilayers of coating on the surface of PDMS

Based on the increasing intensity of green signal on the surface of 25 BLs coated PDMS after 7 days of incubation with *P. aeruginosa* and staining with SYTO9/PI, and the increasing percentage of formed biofilm on the surface of 50 BLs coated PDMS, it can be concluded that contamination of coating surfaces can affect antibiofilm activity of the coating over longer periods of incubation. Therefore, it could be beneficial to enable removal of contaminated surfaces by adding an additional constituent to the multilayer coatings that could biodegradable over an appropriate timescale. Chitosan is a biodegradable and natural polymer that can be degraded by Lysozyme, an enzyme which is present in human urine. Adding chitosan to multilayers of PEI/PAA coating can potentially improve the antimicrobial activity of the coating for longer periods by enabling degradation and removal of surfaces contaminated with bacteria and biofilm. We hypothesized that when a layer of Chitosan degrades, the layers of PEI/PAA above the chitosan layer will peel

away, leaving a new layer of PEI/PAA from below at the surface. In this part of the project was a preliminary investigation into the feasibility of this approach to degradation of contaminated surfaces. As such, only one of each type of sample was produced and investigated in terms of thickness and morphology throughout degradation. Only one sample was investigated in this part of project and 3 thickness measurement were carried out. In initial degradation tests, 50 BLs coating of chitosan/PAA was applied on the surface of PDMS and the sample left in lysozyme with concentration of 1 mg/ml solution for 1 day and 7 days to detect the degradation of coating. The SEM images (Figure 4-50) show that the average thickness of 3 measurements from center and two edges of a single coated sample of 50 Chitosan/PAA BLs coated PDMS, measured when dry, was 16.44 $\pm$ 0.30 µm after deposition. The dry thickness decreased to 3.81 $\pm$ 0.55 µm (average thickness of 3 measurements from center and two edges) after 1 day (76% of the initial thickness was lost), and after 7 days in Lysozyme solution the coating was no longer present (only remnants were observed).

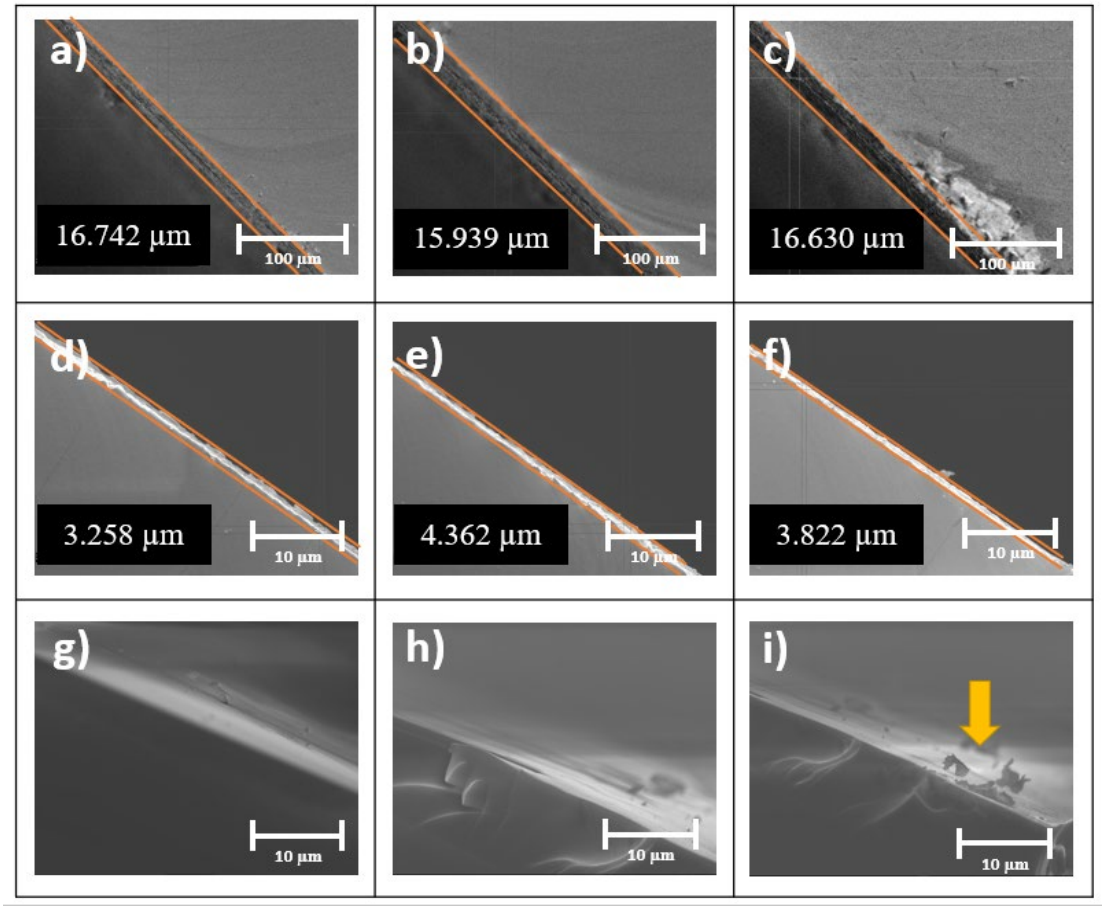

Figure 4-51 SEM images of a) right edge, b) middle, c) left edge of 50 chitosan/PAA BLs coated PDMS, d) right edge, e) middle, f) left edge of 50 chitosan/PAA BLs coated PDMS left in Lysozyme enzyme for 1 day, g) right edge, h) middle and i) left edge of 50 chitosan/PAA BLs coted PDMS left in Lysozyme enzyme for 7 days. The number in each image shows the thickness of coating between the 2 orange lines.

The combination of PEI/PAA multilayers and Chitosan/PAA films is a potential strategy to produce multifunctional coatings where PEI/PAA offers antibiofilm activity and Chitosan/PAA offers degradation of surfaces that may become fouled with biofilm over long-term use. Placing PEI/PAA BLs on top of Chitosan/PAA may restrict access of Lysozyme to the Chitosan layers and might also mechanically constrain the degrading Chitosan and prevent reductions in thickness. To assess this, 2 samples were produced with different thicknesses of PEI/PAA BLs on top of Chitosan/PAA and degradation was assessed of a period of up to 7 days. Below the Chitosan/PAA, 5 BLs of PEI/PAA were deposited to assess whether a fresh surface of antimicrobial PEI/PAA would remain after the expected degradation and removal of the layers above. Coatings with varying numbers of BLs and varying sequences of different compositions could potentially be used to achieve tailored rates of decomposition that could be matched to expected implantation times of urological or other medical devices.

The same procedure for assessing degradation of Chitosan/PAA was carried out for $(PEI/PAA)_5(Chitosan/PAA)_{50}(PEI/PAA)_5$ BLs coated PDMS, and SEM images showed the initial average thickness, measured when dry, with the standard deviation of 25.35 ± 1.792 μm. Based on previous thickness measurements the thickness of 5 PEI/PAA BLs and 50 Chitosan/PAA BLs coated samples were estimated (averagely) 1 and 16.44 μm, respectively (shown in Figure 4-2 and Figure 4-50) and the thickness of $(PEI/PAA)_5(Chitosan/PAA)_{50}(PEI/PAA)_5$ were supposed to be 17.44. However, due to the exponentially growth of thickness and using immersive method of depositing multilayers on the substrate, the results were different. Then the sample were in exposure of Lysozyme solution with the concentration of 1 mg/ml in the incubator with temperature of 37 ℃ for 1, 2 and 7 days. After taking the sample out of Lysozyme solution, SEM images were taken from them by cross sectioning and gold coating them and the thickness of coatings were decreased to average of 18.91, 10.70 and 2.96 μm after 1, 2 and 7 days, respectively. The interfaces between PEI/PAA BLs and Chitosan/PAA cannot be distinguished from the SEM images shown. However, the thickness of the bottom 5 BLs of PEI/PAA coating was estimated to be approximately 1 μm. According to the detected thicknesses for the samples, it can be concluded that 23%, 58% and 95% of chitosan/PAA multilayers were degraded in 1, 2 and 7 days, respectively. Also, according to the thickness of 5 BLs of PEI/PAA and degradation of about 7 μm of the coating after 1 day, it was concluded that top 5 BLs of PEI/PAA was peeled off from the surface by degradation of Chitosan on its bottom layers (Figure 4-51).

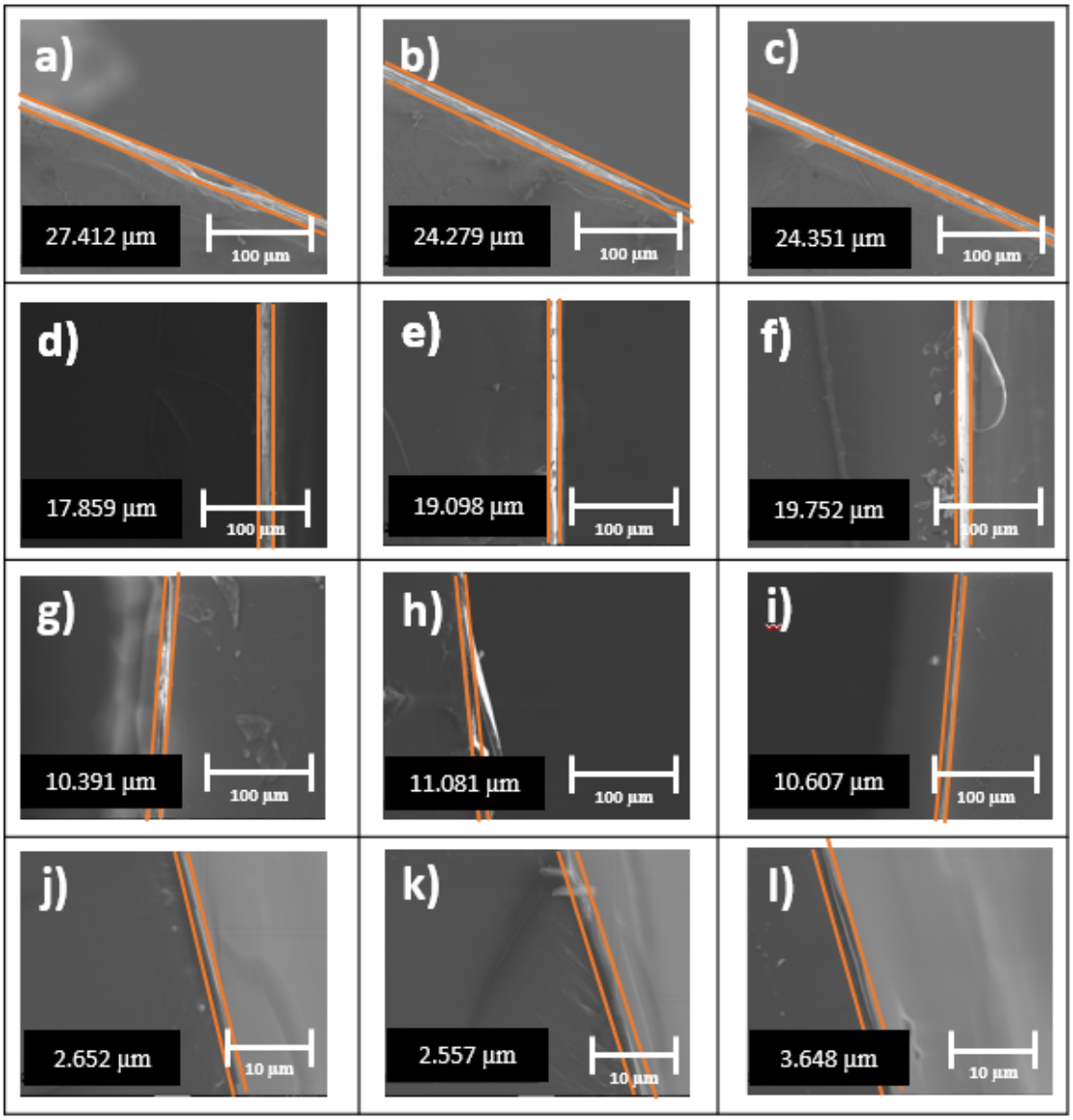

Figure 4-52 SEM images of a) right edge, b) middle, c) left edge of $(PEI/PAA)_5$ $(chitosan/PAA)_{50}$ $(PEI/PAA)_5$ BLs coated PDMS, d) right edge, e) middle, f) left edge of $(PEI/PAA)_5$ $(chitosan/PAA)_{50}$ $(PEI/PAA)_5$ BLs coated PDMS left in lysozyme enzyme for 1 day, g)right edge, h) middle, i) left edge of $(PEI/PAA)_5$ $(chitosan/PAA)_{50}$ $(PEI/PAA)_5$ BLs coted PDMS left in lysozyme enzyme for 2 days, j) right edge, k) middle and l) left edge of $(PEI/PAA)_5$ $(chitosan/PAA)_{50}$ $(PEI/PAA)_5$ BLs coted PDMS left in Lysozyme enzyme for 7 days. The number in each image shows the thickness of coating between the 2 orange lines.

The same assessment was carried out for $(PEI/PAA)_5$ $(Chitosan/PAA)_{50}$ $(PEI/PAA)_{50}$ changed sample and the initial thickness of coating was measured with the SEM imaging (79.30 ± 0.76 µm) which was estimated to be 33.57 µm averagely (1+16.44+16.13) according to previous thickness measurements. Then the sample were in exposure of Lysozyme solution with the concentration of 1 mg/ml in the incubator with temperature of 37 ℃ for 1, 2 and 7 days. After taking the sample out of Lysozyme solution, SEM images were taken from them by cross sectioning and gold coating them

and the thickness of coatings were decreased to average of 52.59, 34.80 and 4.80 µm after 1, 2 and 7 days, respectively (Figure 4-52). According to the thickness measurements, the thickness of the coating for 50 BLs of PEI/PAA BLs should be around 16 µm. However, due to exponential growth of the coating, it is complicated to specify the exact thickness for each portion of the coating. In general, it can be seen that for $(PEI/PAA)_5$ $(Chitosan/PAA)_{50}$ $(PEI/PAA)_{50}$ BL coated PDMS 23%, 58% and 95% of the thicknesses were degraded in 1, 2 and 7 days, respectively which the values are similar to the degradation amount in $(PEI/PAA)_5$ $(Chitosan/PAA)_{50}$ $(PEI/PAA)_5$. However, it can be seen that sandwiching Chitosan/PAA BLs between PEI/PAA BLs reduced the rate of degradation from 76% to around 24% after 1 day of incubation in Lysozyme solution. SEM images of $(PEI/PAA)_5$ $(Chitosan/PAA)_{50}$ $(PEI/PAA)_{50}$ sample after 7 days of incubation showed a gap between two layers which can be due to the degradation of Chitosan multilayers between PEI/PAA non degradable layers. Samples were cross sectioned and placed Lysozyme solution and there is a chance that chitosan degraded from the sides and dissolved in the solution.

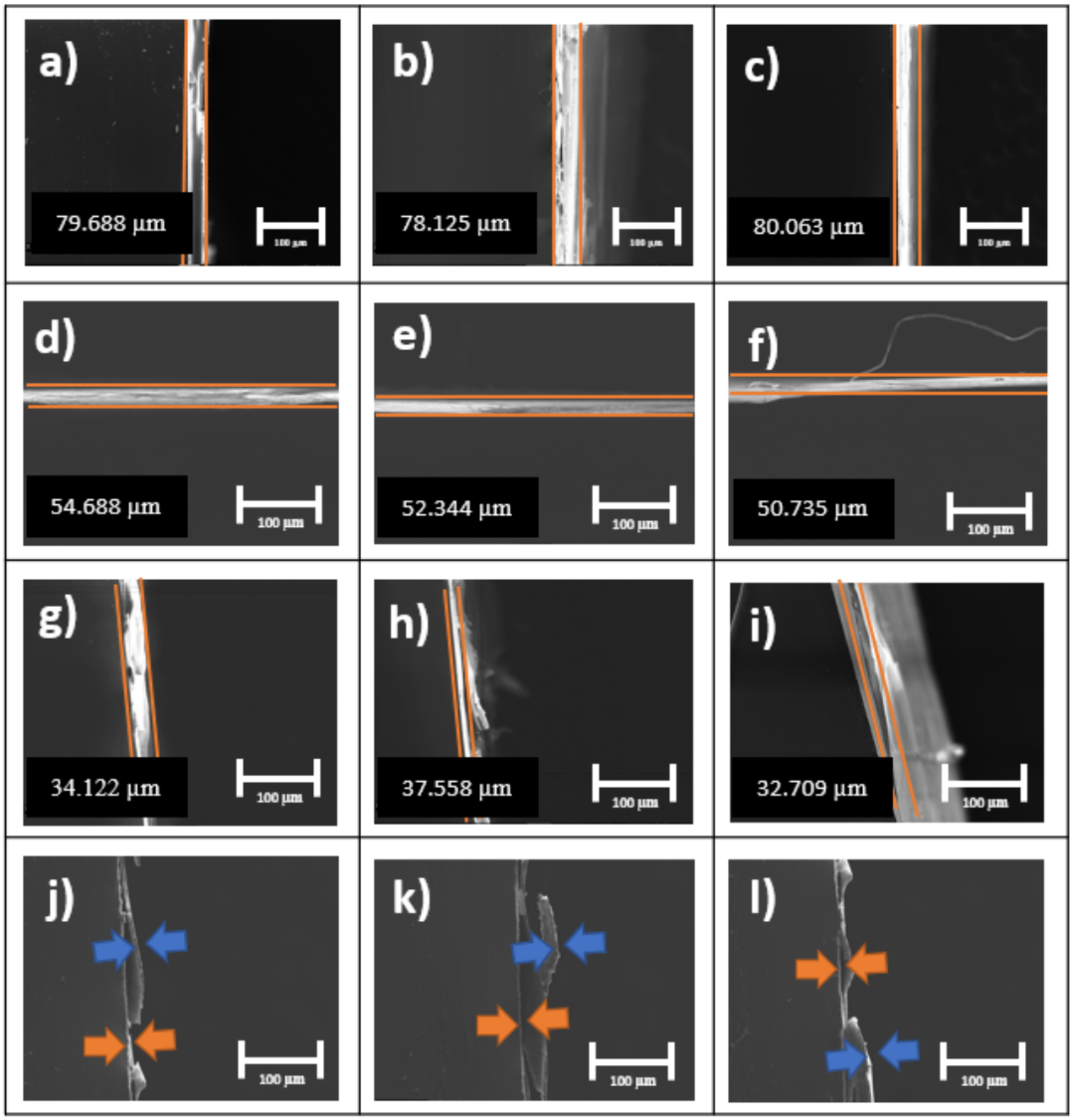

Figure 4-53 SEM images of a) right edge, b) middle, c) left edge of $(PEI/PAA)_5(chitosan/PAA)_{50}$ $(PEI/PAA)_5$ BLs coated PDMS, d) right edge, e) middle, f) left edge of $(PEI/PAA)_5$ $(Chitosan/PAA)_{50}$ $(PEI/PAA)_5$ BLs coated PDMS left in Lysozyme enzyme for 1 day, g) right edge, h) middle, i) left edge of $(PEI/PAA)_5$ $(Chitosan/PAA)_{50}$ $(PEI/PAA)_5$ BLs coted PDMS left in Lysozyme enzyme for 2 day, j) right edge, k) middle and l) left edge of $(PEI/PAA)_5$ $(chitosan/PAA)_{50}$ $(PEI/PAA)_{50}$ BLs coated PDMS left in Lysozyme enzyme for 7 days. The number in each image shows the thickness of coating between the 2 orange lines. Orange and blue arrows in j), k) and l) images show thickness of 5 BLs of PEI/PAA attached to PDMS and 50 BLs PEI/PAA on top, respectively.

Chapter 5 Conclusion

Based on a review of the literature, utilizing LbL assembly is a promising technique for producing multilayer antimicrobial coatings on urinary devices. Although single layer antimicrobial coatings have provided great advantages when deposited onto urinary devices, they suffer from limitations and disadvantages due to complexity of UTI. Combining different antimicrobial agents with different hierarchy and compositions as a coating can potentially help to address biofilm formation in medical devices. LbL assembly has shown promise in providing multilayer coatings on medical devices. The market of urinary devices is growing every year and there is an urgent need for less failure rate devices in this industry therefore, LbL assembly can be the solution to address the UTI challenge. PEI and PAA are commonly used in LbL assembly, are low cost, commercially available, do not require stringent storage conditions, and have proven promising in prior studies of antimicrobial activities. Also, LbL assembly has the advantage that other components can easily be added as additional layers in order to improve the properties (mechanical and/or antimicrobial) of coatings for medical devices such as urinary stents and catheters. In this work, BLs of PEI/PAA were deposited on the surface of PDMS substrates and results confirmed that the thickness of the coating plays an important role in antibiofilm activity. Increasing the number of BLs and thickness, provides more free space between polymeric chain and which allows absorption of more water and lead to softer coating than thinner ones. Investigations showed that bacteria can sense the stiffness of surface and attach less to softer surfaces than stiff ones. Comparing the 5 and 50 BLs coated PDMS sample showed the effect of surface stiffness on biofilm formation and confirmed that softer and thicker surfaces can lead to less biofilm formation. 50 BLs of PEI/PAA showed maximum antibiofilm activity against *P. aeruginosa* in both static and dynamic condition while it has the softest surface among other samples according to the nanoindentation test. On the other hand, the composition of the last layer is another factor that can have an effect on antimicrobial activity which showed the role of surface charge on bacterial growth. 50 BLs coated samples with the last layer of PEI had less biofilm on them than samples with the last layer of PAA. Positively charged surfaces (like PEI) can significantly decrease biofilm formation and damage the membrane of live bacteria while negatively charged surface (like PAA) do not have the same effect (Figure 5-1).

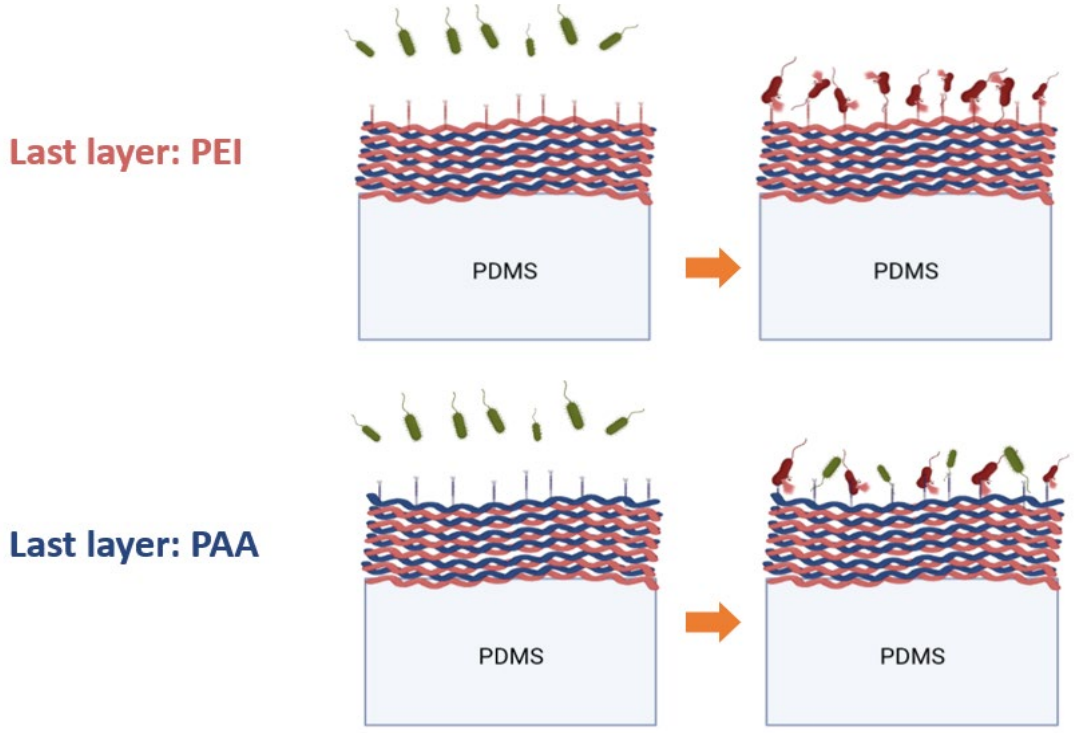

Figure 5-1 Activity of P. aeruginosa against 50 PEI/PAA BLs coated sample with the 2 different compositions of last layer.

Improving the antibiofilm activity of the coating for longer periods of incubation is one of the main objectives in studies on urinary devices and adding Chitosan as a third constituent to BLs of PEI/PAA coating can potentially achieve this by removing contaminated surfaces through biodegradation. The preliminary study in this project showed increasing the thickness of non-degradable top layer of the coating (5 to 50 BLs of PEI/PAA) did not affect on degradation of 50 Chitosan/PAA BLs according to SEM images and more detailed imaging (like confocal microscopy) is needed to have a better understanding and distinguishing the degradation of different layers. Our investigation showed that sandwiching the BLs of degradable Chitosan/PAA between BLs of non-degradable PEI/PAA against Lysozyme decreased the degradation rate of Chitosan and which can lead to controllable degradation for specific period. However, SEM imaging was not able to distinguish the BLs of PEI/PAA and Chitosan/PAA from each other to have a better understanding of what exact percentage of the coating degraded in exposure of Lysozyme.

Chapter 6 Future work

Multilayers of PEI/PAA coating showed promising antimicrobial activity on PDMS and urinary catheter surface against *P. aeruginosa* and more studies are needed regarding other microorganism that can cause UTI. Human urine contains a broad spectrum of bacteria and microbes and testing the antimicrobial activity of PEI/PAA multilayer coating in exposure of them or artificial urine can help to have a better understanding of mechanisms leading the inhibition of biofilm formation and encrustation. *Proteus mirabilis* is one of the important microorganisms that plays an important role in both biofilm formation and encrustation leading to UTIs.

Urine pH is one of the factors that might affect bacterial growth. Increases in pH can increase encrustation rate and cause contamination of coating surfaces [9], [34], [110]. Testing the antibiofilm activity of the applied coating on the surface of urinary catheter by changing under varying pH can be another important study to further investigate the antibiofilm activity of LbL assembled coatings in physiologically relevant conditions.

Manual immersive method in LbL assembly was used in this project to deposit the BLs of PEI/PAA on the substate which can add human errors to the results. Also, providing LbL assembled coating is a long process and for providing 50 BLs of PEI/PAA coating with manual immersive method, at least 10 hours of continues work and concentration is needed which can increase the rate of errors. Using device controlled depositing method can be beneficial for more investigations with less errors by controlling different variables. Computer control depositing methods are not cheap machines. However, they can provide detail-controlled samples at the same time that a person spends on only one sample that might have errors.

On the other hand, providing multifunctional coating would be beneficial to address UTI and adding the thirds constituent can help provide long lasting antimicrobial coating. Degradation of Chitosan between multilayers of PEI/PAA coating is one of the interesting points in improving the antimicrobial activity of multilayer coatings for long term usage. The provided preliminary data regarding the thickness reduction of samples that remained in Lysozyme solution showed that there might be a chance for peeling off the old layers of PEI/PAA BLs and refreshing the coating. Sandwiching the degradable Chitosan between multilayers of PEI and PAA can control the degradation rate of Chitosan and provide multifunctional long-lasting coating on the surface of urinary devices. Peeling off of BLs of PEI/PAA might cause obstructions within catheter lumens, and so further studies on the size of coating debris are needed to understand this potential challenge, which might be overcome by optimizing the thickness of different layers and thus the size of debris.

Appendix A

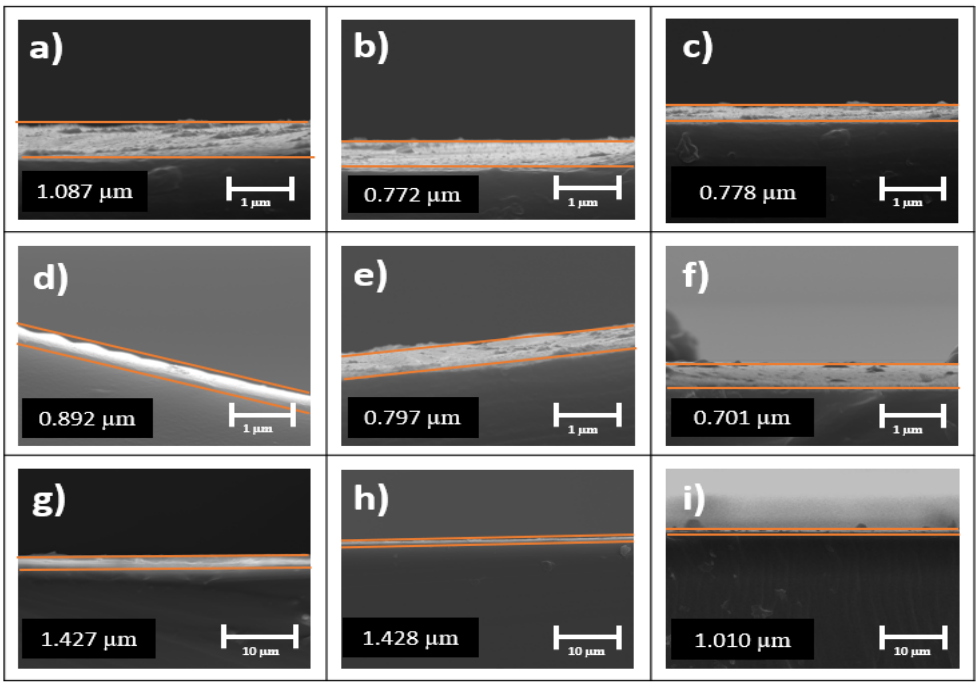

Figure A-1 SEM images of 5 BLs coated a) right edge, b) middle, c) left edge of sample 1, d) right edge, e) middle, f) left edge of sample 2, g) right edge, h) middle and i) left edge of sample 3. The number in each image shows the thickness of coating which is highlighted by the two orange lines.

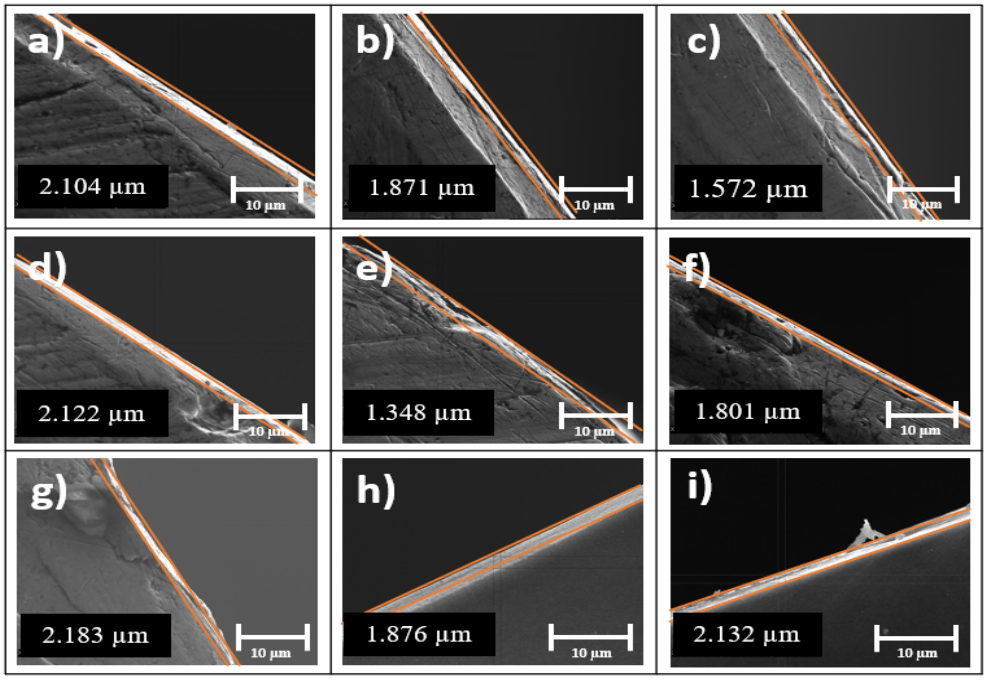

Figure A-2 SEM images of 10 BLs coated a) right edge, b) middle, c) left edge of sample 1, d) right edge, e) middle, f) left edge of sample 2, g) right edge, h) middle and i) left edge of sample 3. The number in each image shows the thickness of coating which is highlighted by the two orange lines.

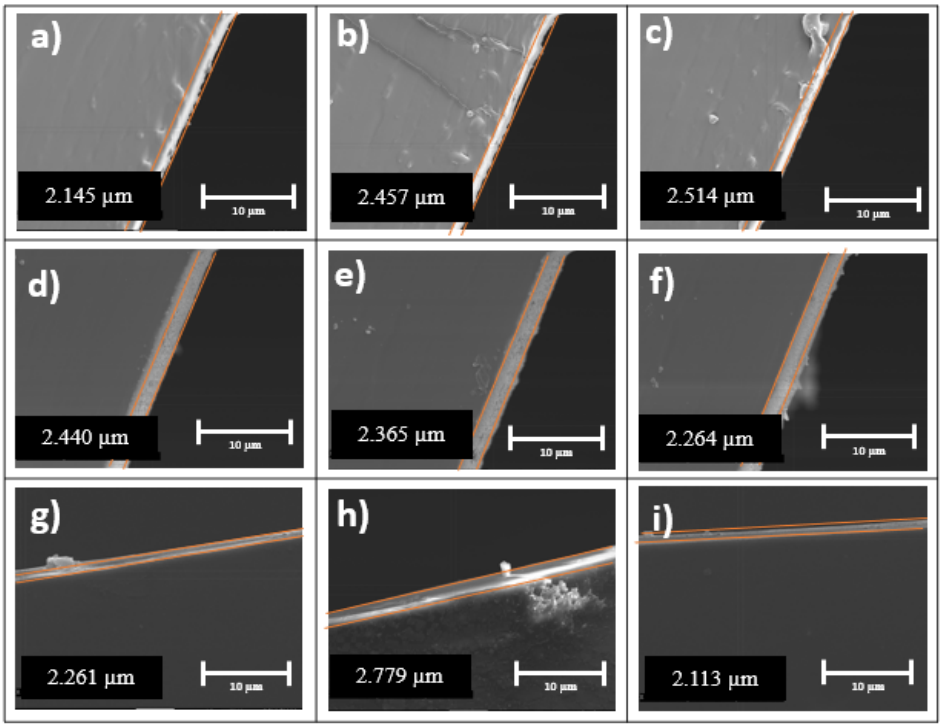

Figure A-3 SEM images of 15 BLs coated a) right edge, b) middle, c) left edge of sample 1, d) right edge, e) middle, f) left edge of sample 2, g) right edge, h) middle and i) left edge of sample 3. The number in each image shows the thickness of coating which is highlighted by the two orange lines.

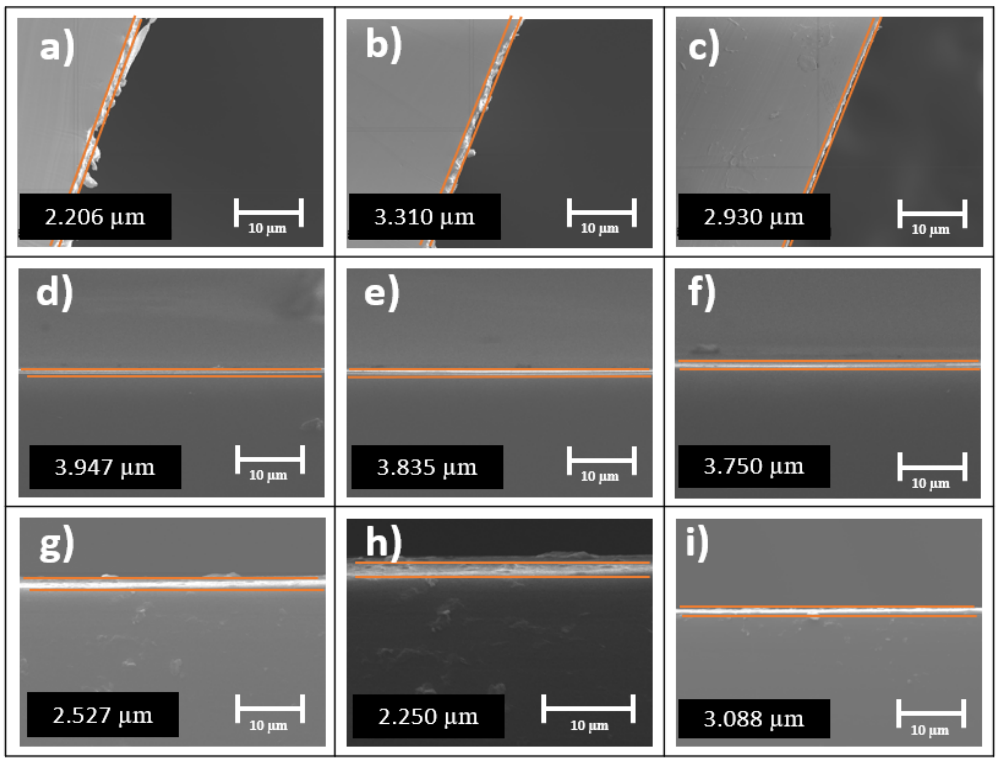

Figure A-4 SEM images of 20 BLs coated a) right edge, b) middle, c) left edge of sample 1, d) right edge, e) middle, f) left edge of sample 2, g) right edge, h) middle and i) left edge of sample 3. The number in each image shows the thickness of coating which is highlighted by the two orange lines.

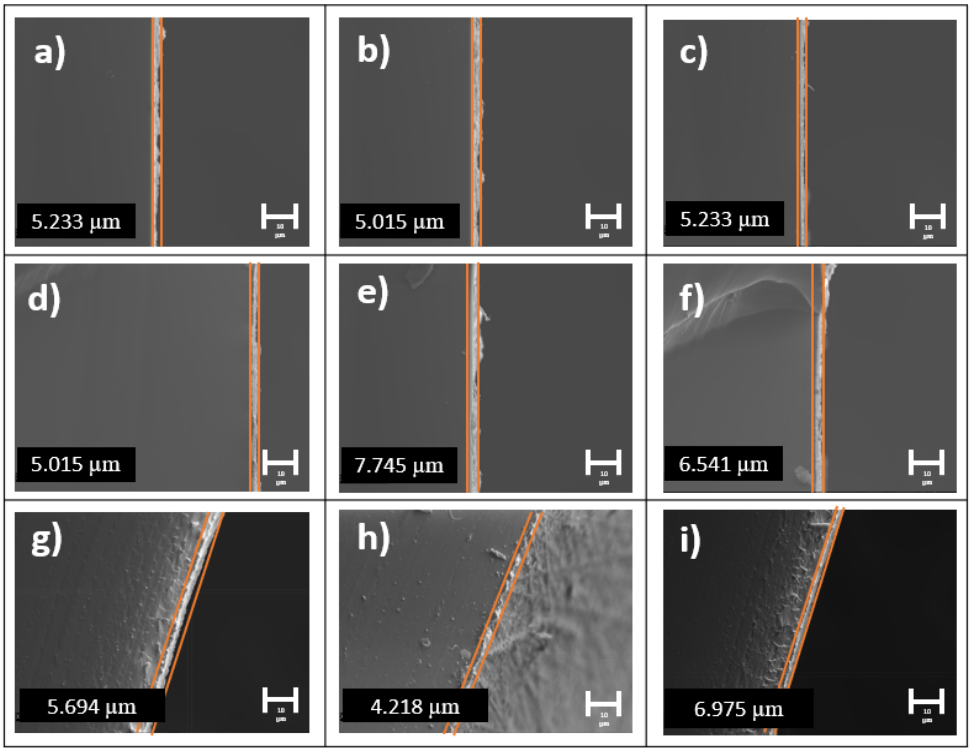

Figure A-5 SEM images of 25 BLs coated a) right edge, b) middle, c) left edge of sample 1, d) right edge, e) middle, f) left edge of sample 2, g) right edge, h) middle and i) left edge of sample 3. The number in each image shows the thickness of coating which is highlighted by the two orange lines.

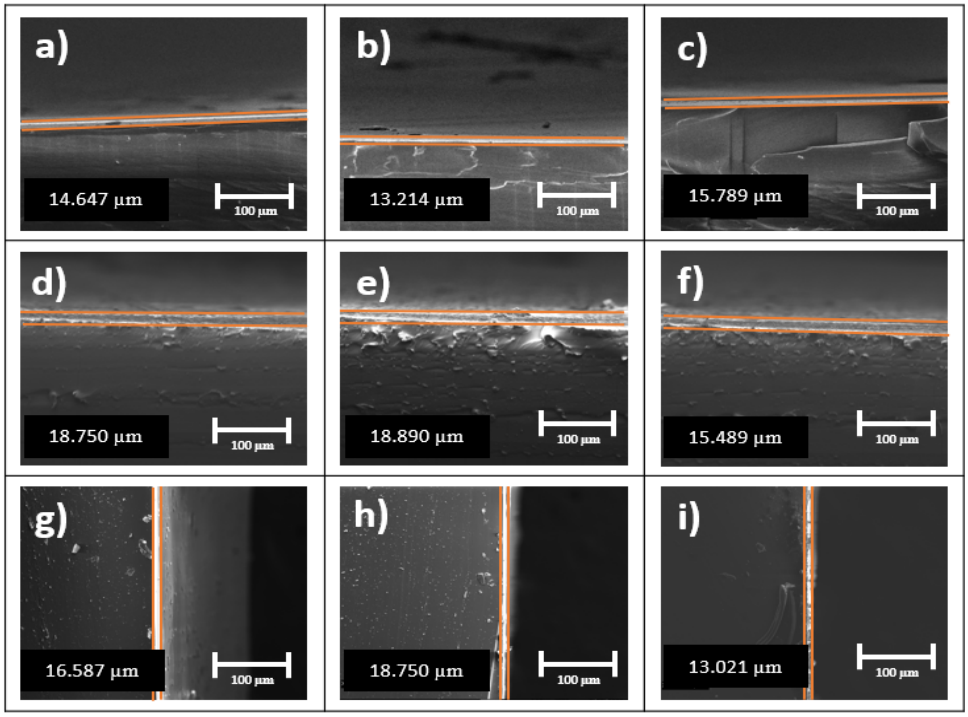

Figure A-6 SEM images of 50 BLs coated a) right edge, b) middle, c) left edge of sample 1, d) right edge, e) middle, f) left edge of sample 2, g) right edge, h) middle and i) left edge of sample 3. The number in each image shows the thickness of coating which is highlighted by the two orange lines.

List of References

[1] T. C. Jones, G. C. Hard, and U. Mohr, *Urinary system*. Springer Science & Business Media, 2013.

[2] R. Luo, S. L. Lee, F. C. Ng, and L. Koh, "Inadvertent placement of a urinary catheter into the ureter : A report of 3 cases and review of the literature," *Asian J. Urol.*, vol. 4, no. 4, pp. 256–261, 2017.

[3] S. J. Lee *et al.*, "Endourology Stent Position Is More Important than α -Blockers or Anticholinergics for Stent-Related Lower Urinary Tract Symptoms after Ureteroscopic Ureterolithotomy : A Prospective Randomized Study," pp. 636–641, 2010.

[4] R. C. L. Feneley, I. B. Hopley, and P. N. T. Wells, "Urinary catheters: history, current status, adverse events and research agenda," *J. Med. Eng. Technol.*, vol. 39, no. 8, pp. 459–470, 2015.

[5] O. O. Abiola, O. O. Ogunwobi, O. T. Williams-Abiola, S. C. Ayeni, and S. O. Adeniyi, "Quality of life and prevalence of depressive symptoms among patients on prolonged indwelling urinary catheters: a study from South west, Nigeria," *Int. J. Med. Med. Sci.*, vol. 8, no. 10, pp. 96–104, 2016.

[6] National Institute for Health and Care Excellence, "Urinary tract infection (lower): antimicrobial prescribing," *Nice*, no. November 2018, pp. 1–29, 2018.

[7] "Improving urinary tract infection treatment in peoples' homes," 2018. [Online]. Available: https://www.england.nhs.uk/atlas_case_study/improving-urinary-tract-infection-treatment-in-peoples-homes/. [Accessed: 10-Jan-2021].

[8] D. G. Maki and P. A. Tambyah, "Engineering out the risk for infection with urinary catheters.," *Emerg. Infect. Dis.*, vol. 7, no. 2, p. 342, 2001.

[9] L. E. Nicolle, "Catheter-related urinary tract infection: practical management in the elderly," *Drugs Aging*, vol. 31, no. 1, pp. 1–10, 2014.

[10] D. J. Stickler, "Clinical complications of urinary catheters caused by crystalline biofilms: something needs to be done," *J. Intern. Med.*, vol. 276, no. 2, pp. 120–129, 2014.

[11] M. Ramstedt *et al.*, "Evaluating efficacy of antimicrobial and antifouling materials for urinary tract medical devices: Challenges and recommendations," *Macromol. Biosci.*, vol. 19, no. 5, p. 1800384, 2019.

[12] E. O. Kehinde *et al.*, "Factors predisposing to urinary tract infection after J ureteral stent insertion," *J. Urol.*, vol. 167, no. 3, pp. 1334–1337, 2002.

[13] A. Nevo, R. Mano, E. Schreter, and D. A. Lifshitz, "Clinical Implications of Stent Culture in Patients with Indwelling Ureteral Stents Prior to Ureteroscopy.," *J. Urol.*, vol. 198, no. 1, pp. 116–121, Jul. 2017.

[14] C. Torrecilla *et al.*, "Reduction of ureteral stent encrustation by modulating the urine pH and inhibiting the crystal film with a new oral composition: a multicenter, placebo controlled, double blind, randomized clinical trial," *BMC Urol.*, vol. 20, pp. 1–12, 2020.

[15] D. J. Cahill, C. H. Fry, and P. J. D. FOXALL, "Variation in urine composition in the human urinary tract: evidence of urothelial function in situ?," *J. Urol.*, vol. 169, no. 3, pp. 871–874, 2003.

[16] X. Li, Z. He, J. Yuan, G. Zeng, Y. He, and M. Lei, "Long-term results of permanent metallic stent implantation in the treatment of benign upper urinary tract occlusion," *Int. J. Urol.*, vol. 14, no. 8, pp. 693–698, 2007.

[17] K. W. Kolewe, J. Zhu, N. R. Mako, S. S. Nonnenmann, and J. D. Schiffman, “Bacterial adhesion is affected by the thickness and stiffness of poly (ethylene glycol) hydrogels,” *ACS Appl. Mater. Interfaces*, vol. 10, no. 3, pp. 2275–2281, 2018.

[18] A. De Grazia, B. K. Somani, F. Soria, D. Carugo, and A. Mosayyebi, “Latest advancements in ureteral stent technology,” *Transl. Androl. Urol.*, vol. 8, no. Suppl 4, p. S436, 2019.

[19] M. Galarza, Á. Giménez, J. Valero, O. P. Pellicer, and J. M. Amigó, “Computational fluid dynamics of ventricular catheters used for the treatment of hydrocephalus: a 3D analysis,” *Child’s Nerv. Syst.*, vol. 30, no. 1, pp. 105–116, 2014.

[20] J. D. P. Valentin *et al.*, “Substrate viscosity plays an important role in bacterial adhesion under fluid flow,” *J. Colloid Interface Sci.*, vol. 552, pp. 247–257, 2019.

[21] F. Song, H. Koo, and D. Ren, “Effects of material properties on bacterial adhesion and biofilm formation,” *J. Dent. Res.*, vol. 94, no. 8, pp. 1027–1034, 2015.

[22] S. A. James, N. Hilal, and C. J. Wright, “Atomic force microscopy studies of bioprocess engineering surfaces–imaging, interactions and mechanical properties mediating bacterial adhesion,” *Biotechnol. J.*, vol. 12, no. 7, p. 1600698, 2017.

[23] F. Pan *et al.*, “Hydrogel networks as underwater contact adhesives for different surfaces,” *Mater. Horizons*, vol. 7, no. 8, pp. 2063–2070, 2020.

[24] X. Zhu and X. J. Loh, “Layer-by-layer assemblies for antibacterial applications,” *Biomater. Sci.*, vol. 3, no. 12, pp. 1505–1518, 2015.

[25] D. Alkekhia, P. T. Hammond, and A. Shukla, “Layer-by-Layer Biomaterials for Drug Delivery,” 2020.

[26] J. J. Richardson, J. Cui, M. Bjornmalm, J. A. Braunger, H. Ejima, and F. Caruso, “Innovation in layer-by-layer assembly,” *Chem. Rev.*, vol. 116, no. 23, pp. 14828–14867, 2016.

[27] I. Choi, R. Suntivich, F. A. Plamper, C. V. Synatschke, A. H. E. Müller, and V. V. Tsukruk, “PH-controlled exponential and linear growing modes of layer-by-layer assemblies of star polyelectrolytes,” *J. Am. Chem. Soc.*, vol. 133, no. 24, pp. 9592–9606, 2011.

[28] M. Ziminska *et al.*, “Nanocomposite-coated porous templates for engineered bone scaffolds: A parametric study of layer-by-layer assembly conditions,” *Biomed. Mater.*, vol. 14, no. 6, 2019.

[29] Q. Wang *et al.*, “Stable and self-healable LbL coating with antibiofilm efficacy based on alkylated polyethyleneimine micelles,” *J. Mater. Chem. B*, vol. 7, no. 24, pp. 3865–3875, 2019.

[30] M. Gultekinoglu *et al.*, “Designing of dynamic polyethyleneimine (PEI) brushes on polyurethane (PU) ureteral stents to prevent infections,” *Acta Biomater.*, vol. 21, pp. 44–54, 2015.

[31] S. J. Gates and A. Shukla, “Layer-by-layer assembly of readily detachable chitosan and poly (acrylic acid) polyelectrolyte multilayer films,” *J. Polym. Sci. Part B Polym. Phys.*, vol. 55, no. 2, pp. 127–131, 2017.

[32] M. Potara, E. Jakab, A. Damert, O. Popescu, V. Canpean, and S. Astilean, “Synergistic antibacterial activity of chitosan–silver nanocomposites on Staphylococcus aureus,” *Nanotechnology*, vol. 22, no. 13, p. 135101, 2011.

[33] F. Dai *et al.*, “Enhanced cellular compatibility of chitosan/collagen multilayers LBL modified nanofibrous mats,” *Mater. Des.*, vol. 205, p. 109717, 2021.

[34] S. Kumar, N. Chandra, L. Singh, M. Z. Hashmi, and A. Varma, *Biofilms in Human Diseases: Treatment and Control*. Springer, 2019.

[35] M. A. Bakar, J. Mckimm, S. Z. Haque, and M. Haque, “Chronic tonsillitis and biofilms : a brief overview of treatment modalities,” pp. 329–337, 2018.

[36] Z. Zhu, Z. Wang, S. Li, and X. Yuan, “Antimicrobial strategies for urinary catheters,” *J. Biomed. Mater. Res. Part A*, vol. 107, no. 2, pp. 445–467, 2019.

[37] A. L. Flores-Mireles, J. N. Walker, M. Caparon, and S. J. Hultgren, “Urinary tract infections: epidemiology, mechanisms of infection and treatment options,” *Nat. Rev. Microbiol.*, vol. 13, no. 5, pp. 269–284, 2015.

[38] M. D. Macia, E. Rojo-Molinero, and A. Oliver, “Antimicrobial susceptibility testing in biofilm-growing bacteria,” *Clin. Microbiol. Infect.*, vol. 20, no. 10, pp. 981–990, 2014.

[39] “OPEN A New Artificial Urine Protocol to Better Imitate Human Urine,” pp. 1–11, 2019.

[40] J. Lo, D. Lange, and B. H. Chew, “Ureteral stents and foley catheters-associated urinary tract infections: the role of coatings and materials in infection prevention,” *Antibiotics*, vol. 3, no. 1, pp. 87–97, 2014.

[41] X.-Y. Sun, C.-Y. Zhang, P. Bhadja, and J.-M. Ouyang, “Preparation, properties, formation mechanisms, and cytotoxicity of calcium oxalate monohydrate with various morphologies,” *CrystEngComm*, vol. 20, no. 1, pp. 75–87, 2018.

[42] P. Singha, J. Locklin, and H. Handa, “A review of the recent advances in antimicrobial coatings for urinary catheters,” *Acta Biomater.*, vol. 50, pp. 20–40, 2017.

[43] A. Majeed *et al.*, “Does antimicrobial coating and impregnation of urinary catheters prevent catheter-associated urinary tract infection? A review of clinical and preclinical studies,” *Expert Rev. Med. Devices*, vol. 16, no. 9, pp. 809–820, 2019.

[44] K. A. Kazmierska, R. Thompson, N. Morris, A. Long, and T. Ciach, “In Vitro Multicompartmental Bladder Model for Assessing Blockage of Urinary Catheters : Effect of Hydrogel Coating on Dynamics of Proteus mirabilis Growth,” *URL*, vol. 76, no. 2, pp. 515.e15-515.e20, 2010.

[45] I. M. Van Meerbeek *et al.*, “Morphing metal and elastomer bicontinuous foams for reversible stiffness, shape memory, and self-healing soft machines,” *Adv. Mater.*, vol. 28, no. 14, pp. 2801–2806, 2016.

[46] H. Q. Raheem, A. A. Al-Thahab, and F. G. Abd, “Different methods for detection sliver nanoparticles produced by proteus mirabilis bacteria,” *Int. J. PharmTech Res.*, vol. 9, no. 4, pp. 368–376, 2016.

[47] S. Meenakumari, K. D. Arunachalam, and A. S. Kumar, “Screening and characterisation of silver nanoparticles for the prevention of biofilm in urinary catheters,” *Asian J. Chem.*, vol. 25, no. 2013, pp. S347–S349, 2013.

[48] S. N. Smith and C. E. Armbruster, *Indwelling Urinary Catheter Model of Proteus mirabilis Infection*, vol. 2021. 2019.

[49] A. Vaterrodt, B. Thallinger, K. Daumann, D. Koch, G. M. Guebitz, and M. Ulbricht, “Antifouling and antibacterial multifunctional polyzwitterion/enzyme coating on silicone catheter material prepared by electrostatic layer-by-layer assembly,” *Langmuir*, vol. 32, no. 5, pp. 1347–1359, 2016.

[50] G. LuTheryn *et al.*, “Bactericidal and anti-biofilm effects of uncharged and cationic ultrasound-responsive nitric oxide microbubbles on Pseudomonas aeruginosa biofilms,” *Front. Cell. Infect. Microbiol.*, p. 1130, 2022.

[51] Q.-Q. Xiang, Y. Gao, Q.-Q. Li, J. Ling, and L.-Q. Chen, “Proteomic profiling reveals the differential toxic responses of gills of common carp exposed to nanosilver and silver nitrate,” *J. Hazard. Mater.*, vol. 394, p. 122562, 2020.

[52] M. Al-qahtani, A. Safan, G. Jassim, and S. Abadla, “Journal of Infection and Public Health Efficacy of anti-microbial catheters in preventing catheter associated urinary tract infections in hospitalized patients : A review on recent updates,” *J. Infect. Public Health*, vol. 12, no. 6, pp. 760–766, 2019.

[53] A. R. El-Nahas, M. Lachine, E. Elsawy, A. Mosbah, and H. El-Kappany, “A randomized controlled trial comparing antimicrobial (silver sulfadiazine)-coated ureteral stents with non-coated stents,” *Scand. J. Urol.*, vol. 52, no. 1, pp. 76–80, Jan. 2018.

[54] A. Abou-Hassan *et al.*, “Potential strategies to prevent encrustations on urinary stents and catheters–thinking outside the box: A European Network of Multidisciplinary Research to Improve Urinary Stents (ENIUS) Initiative,” *Expert Rev. Med. Devices*, vol. 18, no. 7, pp. 697–705, 2021.

[55] S. Zhang, F. Xia, S. Demoustier-Champagne, and A. M. Jonas, “Layer-by-layer assembly in nanochannels: assembly mechanism and applications,” *Nanoscale*, vol. 13, no. 16, pp. 7471–7497, 2021.

[56] A. Z. Panagiotopoulos, “Charge correlation effects on ionization of weak polyelectrolytes,” *J. Phys. Condens. Matter*, vol. 21, no. 42, p. 424113, 2009.

[57] L. Séon, P. Lavalle, P. Schaaf, and F. Boulmedais, “Polyelectrolyte multilayers: a versatile tool for preparing antimicrobial coatings,” *Langmuir*, vol. 31, no. 47, pp. 12856–12872, 2015.

[58] L.-M. Petrila, F. Bucatariu, M. Mihai, and C. Teodosiu, “Polyelectrolyte multilayers: An overview on fabrication, properties, and biomedical and environmental applications,” *Materials (Basel).*, vol. 14, no. 15, p. 4152, 2021.

[59] P. Bieker and M. Schönhoff, “Linear and exponential growth regimes of multilayers of weak polyelectrolytes in dependence on pH,” *Macromolecules*, vol. 43, no. 11, pp. 5052–5059, 2010.

[60] S. T. Dubas and J. B. Schlenoff, “Polyelectrolyte multilayers containing a weak polyacid: construction and deconstruction,” *Macromolecules*, vol. 34, no. 11, pp. 3736–3740, 2001.

[61] D. Balu, *Study of sporadical properties of crosslinked polyelectrolyte multilayers*. Michigan State University, 2010.

[62] B. Demeneix and J. Behr, “Polyethylenimine (PEI),” *Adv. Genet.*, vol. 53, pp. 215–230, 2005.

[63] P. A. Longo, J. M. Kavran, M.-S. Kim, and D. J. Leahy, “Transient mammalian cell transfection with polyethylenimine (PEI),” *Methods Enzymol.*, vol. 529, pp. 227–240, 2013.

[64] G. Gratzl, C. Paulik, S. Hild, J. P. Guggenbichler, and M. Lackner, “Antimicrobial activity of poly (acrylic acid) block copolymers,” *Mater. Sci. Eng. C*, vol. 38, pp. 94–100, 2014.

[65] J. Santiago-Morales, G. Amariei, P. Letón, and R. Rosal, “Antimicrobial activity of poly (vinyl alcohol)-poly (acrylic acid) electrospun nanofibers,” *Colloids Surfaces B Biointerfaces*, vol. 146, pp. 144–151, 2016.

[66] S. S. Shiratori and M. F. Rubner, “pH-dependent thickness behavior of sequentially adsorbed layers of weak polyelectrolytes,” *Macromolecules*, vol. 33, no. 11, pp. 4213–4219, 2000.

[67] Y. Yang, M. Haile, Y. T. Park, F. A. Malek, and J. C. Grunlan, “Super Gas Barrier of All-Polymer Multilayer Thin Films,” pp. 1450–1459, 2011.

[68] D. Yoo, S. S. Shiratori, and M. F. Rubner, “Controlling bilayer composition and surface wettability of sequentially adsorbed multilayers of weak polyelectrolytes,” *Macromolecules*, vol. 31, no. 13, pp. 4309–4318, 1998.

[69] N. Raman, M.-R. Lee, S. P. Palecek, and D. M. Lynn, “Polymer multilayers loaded with antifungal β-peptides kill planktonic Candida albicans and reduce formation of fungal biofilms on the surfaces of

flexible catheter tubes," *J. Control. Release*, vol. 191, pp. 54–62, 2014.

[70] N. Raman *et al.*, "Intraluminal release of an antifungal β-peptide enhances the antifungal and anti-biofilm activities of multilayer-coated catheters in a rat model of venous catheter infection," *ACS Biomater. Sci. Eng.*, vol. 2, no. 1, pp. 112–121, 2016.

[71] S. Srisang and N. Nasongkla, "Layer-by-layer dip coating of Foley urinary catheters by chlorhexidine-loaded micelles," *J. Drug Deliv. Sci. Technol.*, vol. 49, pp. 235–242, 2019.

[72] S. Srisang, N. Wongsuwan, A. Boongird, M. Ungsurungsie, P. Wanasawas, and N. Nasongkla, "Multilayer nanocoating of Foley urinary catheter by chlorhexidine-loaded nanoparticles for prolonged release and anti-infection of urinary tract," *Int. J. Polym. Mater. Polym. Biomater.*, vol. 69, no. 17, pp. 1081–1089, 2020.

[73] F. Fan, C. Zhou, X. Wang, and J. Szpunar, "Layer-by-layer assembly of a self-healing anticorrosion coating on magnesium alloys," *ACS Appl. Mater. Interfaces*, vol. 7, no. 49, pp. 27271–27278, 2015.

[74] S. Pavlukhina and S. Sukhishvili, "Polymer assemblies for controlled delivery of bioactive molecules from surfaces," *Adv. Drug Deliv. Rev.*, vol. 63, no. 9, pp. 822–836, 2011.

[75] C. Correia, "Chitosan Scaffolds Containing Hyaluronic Acid for Cartilage Tissue Engineering," vol. 3512535109, no. d, pp. 1–37.

[76] E. Guzmán *et al.*, "pH-induced changes in the fabrication of multilayers of poly (acrylic acid) and chitosan: fabrication, properties, and tests as a drug storage and delivery system," *Langmuir*, vol. 27, no. 11, pp. 6836–6845, 2011.

[77] J. A. Lichter, K. J. Van Vliet, and M. F. Rubner, "Design of antibacterial surfaces and interfaces: polyelectrolyte multilayers as a multifunctional platform," *Macromolecules*, vol. 42, no. 22, pp. 8573–8586, 2009.

[78] T. Kruk, K. Szczepanowicz, D. Kręgiel, L. Szyk-Warszyńska, and P. Warszyński, "Nanostructured multilayer polyelectrolyte films with silver nanoparticles as antibacterial coatings," *Colloids Surfaces B Biointerfaces*, vol. 137, pp. 158–166, 2016.

[79] K. D. Esmeryan *et al.*, "Early stage anti-bioadhesion behavior of superhydrophobic soot based coatings towards Pseudomonas putida," *Mater. Des.*, vol. 160, pp. 395–404, 2018.

[80] F. Song and D. Ren, "Stiffness of cross-linked poly (dimethylsiloxane) affects bacterial adhesion and antibiotic susceptibility of attached cells," *Langmuir*, vol. 30, no. 34, pp. 10354–10362, 2014.

[81] K. W. Kolewe, S. R. Peyton, and J. D. Schiffman, "Fewer bacteria adhere to softer hydrogels," *ACS Appl. Mater. Interfaces*, vol. 7, no. 35, pp. 19562–19569, 2015.

[82] A. Schneider *et al.*, "Multifunctional Polyelectrolyte Multilayer Films : Combining Mechanical Resistance , Biodegradability , and Bioactivity," pp. 139–145, 2007.

[83] L. Richert *et al.*, "Layer by Layer Buildup of Polysaccharide Films : Physical Chemistry and Cellular Adhesion Aspects," no. 9, pp. 448–458, 2004.

[84] Y. Deng, J. Sun, X. Ni, and D. Xiong, "Multilayers of poly (ethyleneimine)/poly (acrylic acid) coatings on Ti6Al4V acting as lubricated polymer-bearing interface," *J. Biomed. Mater. Res. Part B Appl. Biomater.*, vol. 108, no. 5, pp. 2141–2152, 2020.

[85] B. Domingues *et al.*, "Future Directions for Ureteral Stent Technology: From Bench to the Market," *Adv. Ther.*, vol. 5, no. 1, pp. 1–17, 2022.

[86] A. Armugam *et al.*, "Broad spectrum antimicrobial PDMS-based biomaterial for catheter fabrication," *Biomater. Res.*, vol. 25, no. 1, pp. 1–13, 2021.

[87] M. Ziminska *et al.*, “Nanocomposite-coated porous templates for engineered bone scaffolds: A parametric study of layer-by-layer assembly conditions,” *Biomed. Mater.*, vol. 14, no. 6, p. 65008, 2019.

[88] M. Amerian, M. Amerian, M. Sameti, and E. Seyedjafari, “Improvement of PDMS surface biocompatibility is limited by the duration of oxygen plasma treatment,” *J. Biomed. Mater. Res. Part A*, vol. 107, no. 12, pp. 2806–2813, 2019.

[89] R. Mittal, S. Aggarwal, S. Sharma, S. Chhibber, and K. Harjai, “Urinary tract infections caused by Pseudomonas aeruginosa: a minireview,” *J. Infect. Public Health*, vol. 2, no. 3, pp. 101–111, 2009.

[90] G. M. Alsop, G. T. Waggy, and R. A. Conway, “Bacterial growth inhibition test,” *J. (Water Pollut. Control Fed.*, pp. 2452–2456, 1980.

[91] T. Hryniewicz, K. Rokosz, J. Valíček, and R. Rokicki, “Effect of magnetoelectropolishing on nanohardness and Young’s modulus of titanium biomaterial,” *Mater. Lett.*, vol. 83, pp. 69–72, 2012.

[92] D. Xu *et al.*, “Measuring the elastic modulus of soft biomaterials using nanoindentation,” *J. Mech. Behav. Biomed. Mater.*, vol. 133, p. 105329, 2022.

[93] C. Mcgoverin, J. Robertson, Y. Jonmohamadi, and S. Swift, “Species Dependence of SYTO 9 Staining of Bacteria,” vol. 11, no. September, pp. 1–11, 2020.

[94] CHROMA, “No Title.” [Online]. Available: https://www.chroma.com/spectra-viewer?fluorochromes=10533%2C10406%2C10366%2C10448.

[95] N.- Nag and M. T. Houser, “The effects of age and urine concentration on lysozyme In unne,” pp. 297–302, 1986.

[96] O. Etienne *et al.*, “Degradability of polysaccharides multilayer films in the oral environment: an in vitro and in vivo study,” *Biomacromolecules*, vol. 6, no. 2, pp. 726–733, 2005.

[97] L. Richert *et al.*, “Layer by layer buildup of polysaccharide films: physical chemistry and cellular adhesion aspects,” *Langmuir*, vol. 20, no. 2, pp. 448–458, 2004.

[98] M. Müller, “The anomalous influence of polyelectrolyte concentration on the deposition and nanostructure of poly (ethyleneimine)/poly (acrylic acid) multilayers,” *Molecules*, vol. 24, no. 11, p. 2141, 2019.

[99] Z. Wang, A. A. Volinsky, and N. D. Gallant, “Crosslinking effect on polydimethylsiloxane elastic modulus measured by custom-built compression instrument,” *J. Appl. Polym. Sci.*, vol. 131, no. 22, 2014.

[100] N. Marcus, S. Ashkenazi, Z. Samra, A. Cohen, and G. Livni, “Community-acquired Pseudomonas aeruginosa urinary tract infections in children hospitalized in a tertiary center: relative frequency, risk factors, antimicrobial resistance and treatment,” *Infection*, vol. 36, no. 5, pp. 421–426, 2008.

[101] N. Altaee, M. J. Kadhim, and I. H. Hameed, “Detection of volatile compounds produced by Pseudomonas aeruginosa isolated from UTI patients by gas chromatography-mass spectrometry,” *Int. J. Curr. Pharm. Rev. Res.*, vol. 7, no. 6, pp. 8–24, 2017.

[102] A. Tyagi, V. Singh, M. Bharadwaj, A. Kumar, and K. Thakur, “Isolation and antibacterial susceptibility testing of multi drug resistant Pseudomonas aeruginosa causing urinary tract infections,” *J Chem Pharm Res*, vol. 3, no. 4, pp. 342–347, 2011.

[103] O. Rzhepishevska, S. Hakobyan, R. Ruhal, J. Gautrot, D. Barbero, and M. Ramstedt, “The surface charge of anti-bacterial coatings alters motility and biofilm architecture,” *Biomater. Sci.*, vol. 1, no. 6, pp. 589–602, 2013.

[104] M. Gultekinoglu *et al.*, “Polyethyleneimine brushes effectively inhibit encrustation on polyurethane ureteral stents both in dynamic bioreactor and in vivo,” *Mater. Sci. Eng. C*, vol. 71, pp. 1166–1174, 2017.

[105] Sigma Alrdich, “https://www.sigmaaldrich.com/GB/en/search/pei-mw-25000?focus=products&page=1&perpage=30&sort=relevance&term=pei mw 25000&type=product.” [Online]. Available: https://www.sigmaaldrich.com/GB/en/search/pei-mw-25000?focus=products&page=1&perpage=30&sort=relevance&term=pei mw 25000&type=product.

[106] “www.niddk.nih.gov/health-information/urolo.” .

[107] L. Ballstaedt and B. Woodbury, “Bladder post void residual volume,” 2019.

[108] R. Manikandan, V. Selvaratnam, J. Philip, A. Hanlon, D. G. Machin, and M. Williamson, “Evaluation of flow characteristics of 3-way catheters,” *J. Urol.*, vol. 181, no. 4, pp. 1922–1925, 2009.

[109] J. Nzakizwanayo, H. Pelling, S. Milo, and B. V Jones, “An in vitro bladder model for studying catheter-associated urinary tract infection and associated analysis of biofilms,” in *Proteus mirabilis*, Springer, 2019, pp. 139–158.

[110] L. A. Thornton *et al.*, “The effect of urine concentration and pH on the growth of Escherichia coli in canine urine in vitro,” *J. Vet. Intern. Med.*, vol. 32, no. 2, pp. 752–756, 2018.